

Synthesis of the Two Isomers of Heteroleptic $\text{Rh}_{12}\text{L}_6\text{L}'_6$ Metal-Organic Polyhedra by Screening of Complementary Linkers

Anna Broto-Ribas,^{a,b} María Susana Gutiérrez,^{a,b} Inhar Imaz,^{a,b,*} Arnau Carné-
Sánchez,^{a,b} Felipe Gándara,^c Judith Juanhuix,^d Daniel MasPOCH,^{a,b,e,*}

^a *Catalan Institute of Nanoscience and Nanotechnology (ICN2), CSIC and The Barcelona Institute of Science and Technology, Campus UAB, 08193 Bellaterra, Barcelona, Spain*

^b *Departament de Química, Facultat de Ciències, Universitat Autònoma de Barcelona, 08193, Bellaterra, Spain*

^c *Department of New Architectures in Materials Chemistry, Materials Science Institute of Madrid – CSIC, Sor Juana Inés de la Cruz 3, 28049 Madrid, Spain*

^d *ALBA Synchrotron, 08290 Cerdanyola del Vallès, Barcelona, Spain*

^e *ICREA, Pg. Lluís Companys 23, 08010 Barcelona, Spain*

Table of Contents

S1. Materials and Methods	S3
S2. Experimental Procedures	S5
S2.1 Synthesis of the ligands	S5
S2.2 Synthesis of $\text{Rh}_{12}\mathbf{L}_6\mathbf{L}'_6$	S10
S3. Crystallography	S13
S4. Characterization	S27
S4.1 Characterization of the ligands	S27
S4.2 Characterization of $\text{Rh}_{12}\mathbf{L}_6\mathbf{L}'_6$	S32
S4.2.1 $^1\text{H-NMR}$ of digested $\text{Rh}_{12}\mathbf{L}_6\mathbf{L}'_6$	S32
S4.2.2 UV-vis spectra	S44
S4.2.3 MALDI-TOF spectra	S61
S4.2.4 Powder X-ray diffraction	S73
S4.2.5 N_2 adsorption-desorption isotherms	S85
S4.2.6 CO_2 adsorption-desorption isotherms	S97
S5. References	S109

S1. Materials and Methods

Rhodium acetate was purchased from Acros Organics. 1,3-benzenedicarboxylate (\mathbf{L}^1), sodium carbonate (Na_2CO_3), potassium hydroxide (KOH), potassium carbonate (K_2CO_3), sodium carbonate (Na_2CO_3), hydrochloric acid 37% (HCl). 3-iodobenzoic acid, palladium(II) acetate, (E)-3,3'-(diazene-1,2-diyl)dibenzoic acid (\mathbf{L}^2), 4-*tert*-butylpyridine (tertPy), 5-*tert*-butylbenzene-1,3-dicarboxylic acid (\mathbf{L}^2), dimethyl 5-hydroxyisophthalate and 1-bromobutane, 1-bromohexane, 1-bromododecane, dimethyl naphthalene-2,7-dicarboxylate were purchased from TCI. Triphenylphosphine and HCl 37 % were purchased from Sigma Aldrich. 3-Vinylbenzoic acid was purchased from Alfa Aesar. All deuterated solvents were purchased from Eurisotop. Dimethylformamide (DMF), tetrahydrofuran (THF), methanol (MeOH) and dimethylacetamide (DMA) were purchased from Fischer Chemicals. All the reagents and solvents were used without further purification unless otherwise specified.

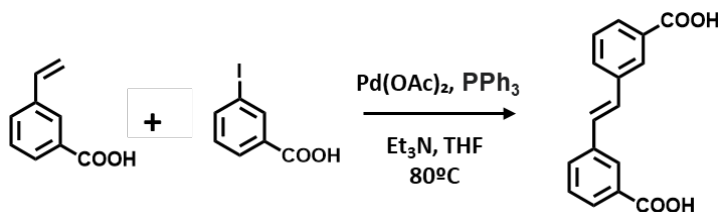
Ultraviolet-visible (UV-Vis) spectra were measured in an Agilent Cary 4000 at room temperature (ca. 25 °C). **Proton Nuclear Magnetic Resonance ($^1\text{H-NMR}$) spectra** were acquired in a Bruker Avance III 250SB NMR and a 360 250SB NMR spectrometer at “Servei d’Anàlisi Química” from Autonomous University of Barcelona (UAB). **Powder X-ray diffraction (PXRD) diagrams** were collected at room temperature on a Panalytical X’pert diffractometer with monochromatic Cu-K α radiation ($\lambda_{\text{Cu}} = 1.5406 \text{ \AA}$). Diffractograms were collected in capillary to keep the samples solvated during the measurement. **Mass Spectroscopy (MALDI-TOF)** measurements were performed using a 4800 Plus MALDI TOF/TOF (ABSCIEX – 2010). The matrix used in each case was trans-2-[3-(4-*tert*-butylphenyl)-2-methyl-2-propenylydene]malononitrile (DCTB) measured in positive mode. **Volumetric N_2 and CO_2 isotherms** were collected at 77 K (N_2) and at 298 K (CO_2) using an

ASAP 2020 (Micromeritics). Before sorption measurements, MOP samples were activated by acetone exchange for 5 days and heating at vacuum at 85 °C overnight. ***Acid digestion of Rh-MOP*** were performed by adding 20 μ L of DCl into a solution of 2 mg of Rh-MOP in 0.45 mL of DMSO- d_6 and heating the resulting solution at 100 °C for 6 hours.

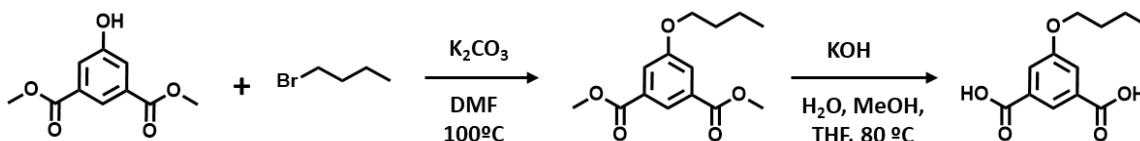
S2. Experimental Procedures

S2.1 Synthesis of the ligands

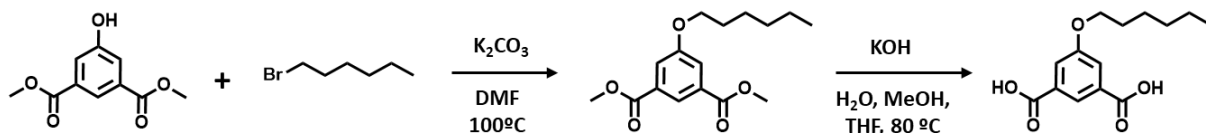
Synthesis of (E)-3,3'-(ethene-1,2-diyl)dibenzoic acid (L¹): 2 g of 3-vinylbenzoic acid (13.5 mmol), 3.34 g of 3-iodobenzoic acid (13.5 mmol), 118 mg of triphenylphosphine (0.45 mmol), triethylamine (20 mL) and 80 mg of palladium(II) acetate (0.36 mmol) were allowed to react in THF (40 ml) at 80 °C for 24 hours. The resulting suspension was filtered, and the obtained solution was evaporated under reduced pressure. The resulting solid was then dissolved in a minimum amount of THF and precipitated with concentrated HCl (12 M). The white solid was separated by centrifugation and washed with small amounts of THF, MeOH and water (2.2 g, yield: 61 %). ¹H NMR (250 MHz, DMSO-d₆): δ 13.05 (s, 1H), 8.21 (s, 1H), 7.91 (d, J = 8.0 Hz, 1H), 7.86 (d, J = 7.9 Hz, 1H), 7.52 (t, J = 7.7 Hz, 1H), 7.45 (s, 1H). ¹³C NMR (250 MHz, DMSO-d₆): δ 168.05, 138.10, 132.17, 131.54, 129.87, 129.47, 129.41, 128.33.



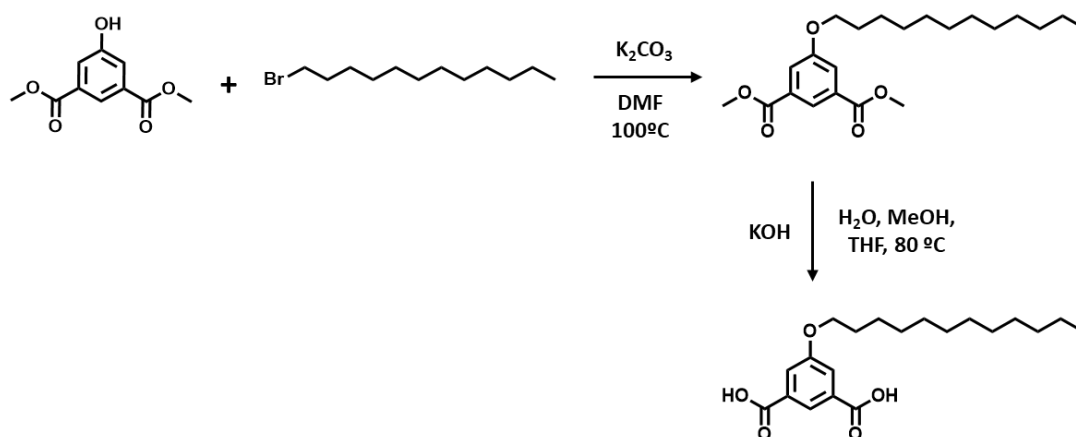
Synthesis of 5-butoxyisophthalic acid (L^{3'}): 2 g of dimethyl 5-hydroxyisophthalate (9.5 mmol) and 3.94 g of K₂CO₃ (28.5 mmol) were mixed in 50 mL of DMF. Then, 1.15 mL of 1-bromobutane (10.6 mmol) was added, and the resulting reaction mixture was heated at 100 °C overnight. Afterwards, DMF was evaporated under reduced pressure, H₂O was added, and the resulting dispersion was centrifugated. The resulting solid was washed several times with H₂O and dried at 85°C vacuum oven obtaining an oil. This oil was dissolved into 40 mL of THF, in which 40 mL of MeOH and 30 mL of 2 M aqueous of KOH solution were added. This mixture was heated at 80 °C overnight. MeOH and THF were evaporated under reduced pressure. The obtained aqueous solution was acidified with HCl forming a white precipitate, which was filtrated, washed several times with H₂O and dried at 85°C at vacuum oven (1.25 g, 55%). ¹H NMR (360 MHz, DMSO-d₆) δ 13.28 (s, 1H), 8.07 (s, 1H) 7.64 (s, 2H), 4.09 (t, J = 6.0 Hz, 2H), 1.73 (p, J = 6.5 Hz, 2H), 1.53 – 1.38 (m, 2H), 0.95 (t, J = 6.8 Hz, 3H).



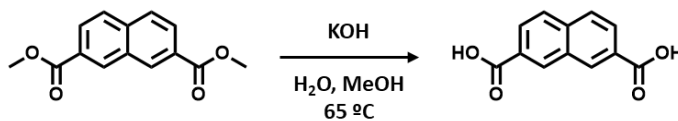
Synthesis of 5-(hexyloxy)isophthalic acid (L⁴): 2 g of dimethyl 5-hydroxyisophthalate (9.5 mmol) and 3.94 g of K₂CO₃ (28.5 mmol) were mixed in 50 mL of DMF. Then, 1.48 mL of 1-bromohexane (10.6 mmol) was added, and the resulting reaction mixture was heated at 100 °C overnight. Afterwards, DMF was evaporated under reduced pressure, H₂O was added, and the resulting dispersion was centrifugated. The obtained solid was washed several times with H₂O and dried at 85°C at vacuum oven to obtain an oil. This oil was dissolved into 40 mL of THF, in which 40 mL of MeOH and 30 mL of 2 M aqueous of KOH solution were added. The resulting mixture was heated at 80 °C overnight. MeOH and THF were evaporated under reduced pressure. The obtained aqueous solution was acidified with HCl forming a white precipitate, which was filtrated, washed several times with H₂O and dried at 85°C at vacuum oven (2.16 g, 86%). ¹H NMR (360 MHz, DMSO-d₆) δ 13.30 (s, 1H), 8.07 (s, 1H), 7.63 (s, 2H), 4.08 (t, J = 6.4 Hz, 2H), 1.74 (p, J = 6.6 Hz, 2H), 1.51 – 1.38 (m, 2H), 1.32 (m, 4H), 0.89 (t, 3H).



Synthesis of 5-(dodecyloxy)isophthalic acid (L^{5'}): 2.55 mL of 1-bromododecane (10.6 mmol) were added into a mixture of 2 g of dimethyl 5-hydroxyisophthalate (9.5 mmol) and 3.94 g of K₂CO₃ (28.5 mmol) in 50 mL of DMF. The reaction mixture was then heated at 100 °C overnight. Afterwards, DMF was evaporated under reduced pressure and H₂O was added to the solid residue to obtain a white dispersion, which was centrifugated and washed three times with H₂O. The resulting solid was dried at 85 °C in vacuum oven overnight to finally obtain a transparent oil. This oil was dissolved into 40 mL of THF, in which 40 mL of MeOH and 30 mL of 2 M aqueous of KOH solution were added. Afterwards, MeOH and THF were evaporated under reduced pressure. The obtained aqueous solution was acidified with HCl forming a white precipitate, which was filtrated and washed several times with H₂O, and finally dried at 85 °C vacuum oven (1.5 g, 45 %). ¹H NMR (360 MHz, DMSO-d₆): δ 13.26, 8.06 (s, 1H), 7.62 (s 2H), 4.06 (t, J = 6.4 Hz, 2H), 1.81 – 1.66 (m, 2H), 1.47 – 1.35 (m, 2H), 1.24 (s, 16H), 0.85 (t, J = 6.6 Hz, 3H).



Synthesis of naphthalene-2,7-dicarboxylic acid (L⁶): 0.5 g of dimethyl naphthalene-2,7-dicarboxylate (2.0 mmol), 1.15 g KOH (20.5 mmol), 9 mL of MeOH and 1 mL of H₂O were heated at 65 °C overnight. Afterwards, MeOH was evaporated under reduced pressure obtaining a water solution. HCl 12M was added, forming a white precipitate, which was filtrated and washed with water (0.40 g, yield: 91%). ¹H NMR (360 MHz, DMSO-d₆): δ 13.24 (s, 2H), 8.80 (s, 2H), 8.12 (s, 4H).



S3.2 Synthesis of $\text{Rh}_{12}\text{L}_6\text{L}'_6$

Synthesis of $\text{Rh}_{12}\text{L}^{1-2}_6\text{L}^{1-6}'_6$: A mixture of 7 eq of L^{1-2} , 5 eq of L^{1-6}' , 5 eq of Na_2CO_3 and 1 eq of rhodium acetate in 2 mL of DMA were sonicated for a few minutes and then, heated at 100 ° C for 72 h. The resulting dispersion was centrifugated to separate the Na_2CO_3 . The brown-green (for $\text{Rh}_{12}\text{L}^1_6\text{L}^{1-6}'_6$) and brown ($\text{Rh}_{12}\text{L}^2_6\text{L}^{1-6}'_6$) solution was precipitated into 10 mL of cold MeOH yielding a green solid which was washed three times with MeOH and dried at vacuum (8 mg; 28 % for $\text{Rh}_{12}\text{L}^1_6\text{L}^{1-6}'_6$; 9 mg; 29 % for $\text{Rh}_{12}\text{L}^1_6\text{L}^{2-6}'_6$; 4 mg; 12 % for $\text{Rh}_{12}\text{L}^1_6\text{L}^{3-6}'_6$, 10 mg; 30 % for $\text{Rh}_{12}\text{L}^1_6\text{L}^{4-6}'_6$; 20 mg; 54 % for $\text{Rh}_{12}\text{L}^1_6\text{L}^{5-6}'_6$; 2 mg; 7 % for $\text{Rh}_{12}\text{L}^1_6\text{L}^{6-6}'_6$; 0.5 mg; 2 % for $\text{Rh}_{12}\text{L}^2_6\text{L}^{1-6}'_6$; 6 mg; 21% for $\text{Rh}_{12}\text{L}^2_6\text{L}^{1-6}'_6$; 4 mg; 13 % for $\text{Rh}_{12}\text{L}^2_6\text{L}^{2-6}'_6$; 2.5 mg; 8 % for $\text{Rh}_{12}\text{L}^2_6\text{L}^{3-6}'_6$; 4.5 mg; 14 % for $\text{Rh}_{12}\text{L}^2_6\text{L}^{4-6}'_6$; 10 mg; 27% for $\text{Rh}_{12}\text{L}^2_6\text{L}^{5-6}'_6$).

Crystallization of $\text{Rh}_{12}\text{L}^1_6\text{L}^{1-6}'_6$: 2 mg of $\text{Rh}_{12}\text{L}^1_6\text{L}^{1-6}'_6$ were dissolved in 0.5 mL of DMA and then, 150 μL of a 4-hydroxypyridine solution (3 mg of 4-hydroxypyridine in 1 mL of DMA) were added. Purple parallelepiped crystals were obtained by slow ether vapor diffusion into this solution.

Crystallization of $\text{Rh}_{12}\text{L}^1_6\text{L}^{2-6}'_6$: 2 mg of $\text{Rh}_{12}\text{L}^1_6\text{L}^{2-6}'_6$ were dissolved in 0.5 mL of DMF and then, 120 μL of a 4-hydroxypyridine solution (3.6 mg of isonicotinic acid in 1 mL of DMF) were added. Purple parallelepiped crystals were obtained by slow ether vapor diffusion into this solution.

Crystallization of $\text{Rh}_{12}\text{L}^1_6\text{L}^{3-6}'_6$: 2 mg of $\text{Rh}_{12}\text{L}^1_6\text{L}^{3-6}'_6$ were dissolved in 0.5 mL of DMA and then, 200 μL of an isonicotinic acid solution (3.5 mg of isonicotinic acid in 1 mL of DMA) were added. Purple parallelepiped crystals were obtained by slow ether vapor diffusion into this solution.

Crystallization of Rh₁₂L¹₆L^{4'}₆: 2 mg of Rh₁₂L¹₆L^{4'}₆ were dissolved in 0.5 mL of DMF and then, 200 μL of an isonicotinic acid solution (3.3 mg of isonicotinic acid in 1 mL of DMA) were added. Purple cubic crystals were obtained by slow ether vapor diffusion into this solution.

Crystallization of Rh₁₂L¹₆L^{5'}₆: 2 mg of Rh₁₂L¹₆L^{5'}₆ were dissolved in 0.5 mL of DMA and then, 120 μL of an isonicotinic acid solution (3.9 mg of isonicotinic acid in 1 mL of DMF) were added. Purple cubic crystals were obtained by slow ether vapor diffusion into this solution.

Crystallization of Rh₁₂L¹₆L^{6'}₆: 2 mg of Rh₁₂L¹₆L^{6'}₆ were dissolved in 0.5 mL of DMF and then, 120 μL of an isonicotinic acid solution (3.9 mg of isonicotinic acid in 1 mL of DMF) were added. Purple parallelepiped crystals were obtained by slow ether vapor diffusion into this solution.

Crystallization of Rh₁₂L²₆L^{6'}₆: 1 mg of Rh₁₂L²₆L^{6'}₆ were dissolved in 0.5 mL of DMF and then, 120 μL of isonicotinic acid solution (3.6 mg isonicotinic acid in 1 mL of DMA) were added. Purple parallelepiped crystals were obtained by slow ether vapor diffusion into this solution.

Crystallization of Rh₁₂L²₆L^{1'}₆: 2 mg of Rh₁₂L²₆L^{1'}₆ were dissolved in 0.5 mL of DMA and then, 200 μL tert-butylpyridine solution (3.5 μL tert-butylpyridine in 1 mL of DMA) were added. Purple parallelepiped crystals were obtained by slow ether vapor diffusion into this solution.

Crystallization of Rh₁₂L²₆L^{2'}₆: 2 mg of Rh₁₂L²₆L^{2'}₆ were first dissolved in 20 mL of DMF. Green parallelepiped crystals were obtained by slow ether vapor diffusion into this solution.

Crystallization of Rh₁₂L²₆L^{3'}₆: 2 mg of Rh₁₂L²₆L^{3'}₆ were dissolved in 0.5 mL of DMA and then, 200 μL tert-butylpyridine solution (4.1 μL tert-butylpyridine in 1 mL of DMA) were added. Purple parallelepiped crystals were obtained by slow ether vapor diffusion into this solution.

Crystallization of Rh₁₂L²₆L⁴₆: 2 mg of Rh₁₂L²₆L⁴₆ were dissolved in 0.5 mL of DMF and then, 120 μL of isonicotinic acid solution (3.8 mg isonicotinic acid in 1 mL of DMF) were added. Purple rhombic crystals were obtained by slow ether vapor diffusion into this solution.

Crystallization of Rh₁₂L²₆L⁵₆: Hexagonal crystals of Rh₁₂L²₆L⁵₆ were obtained by slow evaporation of a solution of 50 mg of Rh₁₂L²₆L⁵₆ in 25 mL THF.

S3. Crystallography

Crystallographic data for $\text{Rh}_{12}\text{L}^1_6\text{L}^{1-6'}_6$ MOPs and $\text{Rh}_{12}\text{L}^2_6\text{L}^{1,3-6'}_6$ MOPs were collected at 100 K at XALOC beamline at ALBA synchrotron (X-ray wavelength 0.82653 Å).¹ Data were indexed, integrated and scaled using the XDS program.² Crystallographic data for $\text{Rh}_{12}\text{L}^2_6\text{L}^{2'}_6$ was collected at 'Bruker APEX-II CCD' at 150 K. Absorption correction was not applied in the case of $\text{Rh}_{12}\text{L}^1_6\text{L}^{1-6'}_6$ MOPs and $\text{Rh}_{12}\text{L}^2_6\text{L}^{1,3-6'}_6$ MOPs. Semiempirical multi-scan absorption correction was applied to $\text{Rh}_{12}\text{L}^2_6\text{L}^{2'}_6$ using SADAbs.³ The structures were solved by direct methods and subsequently refined by correction of F2 against all reflections, using SHELXT2018 within Olex2 package.^{4,5} All non-hydrogen atoms were refined with anisotropic thermal parameters by full-matrix least-squares calculations on F2 using the program SHELXL2018.⁴ The hydrogen atoms were calculated in their expected positions with the HFIX instruction of SHELXL2018 and refined as riding atoms with $\text{Uiso(H)} = 1.5 \text{ Ueq(C)}$. We treated the presence of solvent molecules in the cavities of all structures running solvent mask using Olex2 solvent mask.^{6,7} Thermal motion of some benzene rings and some coordinated solvents and pyridines of $\text{Rh}_{12}\text{L}_6\text{L}'_6$ MOPs was restrained by FLAT, DELU and SIMU. Thermal motion of $\text{Rh}_{12}\text{L}^1_6\text{L}^{1'}_6$, $\text{Rh}_{12}\text{L}^2_6\text{L}^{2'}_6$ and $\text{Rh}_{12}\text{L}^2_6\text{L}^{6'}_6$ was also restrained with EADPs restraints on the DMF or DMA moieties and in some positions of the benzene rings and tBut groups of $\text{Rh}_{12}\text{L}^2_6\text{L}^{2'}_6$. The rotation of the three tBut groups of $\text{L}^{2'}$ of $\text{Rh}_{12}\text{L}^2_6\text{L}^{2'}_6$ and the coordinated pyridines of $\text{Rh}_{12}\text{L}^2_6\text{L}^{3'}_6$ was modeled splitting them in two parts. Due to their high mobility the positions corresponding to the four, six and twelve carbons of the OC_4 , OC_6 and OC_{12} carbon chains of $\text{Rh}_{12}\text{L}^{1-2}_6\text{L}^{3,4,5'}_6$ were not well defined; constraints as EADP, DELU, RIGU and DFIX have been applied in the proposed model. Hydrogen atoms were inserted at calculated positions in the three structures. Reflections where $I(\text{obs})$ and $I(\text{calc})$ differ more than 10 times Σ (W) were omitted, ($\text{Rh}_{12}\text{L}^1_6\text{L}^{1'}_6$) (-1 -1 4); ($\text{Rh}_{12}\text{L}^1_6\text{L}^{3'}_6$) (0 2 10) (-3 4 14) (-4 4 16) (-3 12

18) $(-1 \ 10 \ 1)$; $(\text{Rh}_{12}\mathbf{L}^1\mathbf{L}^4_6)$ $(0 \ 5 \ 10)$ $(-3 \ 6 \ 12)$ $(-5 \ 6 \ 7)$ $(-2 \ 3 \ 7)$ $(-7 \ 7 \ 4)$; $(\text{Rh}_{12}\mathbf{L}^1\mathbf{L}^6_6)$ $(0 \ 6 \ 9)$ $(-4 \ 5$
 15) $(-3 \ 6 \ 3)$ $(-2 \ 3 \ 7)$; $(\text{Rh}_{12}\mathbf{L}^2\mathbf{L}^6_6)$ $(2 \ -3 \ 3)$ $(-1 \ 10 \ 0)$ $(-1 \ 0 \ 4)$ $(2 \ 0 \ 5)$ $(0 \ -5 \ 8)$ $(-3 \ -4 \ 3)$ $(-1 \ -2 \ 7)$ $(-2 \ -$
 6) $(3 \ -1 \ 12)$; $(\text{Rh}_{12}\mathbf{L}^2\mathbf{L}^1_6)$ $(-3 \ 6 \ 9)$ $(-5 \ 5 \ 2)$; $(\text{Rh}_{12}\mathbf{L}^2\mathbf{L}^2_6)$ $(-1 \ 0 \ 1)$ $(2 \ 0 \ 0)$ $(0 \ -1 \ 1)$; $(\text{Rh}_{12}\mathbf{L}^2\mathbf{L}^3_6)$
 $(0 \ 5 \ 1)$; $(\text{Rh}_{12}\mathbf{L}^2\mathbf{L}^5_6)$ $(-4 \ 4 \ 1)$ $(-1 \ 5 \ 3)$ $(-4 \ 7 \ 1)$.

S3.1 Crystal data and structure refinement for Rh₁₂L¹₆L^{1'}₆

Identification code	2176188
Formula	C ₂₀₆ H ₁₈₀ N ₁₄ O ₆₈ Rh ₁₂
Formula weight (g.mol ⁻¹)	5174.55
Temperature (K)	100
Wavelength (Å)	0.82656
Crystal system	triclinic
Space group	P-1
Unit cell dimensions	a = 20.10034(7); b = 21.47025(6); c = 23.37885(8) α = 99.5536(3); β = 109.2065(3); γ = 113.9476(7)
Volume (Å ³)	8166.45(6)
Z	1
Density calculated (g/cm ⁻³)	1.052
Absorption coefficient (mm ⁻¹)	0.971
F(000)	2598.0
Crystal size (mm)	0.18 × 0.18 × 0.16
2Theta range for data collection (°)	2.574 to 67.602
Index ranges	-27 ≤ h ≤ 23, -28 ≤ k ≤ 28, 0 ≤ l ≤ 31
Reflection collected	103894
Independent reflections	31293 [R _{int} = 0.0951, R _{sigma} = 0.0958]
Refinement method	Full-matrix least-squares on F ²
Data / restraints / parameters	31293/126/1268
Goodness-of-fit on F ²	1.043
Final R indices [I > 2σ(I)]	R ₁ = 0.0796, wR ₂ = 0.2431
R indices (all data)	R ₁ = 0.0823, wR ₂ = 0.2478
Largest diff. peak and hole	2.49, -2.02 e Å ⁻³

S3.2 Crystal data and structure refinement for Rh₁₂L¹₆L²₆

Identification code	2176191
Formula	C ₂₀₄ H ₁₆₈ N ₆ O ₆₆ Rh ₁₂
Formula weight (g.mol ⁻¹)	4982.26
Temperature (K)	100
Wavelength (Å)	0.82653
Crystal system	Trigonal
Space group	R-3c
Unit cell dimensions	a = 31.480(5); b = 31.480(5); c = 72.390(5) α = 90; β = 90; γ = 120
Volume (Å ³)	62126.7
Z	6
Density calculated (g/cm ⁻³)	0.799
Absorption coefficient (mm ⁻¹)	0.762
F(000)	14940.0
Crystal size (mm)	0.09 x 0.09 x 0.04
2Theta range for data collection (°)	4.78 to 54.664
Index ranges	-34 ≤ h ≤ 34, -34 ≤ k ≤ 34, -80 ≤ l ≤ 80
Reflection collected	170930
Independent reflections	170930 [Rint = 0.1021, Rsigma = 0.0360]
Refinement method	Full-matrix least-squares on F ²
Data / restraints / parameters	9423/37/421
Goodness-of-fit on F ²	1.567
Final R indices [I > 2σ(I)]	R ₁ = 0.1427, wR ₂ = 0.3901
R indices (all data)	R ₁ = 0.1717, wR ₂ = 0.4292
Largest diff. peak and hole	2.01/-0.64

S3.3 Crystal data and structure refinement for Rh₁₂L¹₆L^{3'}₆

Identification code	2176185
Formula	C ₂₀₄ H ₁₄₄ N ₆ O ₇₂ Rh ₁₂
Formula weight (g.mol ⁻¹)	5066.16
Temperature (K)	100
Wavelength (Å)	0.82656
Crystal system	trigonal
Space group	R-3c
Unit cell dimensions	a = 31.4131(2); b = 31.4131(2); c = 72.4411(2) α = 90; β = 90; γ = 120
Volume (Å ³)	61906.6(8)
Z	6
Density calculated (g/cm ⁻³)	0.815
Absorption coefficient (mm ⁻¹)	0.768
F(000)	15156.0
Crystal size (mm)	0.12 × 0.11 × 0.09
2Theta range for data collection (°)	2.178 to 49.842
Index ranges	0 ≤ h ≤ 27, 0 ≤ k ≤ 16, -73 ≤ l ≤ 73
Reflection collected	142271
Independent reflections	7642 [R _{int} = 0.0648, R _{sigma} = 0.0268]
Refinement method	Full-matrix least-squares on F ²
Data / restraints / parameters	7642/62/406
Goodness-of-fit on F ²	1.343
Final R indices [I > 2σ(I)]	R ₁ = 0.1098, wR ₂ = 0.3219
R indices (all data)	R ₁ = 0.1240, wR ₂ = 0.3447
Largest diff. peak and hole	1.45, -0.46 e Å ⁻³

S3.4 Crystal data and structure refinement for Rh₁₂L¹₆L^{4'}₆

Identification code	2176186
Formula	C ₂₁₆ H ₁₈₀ N ₆ O ₇₂ Rh ₁₂
Formula weight (g.mol ⁻¹)	5246.57
Temperature (K)	100
Wavelength (Å)	0.82656
Crystal system	trigonal
Space group	R-3c
Unit cell dimensions	a = 31.2593(3); b = 31.2593(3); c = 73.3075(10) α = 90; β = 90; γ = 120
Volume (Å ³)	62035.1(15)
Z	6
Density calculated (g/cm ⁻³)	0.843
Absorption coefficient (mm ⁻¹)	0.768
F(000)	15804.0
Crystal size (mm)	0.12 × 0.11 × 0.09
2Theta range for data collection (°)	3.03 to 58.18
Index ranges	0 ≤ h ≤ 31, 0 ≤ k ≤ 18, -86 ≤ l ≤ 86
Reflection collected	213203
Independent reflections	11763 [R _{int} = 0.0930, R _{sigma} = 0.0361]
Refinement method	Full-matrix least-squares on F ²
Data / restraints / parameters	11763/29/436
Goodness-of-fit on F ²	1.057
Final R indices [I > 2σ(I)]	R ₁ = 0.0695, wR ₂ = 0.2399
R indices (all data)	R ₁ = 0.0846, wR ₂ = 0.2525
Largest diff. peak and hole	1.01, -0.61 e Å ⁻³

S3.5 Crystal data and structure refinement for Rh₁₂L¹₆L⁵₆

Identification code	2176187
Formula	C ₂₅₂ H ₂₅₂ N ₆ O ₇₂ Rh ₁₂
Formula weight (g.mol ⁻¹)	5751.50
Temperature (K)	100
Wavelength (Å)	0.82656
Crystal system	trigonal
Space group	R-3c
Unit cell dimensions	a = 31.6843(5); b = 31.6843(5); c = 72.349(2) α = 90; β = 90; γ = 120
Volume (Å ³)	62900(3)
Z	6
Density calculated (g/cm ⁻³)	0.911
Absorption coefficient (mm ⁻¹)	0.763
F(000)	17532.0
Crystal size (mm)	0.09 × 0.07 × 0.06
2Theta range for data collection (°)	2.99 to 48.814
Index ranges	0 ≤ h ≤ 27, 0 ≤ k ≤ 15, -71 ≤ l ≤ 72
Reflection collected	134519
Independent reflections	7315 [R _{int} = 0.1340, R _{sigma} = 0.0505]
Refinement method	Full-matrix least-squares on F ²
Data / restraints / parameters	7315/101/394
Goodness-of-fit on F ²	1.245
Final R indices [I > 2σ(I)]	R1 = 0.1105, wR2 = 0.3237
R indices (all data)	R1 = 0.1354, wR2 = 0.3509
Largest diff. peak and hole	1.46, -0.48 e Å ⁻³

S3.6 Crystal data and structure refinement for Rh₁₂L¹₆L^{6'}₆

Identification code	2176189
Formula	C ₂₀₄ H ₁₂₀ N ₆ O ₆₆ Rh ₁₂
Formula weight (g.mol ⁻¹)	4945.97
Temperature (K)	100
Wavelength (Å)	0.82656
Crystal system	trigonal
Space group	R-3
Unit cell dimensions	a = 29.1065(5); b = 29.1065(5); c = 56.2463(9) α = 90; β = 90; γ = 120
Volume (Å ³)	41267.1(16)
Z	3
Density calculated (g/cm ⁻³)	0.597
Absorption coefficient (mm ⁻¹)	0.574
F(000)	7362.0
Crystal size (mm)	0.07 × 0.07 × 0.04
2Theta range for data collection (°)	2.526 to 50.966
Index ranges	0 ≤ h ≤ 25, 0 ≤ k ≤ 26, -58 ≤ l ≤ 58
Reflection collected	100303
Independent reflections	10826 [R _{int} = 0.0810, R _{sigma} = 0.0503]
Refinement method	Full-matrix least-squares on F ²
Data / restraints / parameters	10826/88/385
Goodness-of-fit on F ²	1.029
Final R indices [I > 2σ(I)]	R1 = 0.0648, wR2 = 0.2102
R indices (all data)	R1 = 0.0864, wR2 = 0.2286
Largest diff. peak and hole	0.72, -0.36 e Å ⁻³

S3.7 Crystal data and structure refinement for Rh₁₂L²₆L⁶₆

Identification code	2176190
Formula	C ₁₉₅ H ₁₁₅ N ₁₉ O ₆₇ Rh ₁₂
Formula weight (g.mol ⁻¹)	5030.97
Temperature (K)	100
Wavelength (Å)	0.82656
Crystal system	triclinic
Space group	P-1
Unit cell dimensions	a = 22.9616(5); b = 27.9645(4); c = 29.9154(4) α = 87.892(2); β = 68.779(2); γ = 77.069(2)
Volume (Å ³)	17431.7(6)
Z	2
Density calculated (g/cm ⁻³)	0.959
Absorption coefficient (mm ⁻¹)	0.908
F(000)	4988.0
Crystal size (mm)	0.16 × 0.14 × 0.07
2Theta range for data collection (°)	1.7 to 59.768
Index ranges	-25 ≤ h ≤ 27, -33 ≤ k ≤ 33, 0 ≤ l ≤ 35
Reflection collected	188103
Independent reflections	57778 [R _{int} = 0.0481, R _{sigma} = 0.0526]
Refinement method	Full-matrix least-squares on F ²
Data / restraints / parameters	57778/451/2464
Goodness-of-fit on F ²	1.170
Final R indices [I > 2σ(I)]	R ₁ = 0.1123, wR ₂ = 0.3103
R indices (all data)	R ₁ = 0.1379, wR ₂ = 0.3414
Largest diff. peak and hole	2.70, -0.98 e Å ⁻³

S3.8 Crystal data and structure refinement for Rh₁₂L₂₆L'₆

Identification code	2095292
Formula	C ₁₈₆ H ₁₅₀ N ₁₈ O ₅₄ Rh ₁₂
Formula weight (g.mol ⁻¹)	4736.15
Temperature (K)	100
Wavelength (Å)	0.82653
Crystal system	trigonal
Space group	R-3c
Unit cell dimensions	a = 31.163; b = 31.163; c = 69.154 $\alpha = 90^\circ$; $\beta = 90^\circ$; $\gamma = 120^\circ$
Volume/Å ³	58160.2
Z	6
Density calculated (g/cm ⁻³)	0.811
Absorption coefficient (mm ⁻¹)	0.809
F(000)	14184.0
Crystal size (mm)	0.11 x 0.095 x 0.088
2Theta range for data collection (°)	3.04 to 49.344
Index ranges	0 ≤ h ≤ 27, 0 ≤ k ≤ 15, -69 ≤ l ≤ 69
Reflections collected	131593
Independent reflections	6990 [Rint = 0.0673, Rsigma = 0.0272]
Refinement method	Full-matrix least-squares on F ²
Data / restraints / parameters	6990/233/374
Goodness-of-fit on F ²	1.366
Final R indices [I > 2sigma(I)]	R ₁ = 0.1002, wR ₂ = 0.3216
R indices (all data)	R ₁ = 0.1108, wR ₂ = 0.3418
Largest diff. peak and hole	1.07, -0.36 e Å ⁻³

S3.9 Crystal data and structure refinement for Rh₁₂L²₆L^{2'}₆

Identification code	2095294
Formula	C ₁₈₀ H ₁₇₆ N ₂₀ O ₆₂ Rh ₁₂
Formula weight (g.mol ⁻¹)	4846.32
Temperature (K)	150
Wavelength (Å)	1.54178
Crystal system	Triclinic
Space group	P-1
Unit cell dimensions	a = 19.1839(14); b = 19.3591(14); c = 21.9788(17) α = 98.356(5); β = 109.317(5); γ = 109.104(4)
Volume (Å ³)	6978.3(9)
Z	1
Density calculated (g/cm ⁻³)	1.153
Absorption coefficient (mm ⁻¹)	6.108
F(000)	2432.0
Crystal size (mm)	0.08 × 0.08 × 0.04
2Theta range for data collection (°)	4.444 to 101.764
Index ranges	-19 ≤ h ≤ 19, -19 ≤ k ≤ 19, -22 ≤ l ≤ 22
Reflection collected	45605
Independent reflections	14581 [R _{int} = 0.1814, R _{sigma} = 0.2072]
Refinement method	Full-matrix least-squares on F ²
Data / restraints / parameters	14581/470/1190
Goodness-of-fit on F ²	0.923
Final R indices [I > 2σ(I)]	R ₁ = 0.0805, wR ₂ = 0.1989
R indices (all data)	R ₁ = 0.1575, wR ₂ = 0.2416
Largest diff. peak and hole	1.46, -1.07 e Å ⁻³

S3.10 Crystal data and structure refinement for $\text{Rh}_{12}\text{L}^2_6\text{L}^{3'}_6$

Identification code	2176184
Formula	$\text{C}_{234}\text{H}_{252}\text{N}_{24}\text{O}_{60}\text{Rh}_{12}$
Formula weight ($\text{g}\cdot\text{mol}^{-1}$)	5595.50
Temperature (K)	100
Wavelength (\AA)	0.82656
Crystal system	trigonal
Space group	R-3
Unit cell dimensions	$a = 33.9017(2)$; $b = 33.9017(2)$; $c = 23.6843(7)$ $\alpha = 90$; $\beta = 90$; $\gamma = 120$
Volume (\AA^3)	23574.0(8)
Z	3
Density calculated (g/cm^3)	1.182
Absorption coefficient (mm^{-1})	1.014
F(000)	8532.0
Crystal size (mm)	$0.11 \times 0.09 \times 0.03$
2Theta range for data collection ($^\circ$)	3.796 to 66.798
Index ranges	$0 \leq h \leq 38$, $0 \leq k \leq 38$, $-31 \leq l \leq 31$
Reflection collected	99905
Independent reflections	12006 [$R_{\text{int}} = 0.0791$, $R_{\text{sigma}} = 0.0517$]
Refinement method	Full-matrix least-squares on F ²
Data / restraints / parameters	12006/100/524
Goodness-of-fit on F ²	0.985
Final R indices [$I > 2\sigma(I)$]	$R_1 = 0.0806$, $wR_2 = 0.2342$
R indices (all data)	$R_1 = 0.1094$, $wR_2 = 0.2602$
Largest diff. peak and hole	2.32, -0.45 e \AA^{-3}

S3.11 Crystal data and structure refinement for Rh₁₂L²₆L⁴'₆

Identification code	2176183
Formula	C ₂₀₄ H ₁₆₈ N ₁₈ O ₇₂ Rh ₁₂
Formula weight (g.mol ⁻¹)	5258.47
Temperature (K)	100
Wavelength (Å)	0.82656
Crystal system	trigonal
Space group	R-3
Unit cell dimensions	a = 28.4941(2); b = 28.4941(2); c = 46.4950(5) α = 90; β = 90; γ = 120
Volume (Å ³)	32692.4(6)
Z	3
Density calculated (g/cm ⁻³)	0.801
Absorption coefficient (mm ⁻¹)	0.730
F(000)	7902.0
Crystal size (mm)	0.11 × 0.07 × 0.06
2Theta range for data collection (°)	5.18 to 44.134
Index ranges	0 ≤ h ≤ 21, 0 ≤ k ≤ 22, -42 ≤ l ≤ 42
Reflection collected	55567
Independent reflections	5693 [R _{int} = 0.0300, R _{sigma} = 0.0178]
Refinement method	Full-matrix least-squares on F ²
Data / restraints / parameters	5693/398/370
Goodness-of-fit on F ²	2.486
Final R indices [I > 2σ(I)]	R ₁ = 0.1742, wR ₂ = 0.4732
R indices (all data)	R ₁ = 0.1821, wR ₂ = 0.5059
Largest diff. peak and hole	2.27, -0.69 e Å ⁻³

S3.12 Crystal data and structure refinement for Rh₁₂L²₆L^{5'}₆

Identification code	2095293
Formula	C ₂₂₈ H ₂₆₄ N ₁₂ O ₆₆ Rh ₁₂
Formula weight (g.mol ⁻¹)	5463.42
Temperature (K)	100
Wavelength (Å)	0.82653
Crystal system	Trigonal
Space group	R-3
Unit cell dimensions	a = 26.590; b = 26.590; c = 43.610 α = 90°; β = 90°; γ = 120°
Volume (Å ³)	26702.6
Z	3
Density calculated (g/cm ⁻³)	1.019
Absorption coefficient (mm ⁻¹)	0.894
F(000)	8352.0
Crystal size (mm)	0.34 × 0.18 × 0.04
2Theta range for data collection (°)	2.992 to 49.866
Index ranges	0 ≤ h ≤ 22, 0 ≤ k ≤ 23, -44 ≤ l ≤ 44
Reflections collected	64408
Independent reflections	6603 [R _{int} = 0.0718, R _{sigma} = 0.0802]
Refinement method	Full-matrix least-squares on F ²
Data / restraints / parameters	6603/194/412
Goodness-of-fit on F ²	1.060
Final R indices [I > 2σ(I)]	R ₁ = 0.0808, wR ₂ = 0.2689
R indices (all data)	R ₁ = 0.1044, wR ₂ = 0.2975
Largest diff. peak and hole	0.60, -0.47 e Å ⁻³

S4. Characterization

S4.1 Characterization of the ligands

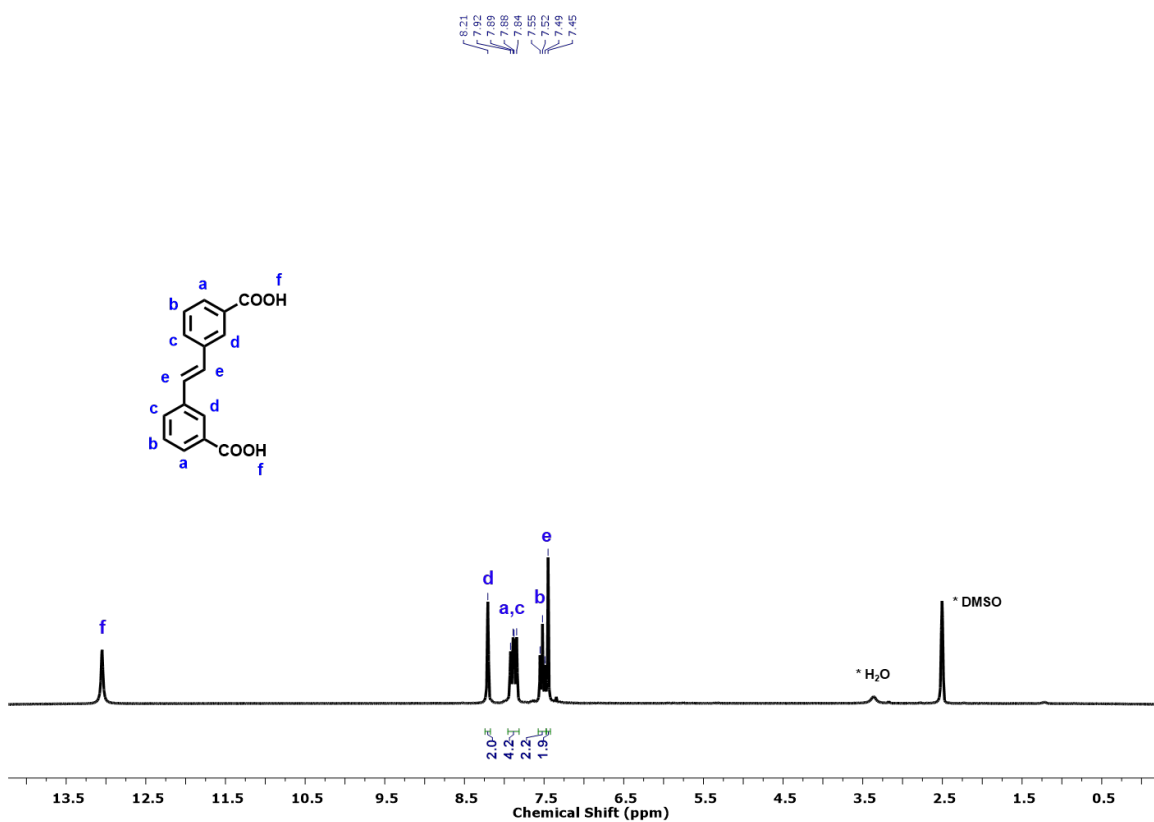


Figure S1. ¹H NMR spectrum (250 MHz, DMSO-d₆) of (E)-3,3'-(ethene-1,2-diyl)dibenzoic acid.

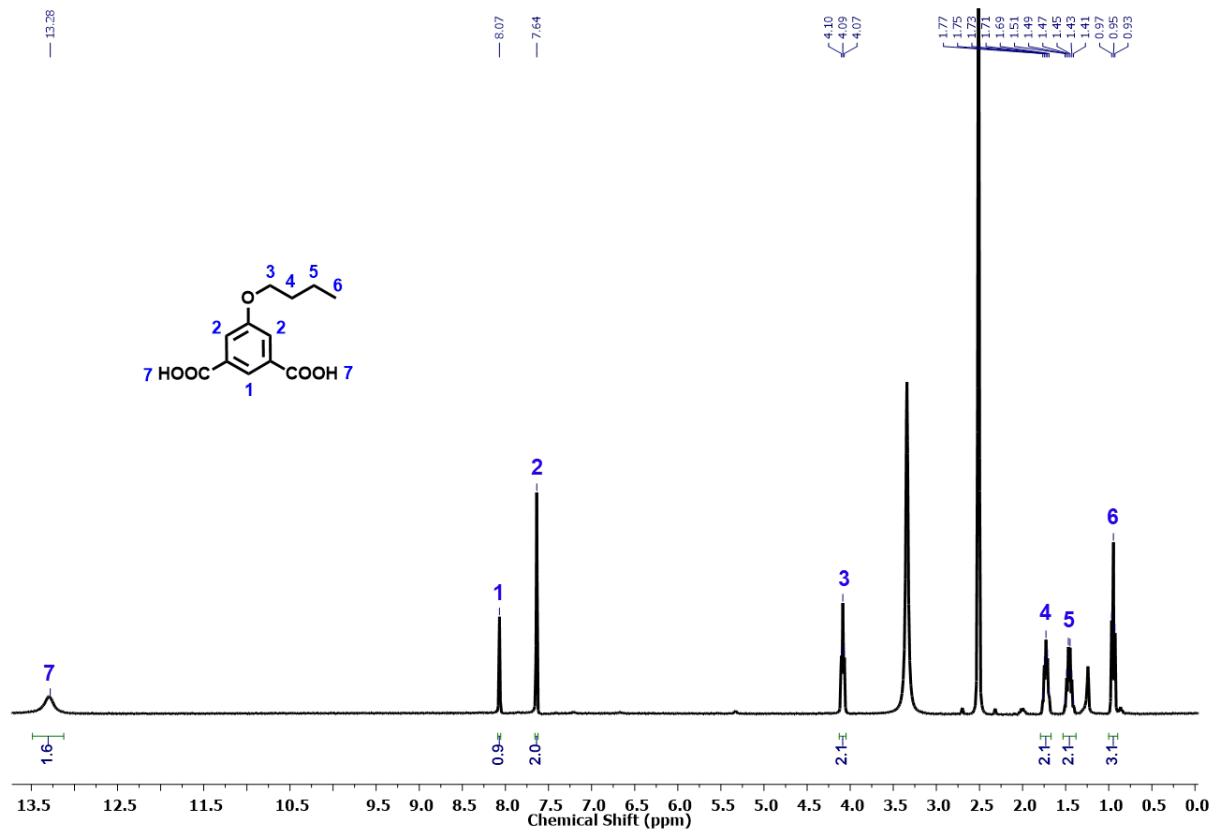


Figure S2. ^1H NMR spectrum (400 MHz, DMSO-d_6) of 5-butoxyisophthalic acid.

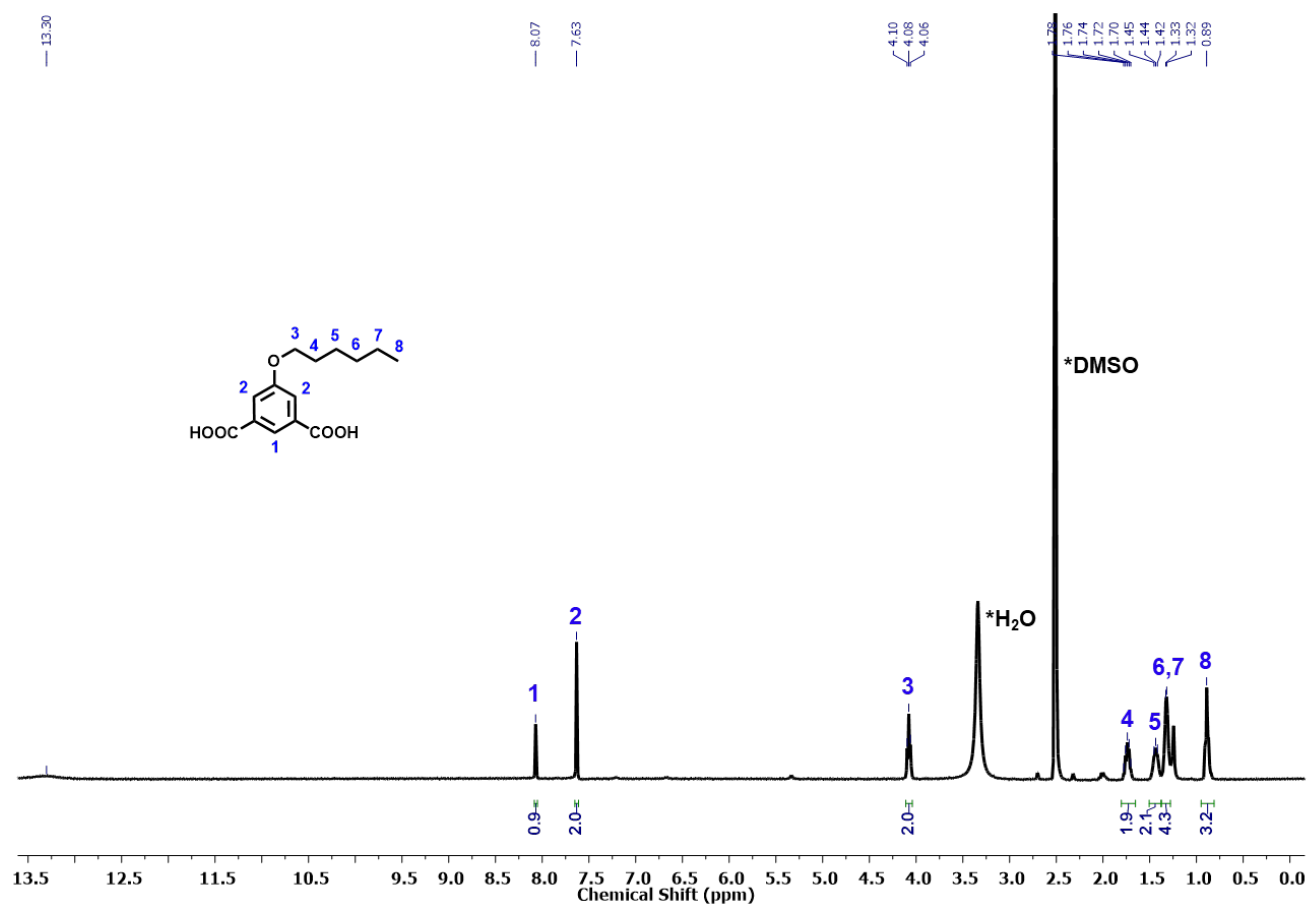


Figure S3. ¹H NMR spectrum (400 MHz, DMSO-d₆) of 5-(hexyloxy)isophthalic acid.

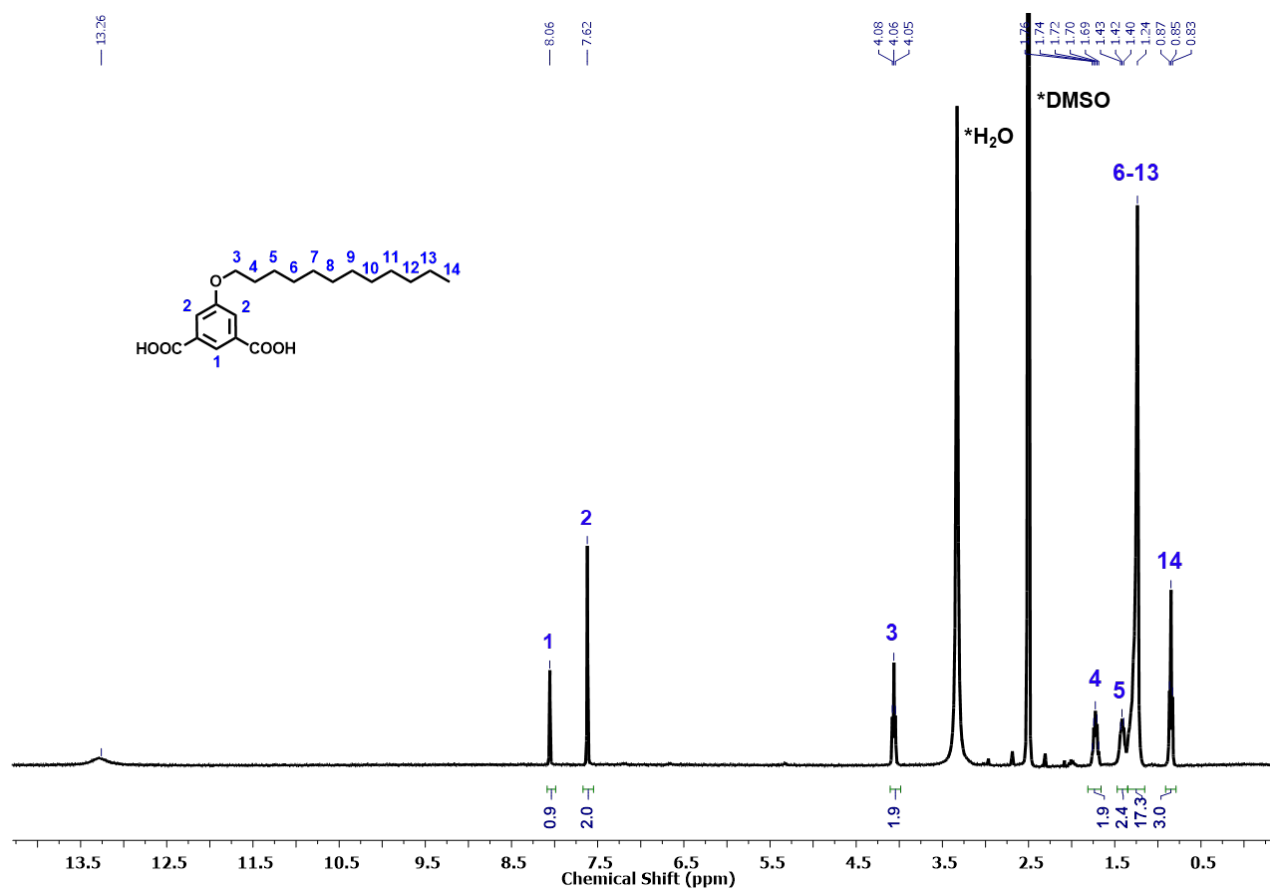


Figure S4. ¹H NMR spectrum (400 MHz, DMSO-d₆) of 5-(dodecyloxy)isophthalic acid.

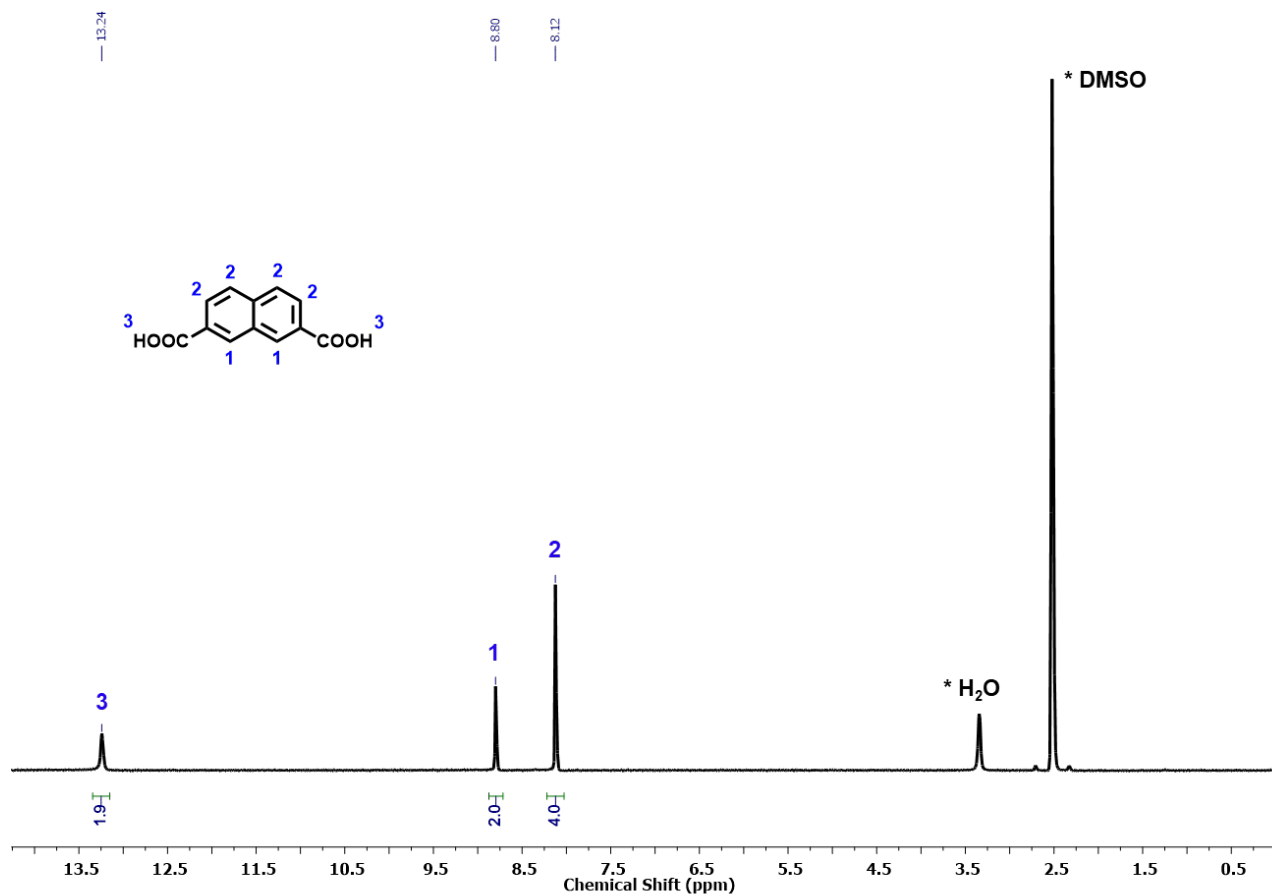


Figure S5. ¹H NMR spectrum (400 MHz, DMSO-d₆) of naphthalene-2,7-dicarboxylic acid.

S4.2 Characterization of $\text{Rh}_{12}\text{L}_6\text{L}'_6$

S4.2.1 $^1\text{H-NMR}$ of digested $\text{Rh}_{12}\text{L}_6\text{L}'_6$

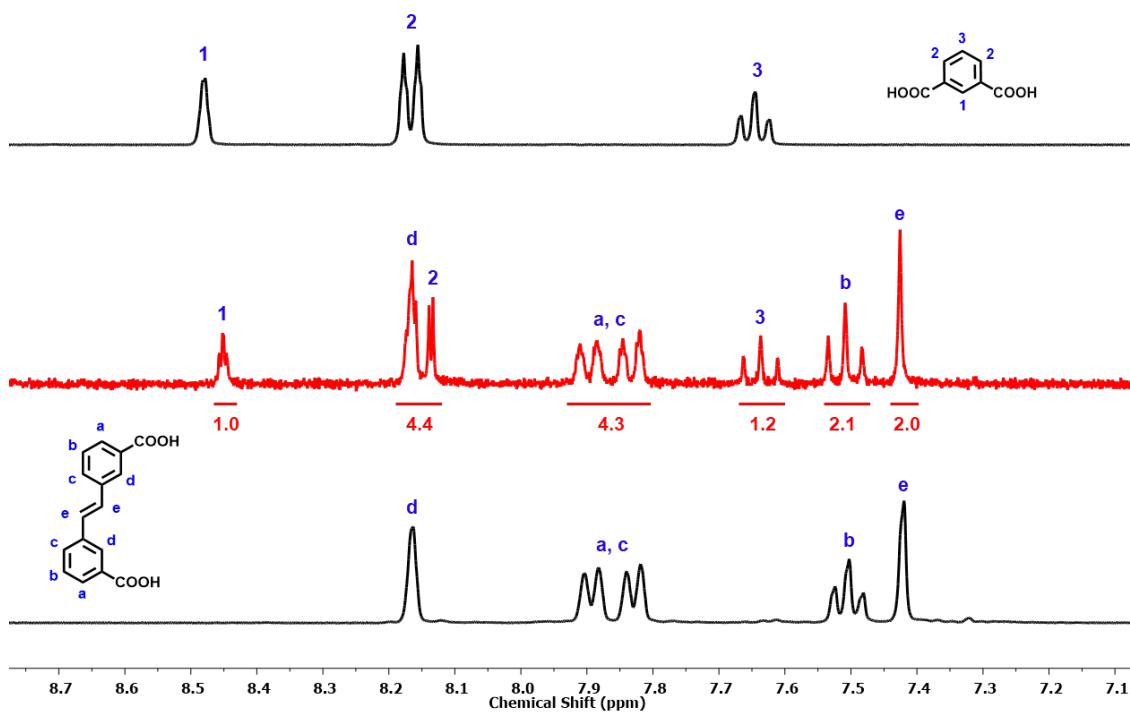


Figure S6. $^1\text{H-NMR}$ spectra (400 MHz, DMSO-d_6) of digested $\text{Rh}_{12}\text{L}^1\text{L}'_6$ (middle), the L' ligand (top) and L^1 (bottom) The integrals of the assigned protons revealed that the molar ratio between the two linkers in the digested MOP is 1:1 as expected from the structure of the MOP.

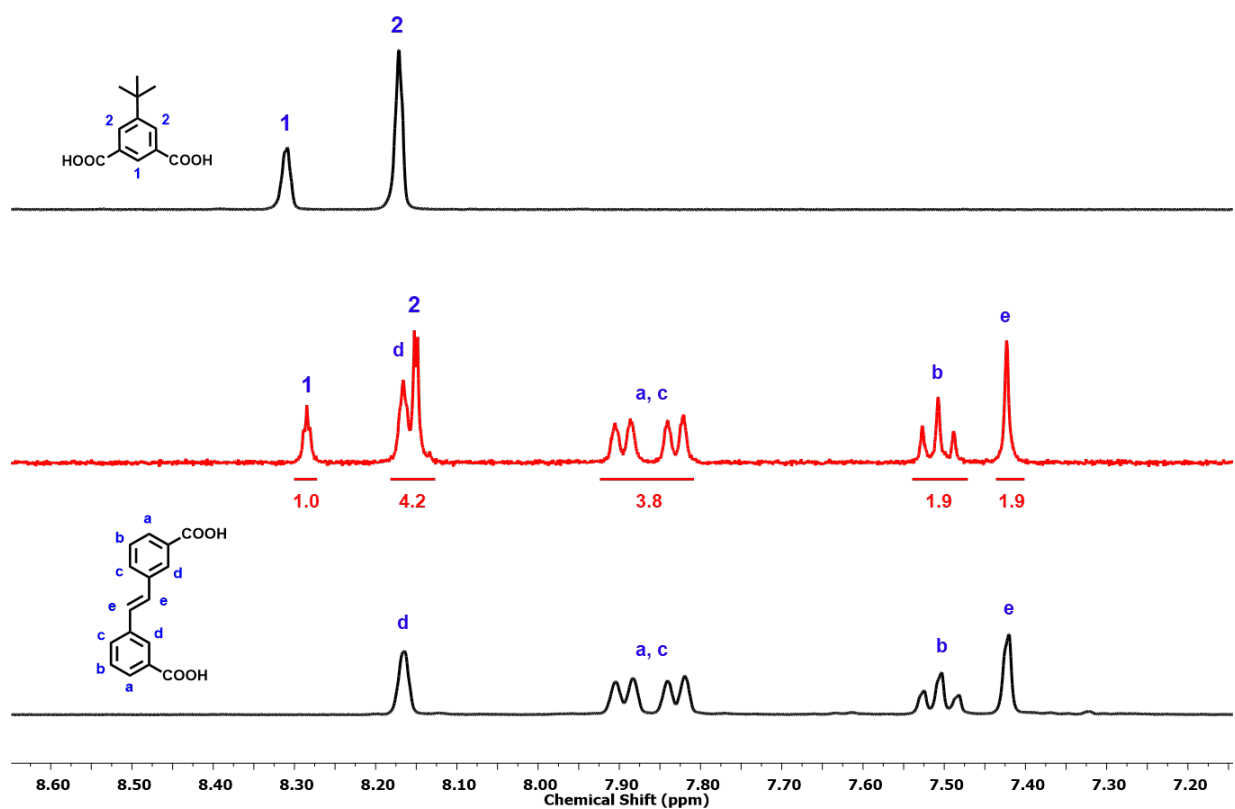


Figure S7. ¹H-NMR spectra (400 MHz, DMSO-d₆) of digested Rh₁₂L¹L^{2'}₆ (middle), the L^{2'} ligand (top) and L¹ (bottom) The integrals of the assigned protons revealed that the molar ratio between the two linkers in the digested MOP is 1:1 as expected from the structure of the MOP

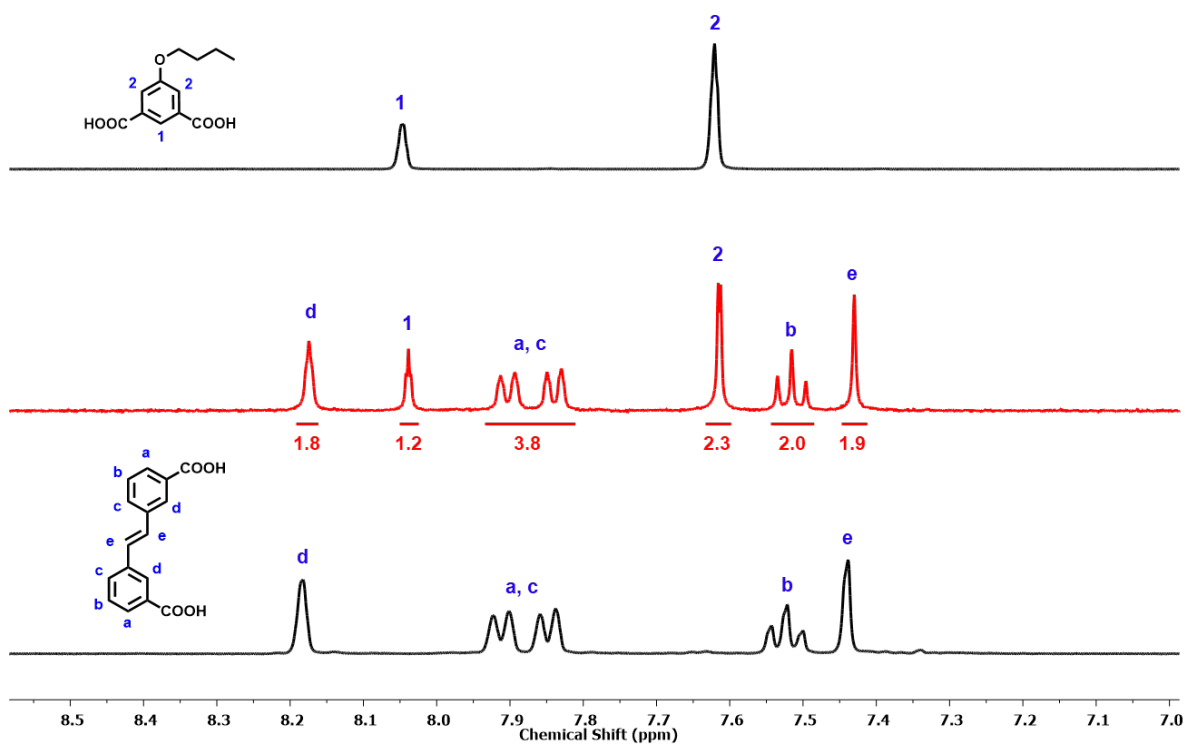


Figure S8. ¹H-NMR spectra (400 MHz, DMSO-d₆) of digested Rh₁₂L¹L^{3'}₆ (middle), the L^{3'} ligand (top) and L¹ (bottom). The integrals of the assigned protons revealed that the molar ratio between the two linkers in the digested MOP is 1:1 as expected from the structure of the MOP.

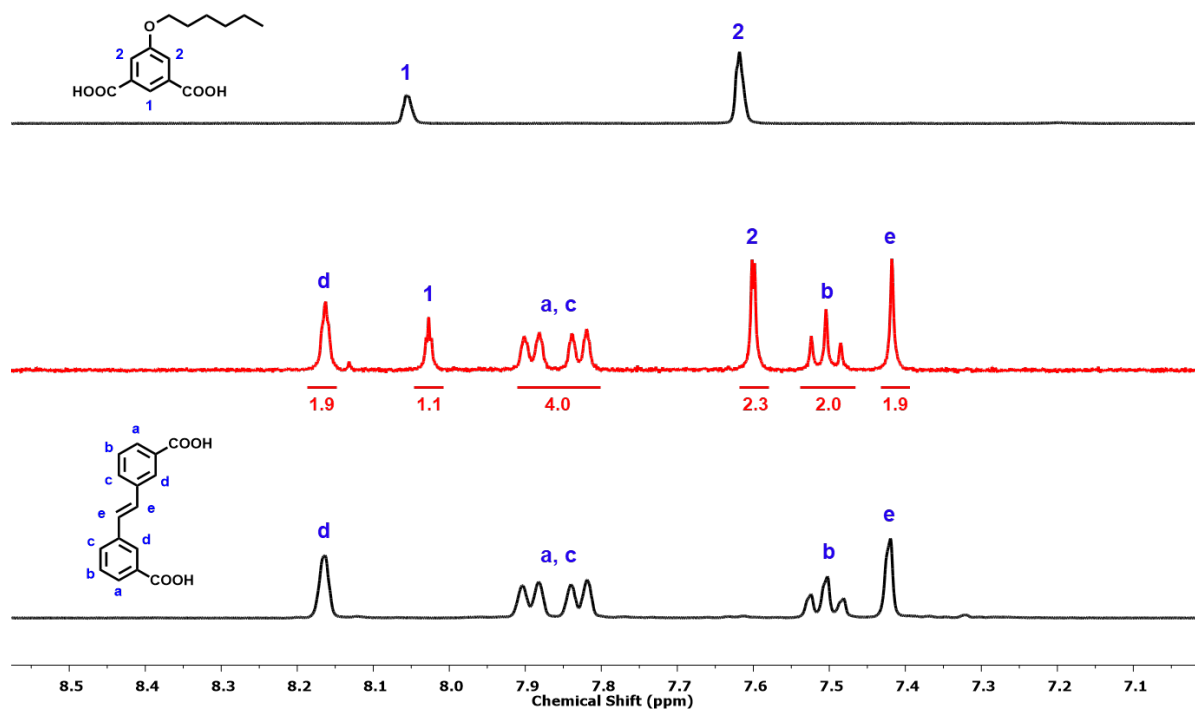


Figure S9. $^1\text{H-NMR}$ spectra (400 MHz, DMSO-d_6) of digested $\text{Rh}_{12}\text{L}^1\text{L}^{4'}_6$ (middle), the $\text{L}^{4'}$ ligand (top) and L^1 (bottom) The integrals of the assigned protons revealed that the molar ratio between the two linkers in the digested MOP is 1:1 as expected from the structure of the MOP

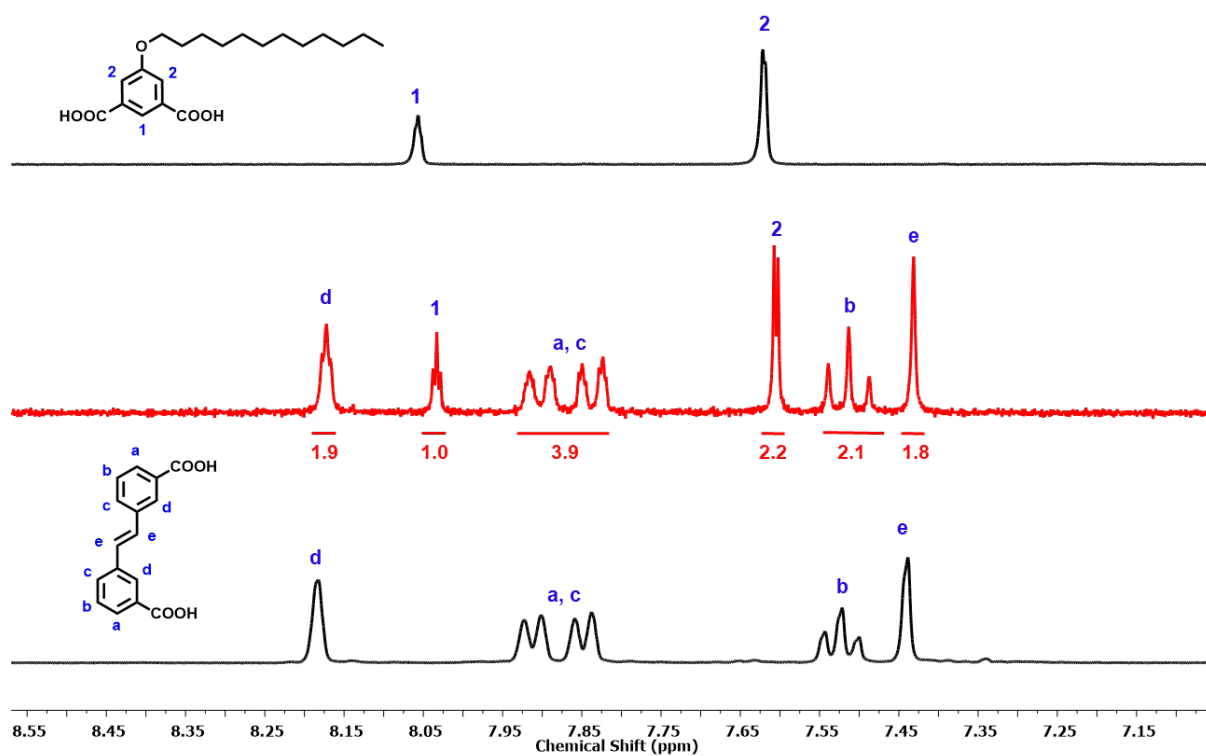


Figure S10. ¹H-NMR spectra (400 MHz, DMSO-d₆) of digested Rh₁₂L₁₆L₅₆ (middle), the L⁵ ligand (top) and L¹ (bottom) The integrals of the assigned protons revealed that the molar ratio between the two linkers in the digested MOP is 1:1 as expected from the structure of the MOP

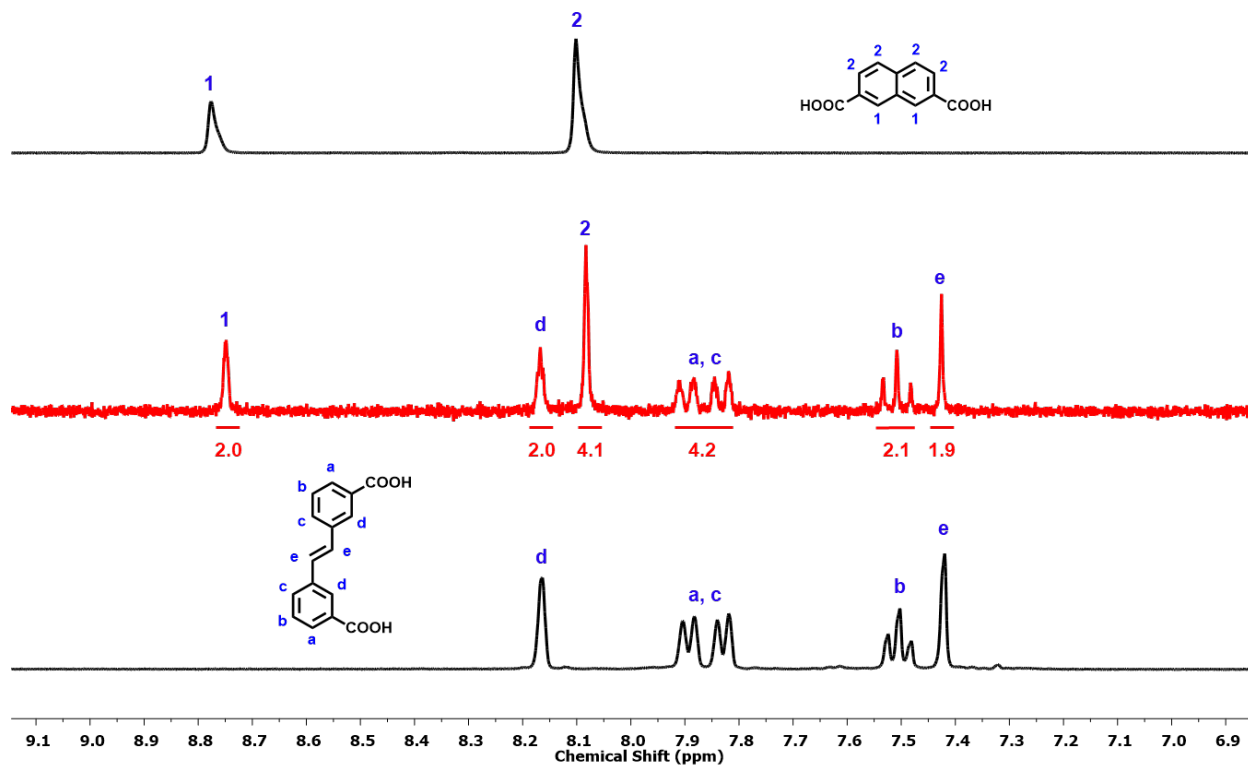


Figure S11. ¹H-NMR spectra (400 MHz, DMSO-d₆) of digested Rh₁₂L⁶L^{6'} (middle), the L^{6'} ligand (top) and L¹ (bottom) The integrals of the assigned protons revealed that the molar ratio between the two linkers in the digested MOP is 1:1 as expected from the structure of the MOP

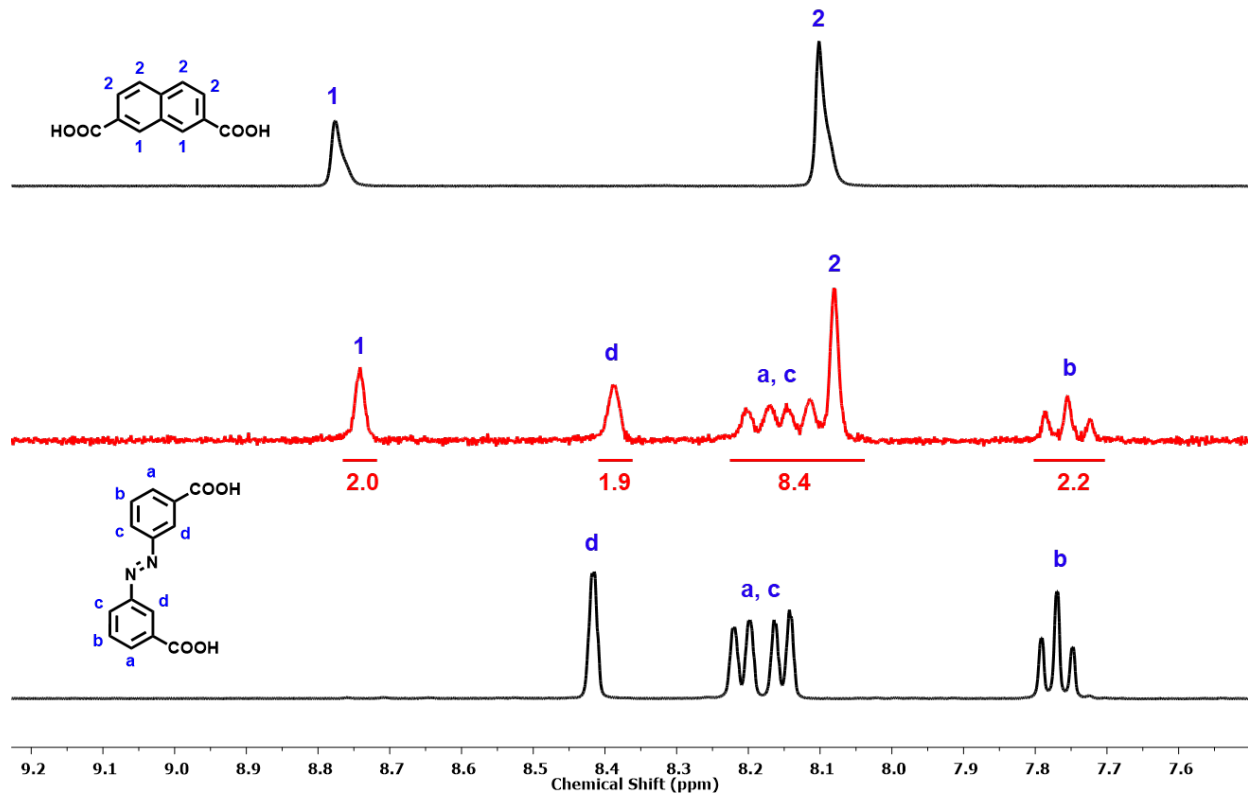


Figure S12. ¹H-NMR spectra (400 MHz, DMSO-d₆) of digested Rh₁₂L²₆L^{6'}₆ (middle), the L^{6'} ligand (top) and L² (bottom) The integrals of the assigned protons revealed that the molar ratio between the two linkers in the digested MOP is 1:1 as expected from the structure of the MOP

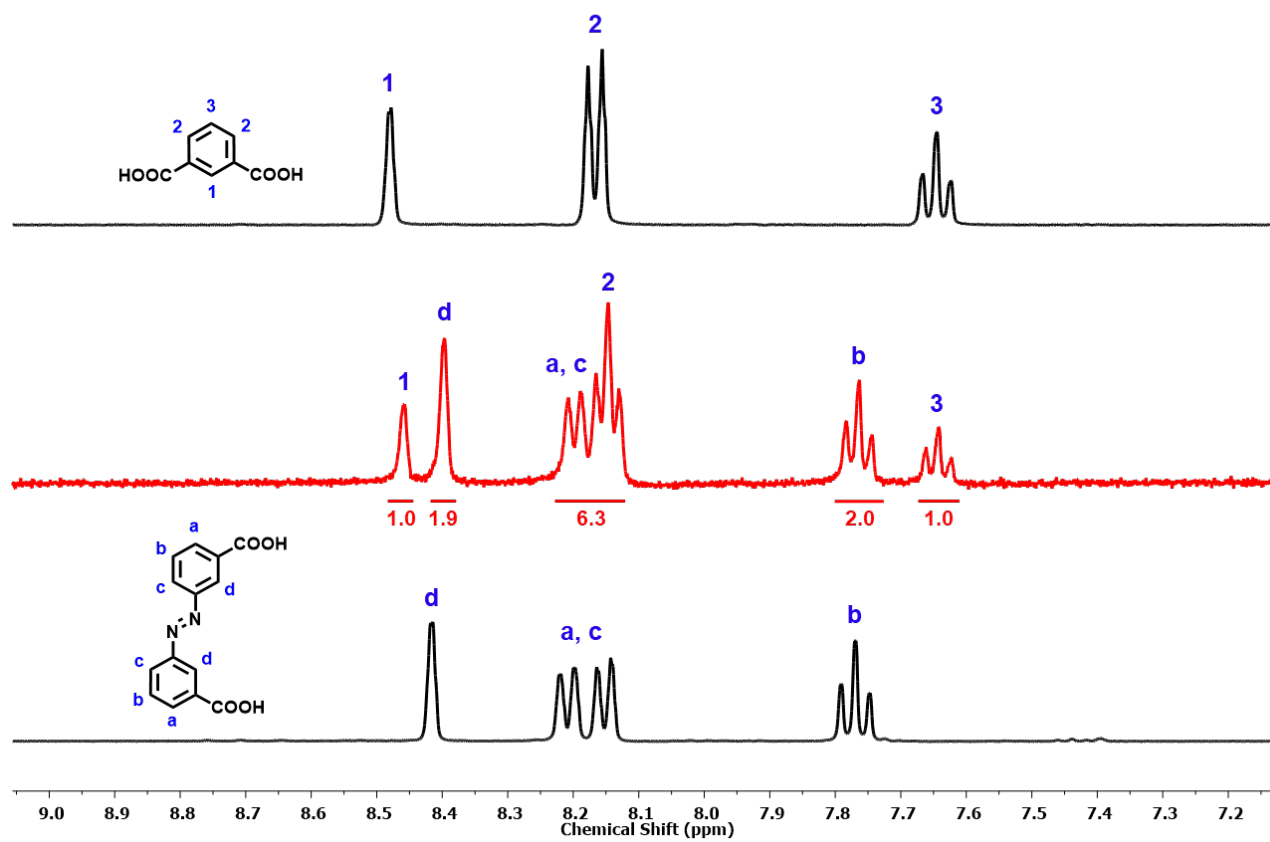


Figure S13. ¹H-NMR spectra (400 MHz, DMSO-d₆) of digested Rh₁₂L₂L'₆ (middle), the L^{3'} ligand (top) and L² (bottom) The integrals of the assigned protons revealed that the molar ratio between the two linkers in the digested MOP is 1:1 as expected from the structure of the MOP

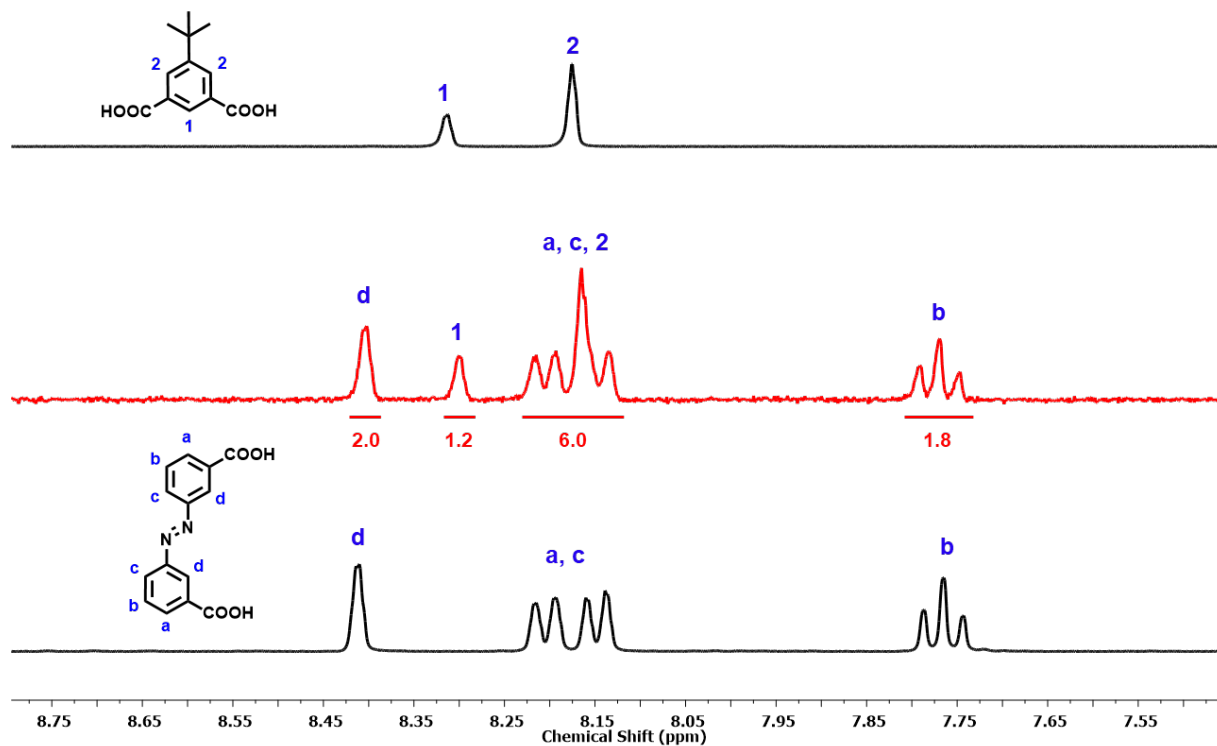


Figure S14. ¹H-NMR spectra (400 MHz, DMSO-d₆) of digested Rh₁₂L²₆L^{2'}₆ (middle), the L^{2'} ligand (top) and L² (bottom) The integrals of the assigned protons revealed that the molar ratio between the two linkers in the digested MOP is 1:1 as expected from the structure of the MOP

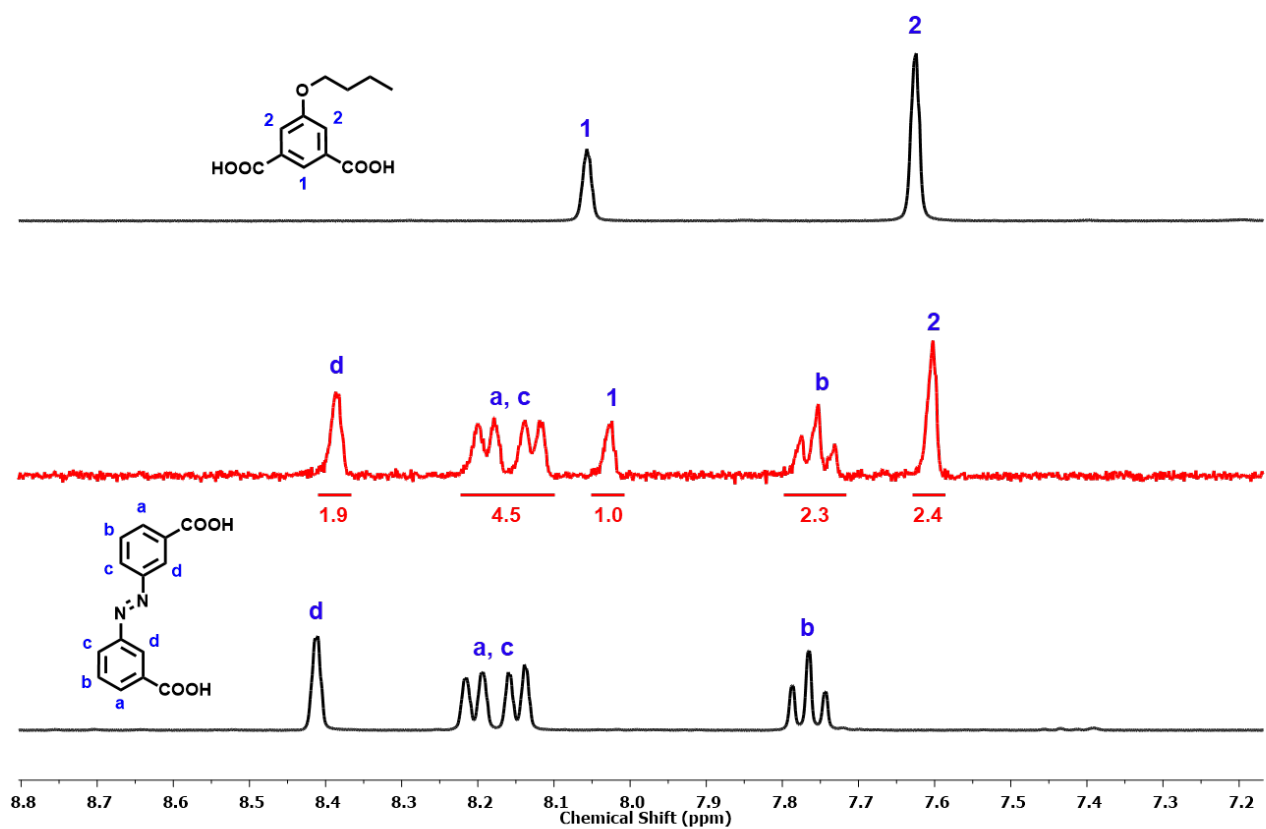


Figure S15. $^1\text{H-NMR}$ spectra (400 MHz, DMSO-d_6) of digested $\text{Rh}_{12}\text{L}^2_6\text{L}^3'_6$ (middle), the L^3 ligand (top) and L^2 (bottom) The integrals of the assigned protons revealed that the molar ratio between the two linkers in the digested MOP is 1:1 as expected from the structure of the MOP

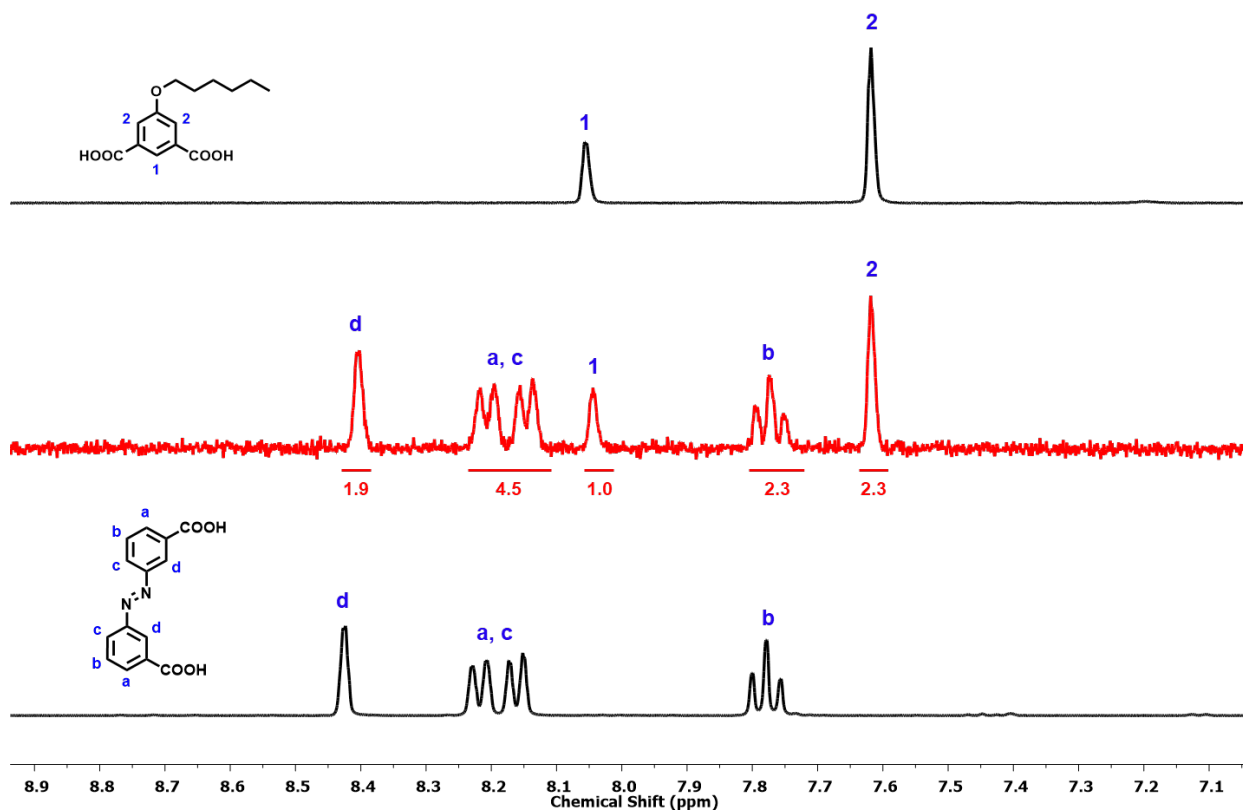


Figure S16. ¹H-NMR spectra (400 MHz, DMSO-d₆) of digested Rh₁₂L²L⁴₆ (middle), the L⁴ ligand (top) and L² (bottom). The integrals of the assigned protons revealed that the molar ratio between the two linkers in the digested MOP is 1:1 as expected from the structure of the MOP.

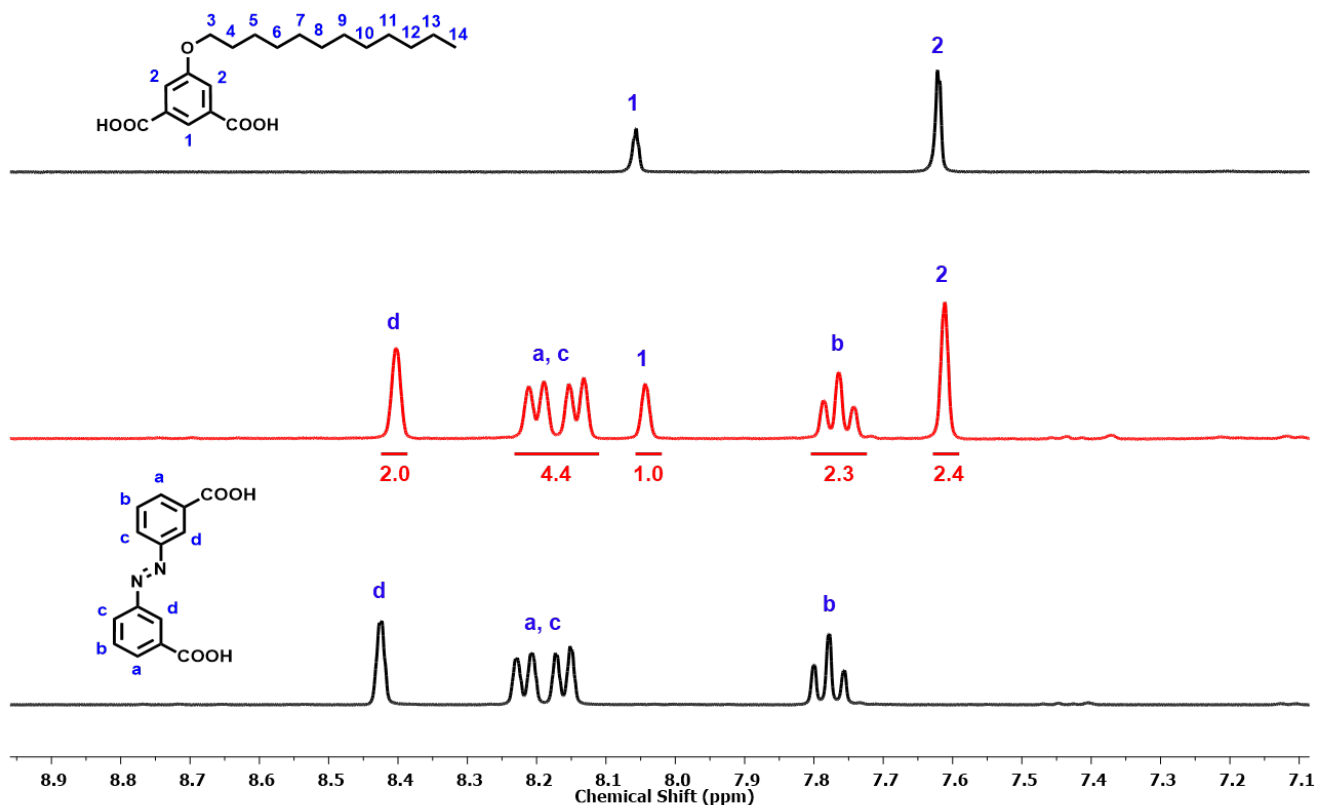


Figure S17. ¹H-NMR spectra (400 MHz, DMSO-d₆) of digested Rh₁₂L²₆L^{5'} (middle), the L^{5'} ligand (top) and L² (bottom) The integrals of the assigned protons revealed that the molar ratio between the two linkers in the digested MOP is 1:1 as expected from the structure of the MOP

S5.2.2 UV-Vis spectra

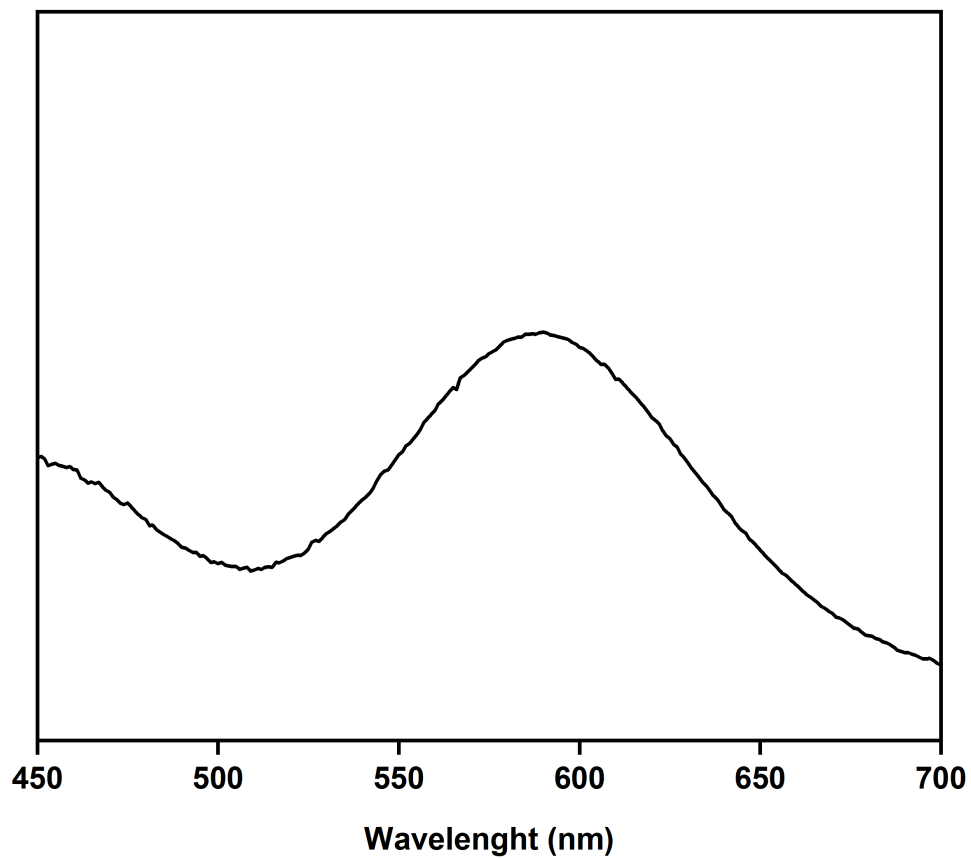


Figure S18. UV-Vis spectrum of a DMF solution of $\text{Rh}_{12}\text{L}^1\text{L}'_6$. The maximum of adsorption band I (λ_{max}) of $\text{Rh}_{12}\text{L}^1\text{L}'_6$ is centered at 590 nm.

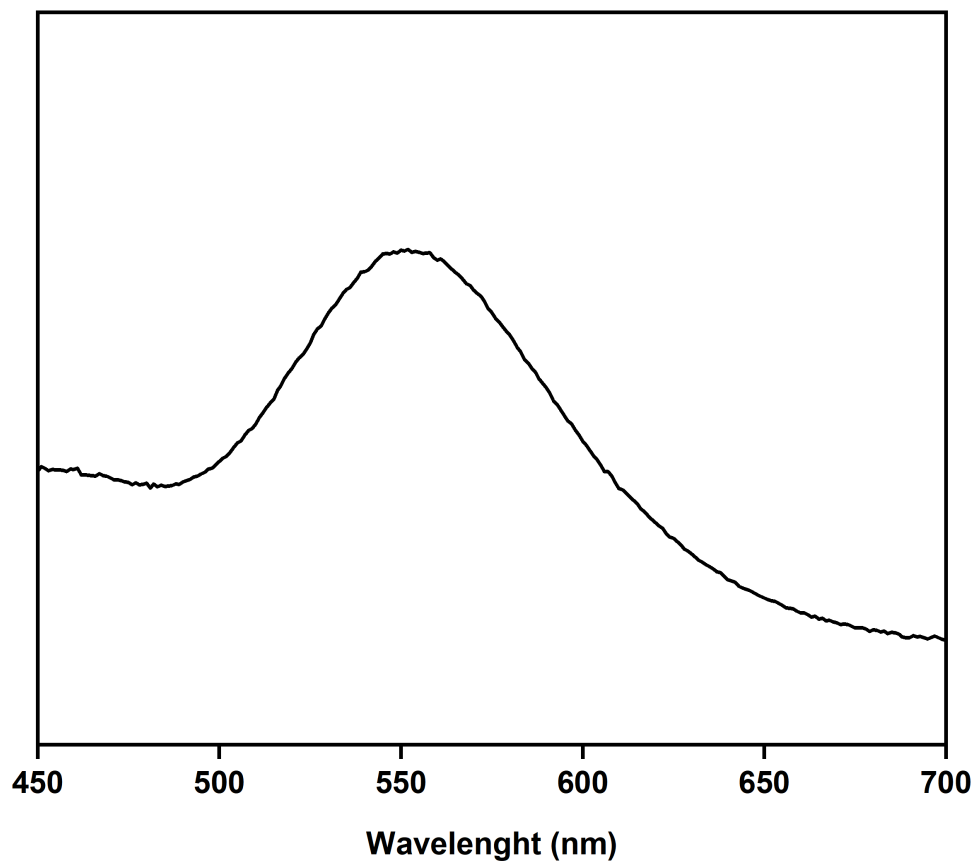


Figure S19. UV-Vis spectrum of a DMF solution of $\text{Rh}_{12}\text{L}^1_6\text{L}'_6$ coordinated to six equivalents of 4-hydroxypyridine. The maximum of adsorption band I (λ_{max}) of $\text{Rh}_{12}\text{L}^1_6\text{L}'_6$ is centered at 552 nm.

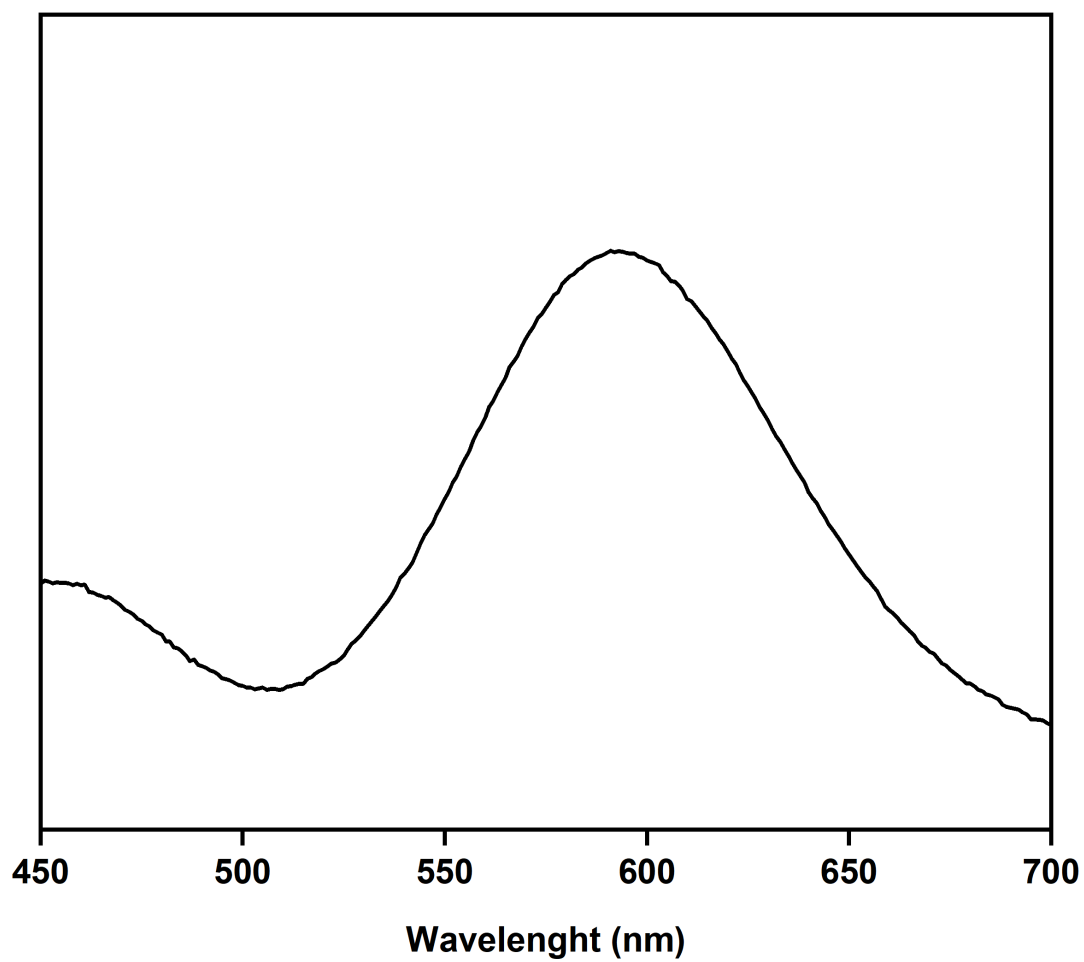


Figure S20. UV-Vis spectrum of a DMF solution of Rh₁₂L¹L^{2'}₆. The maximum of adsorption band I (λ_{max}) of Rh₁₂L¹L^{2'}₆ is centered at 593 nm.

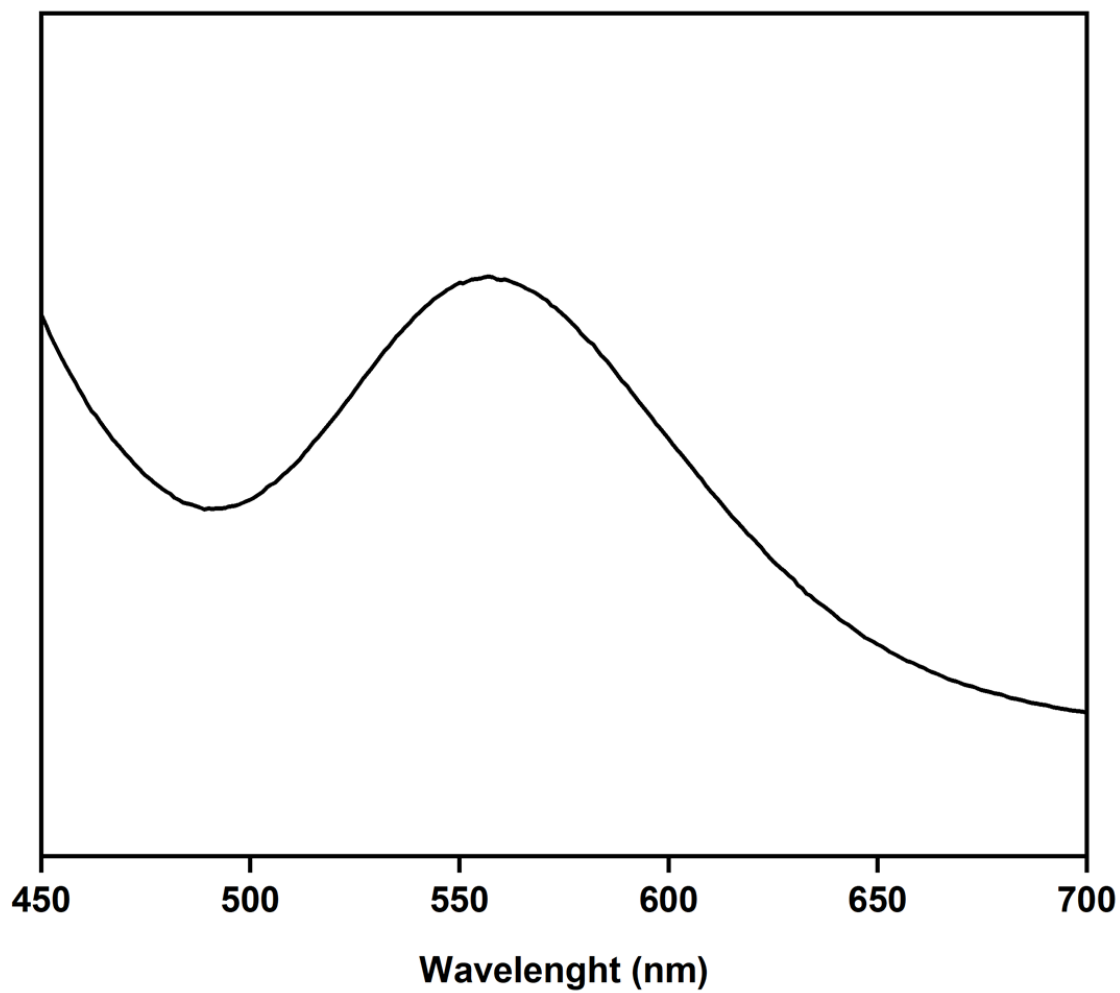


Figure S21. UV-Vis spectrum of a DMF solution of $\text{Rh}_{12}\text{L}^1_6\text{L}'_6$ coordinated to six equivalents of isonicotinic acid. The maximum of adsorption band I (λ_{max}) of $\text{Rh}_{12}\text{L}^1_6\text{L}'_6$ is centered at 557 nm.

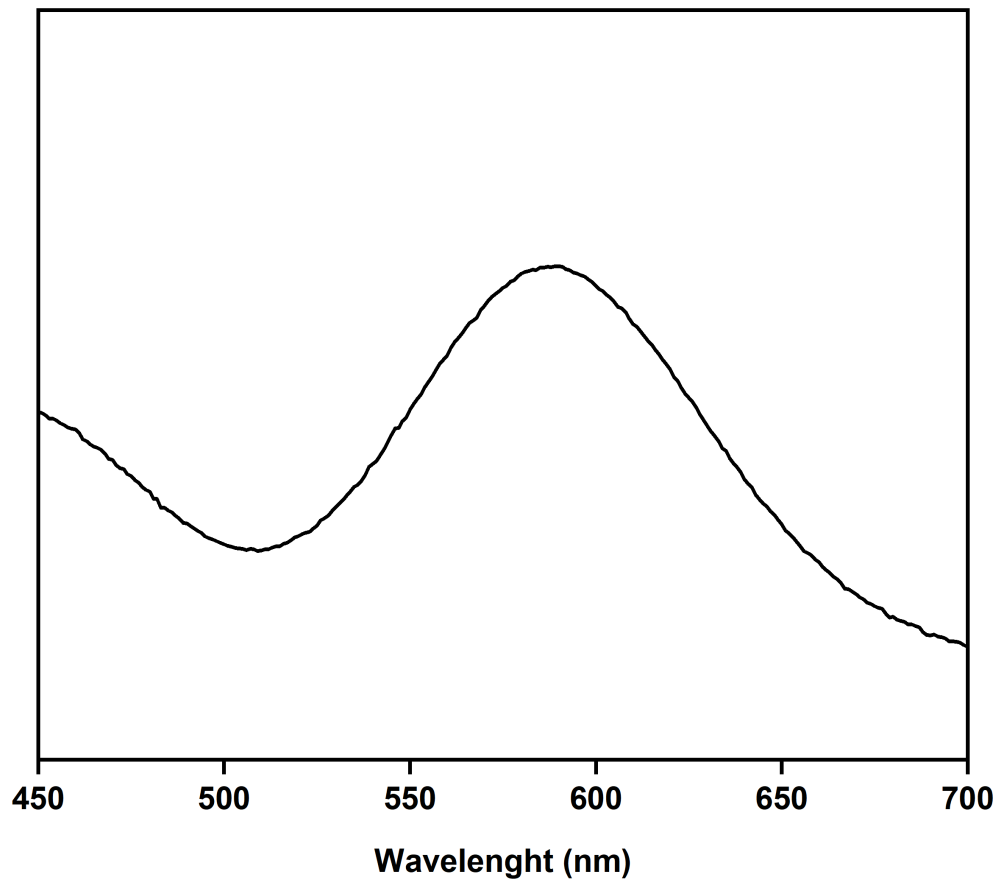


Figure S22. UV-Vis spectrum of a DMF solution of Rh₁₂L¹⁶L^{3'}₆. The maximum of adsorption band I (λ_{max}) of Rh₁₂L¹⁶L^{3'}₆ is centered at 589 nm.

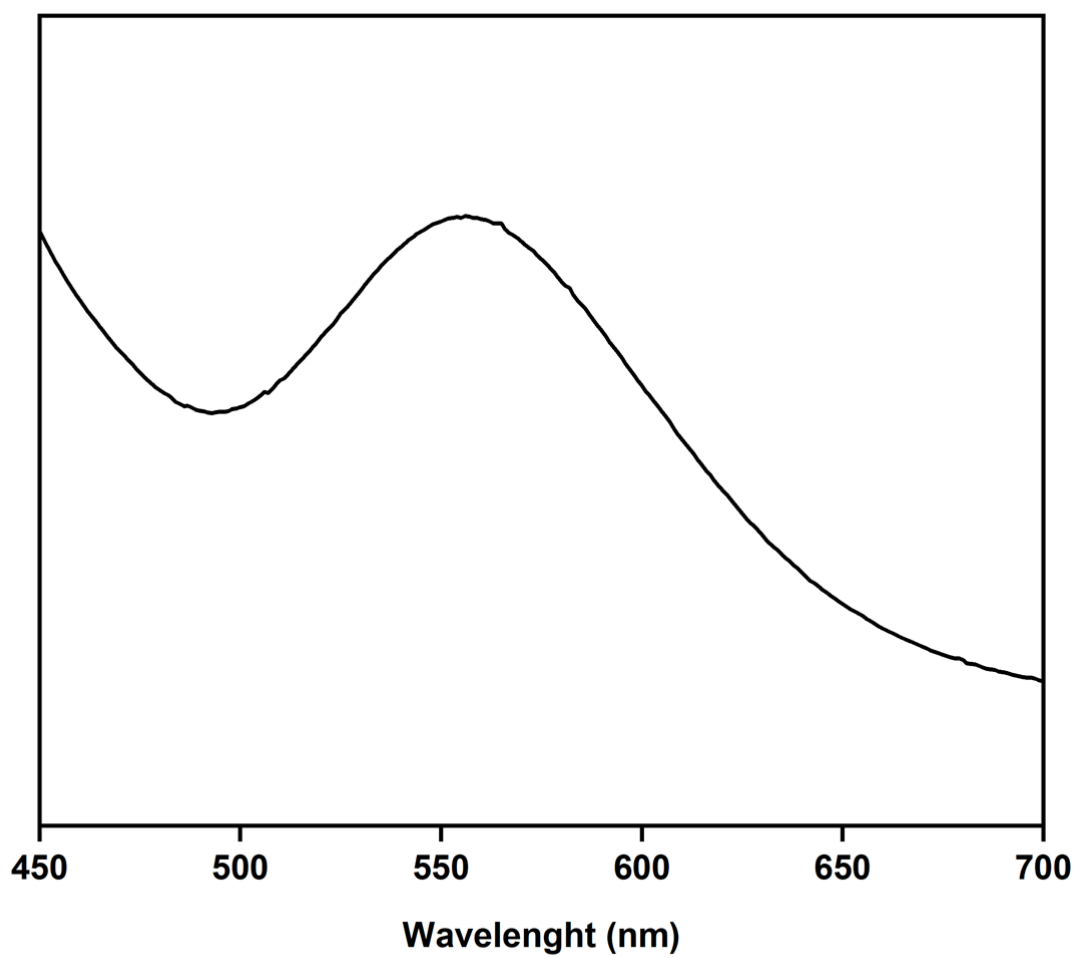


Figure S23. UV-Vis spectrum of a DMF solution of $\text{Rh}_{12}\text{L}^1\text{L}^{3'6}$ coordinated to six equivalents of isonicotinic acid. The maximum of adsorption band I (λ_{max}) of $\text{Rh}_{12}\text{L}^1\text{L}^{3'6}$ is centered at 556 nm.

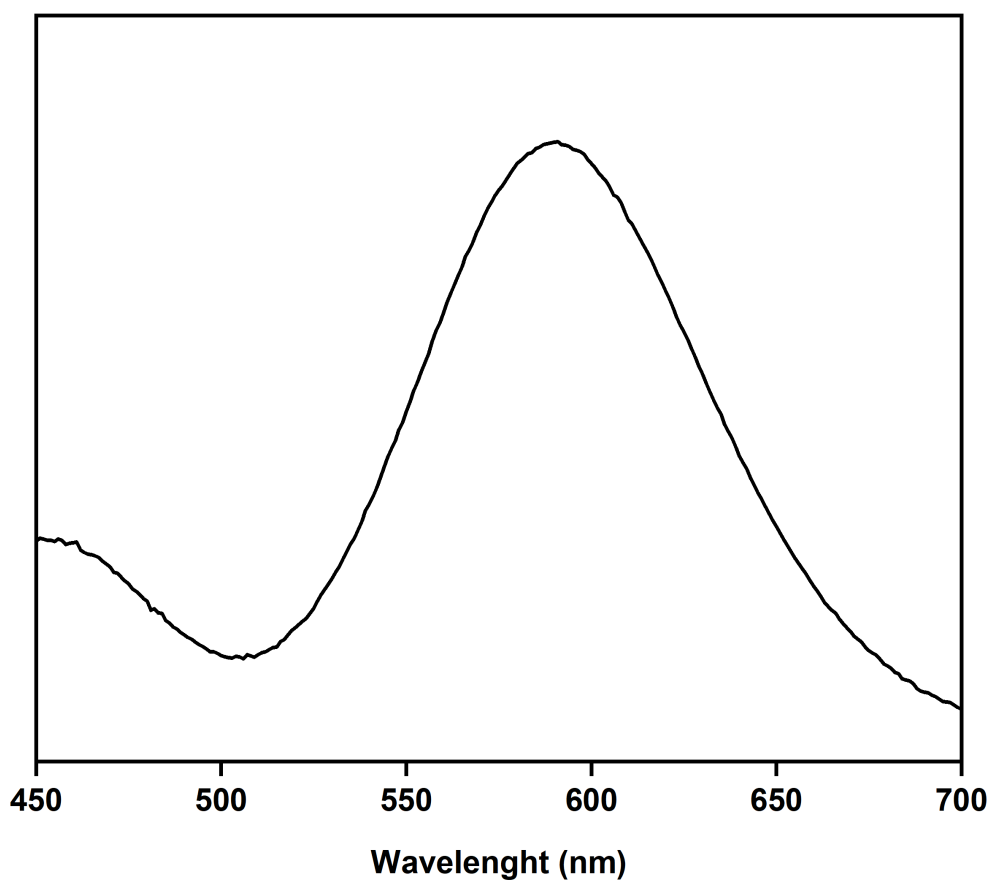


Figure S24: UV-vis spectrum of a DMF solution of Rh₁₂L₁₆L'₆. The maximum of adsorption band I (λ_{max}) of Rh₁₂L₁₆L'₆ is centered at 591 nm.

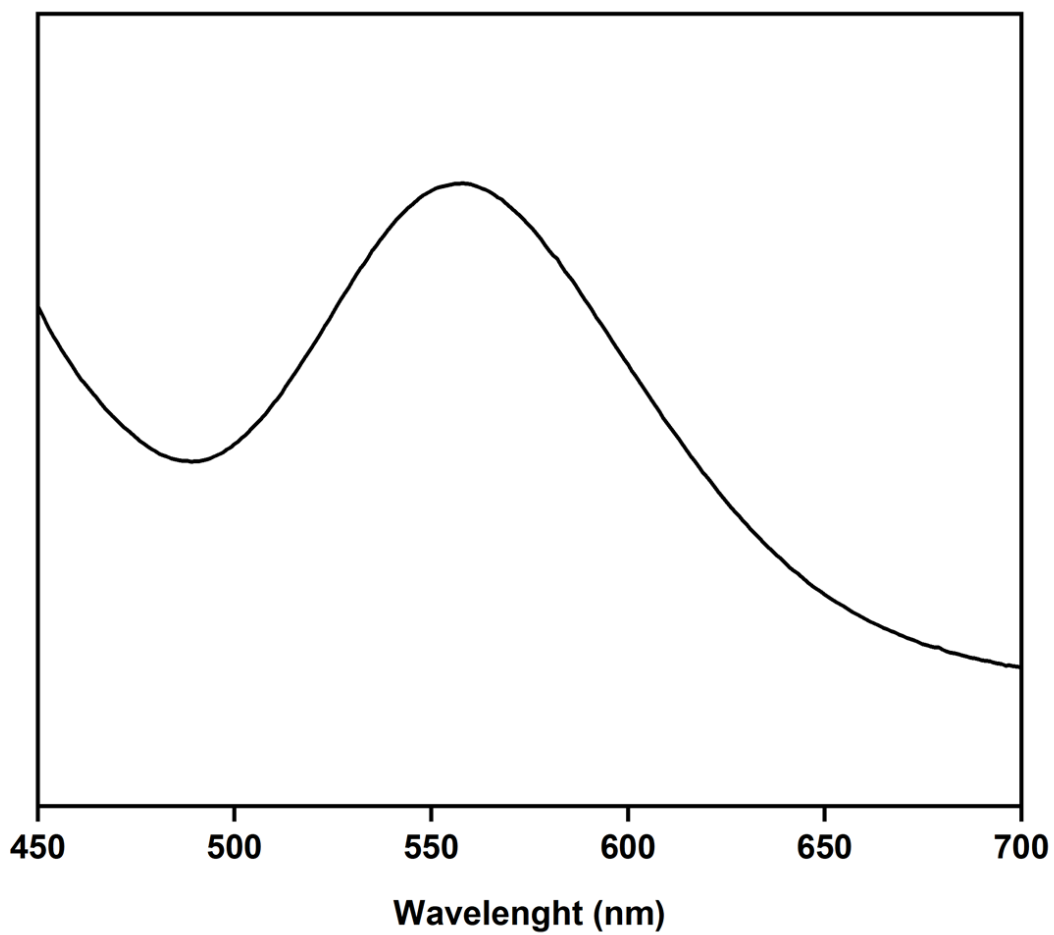


Figure S25. UV-Vis spectrum of a DMF solution of $\text{Rh}_{12}\text{L}^1_6\text{L}'_6$ coordinated to six equivalents of isonicotinic acid. The maximum of adsorption band I (λ_{max}) of $\text{Rh}_{12}\text{L}^1_6\text{L}'_6$ is centered at 558 nm.

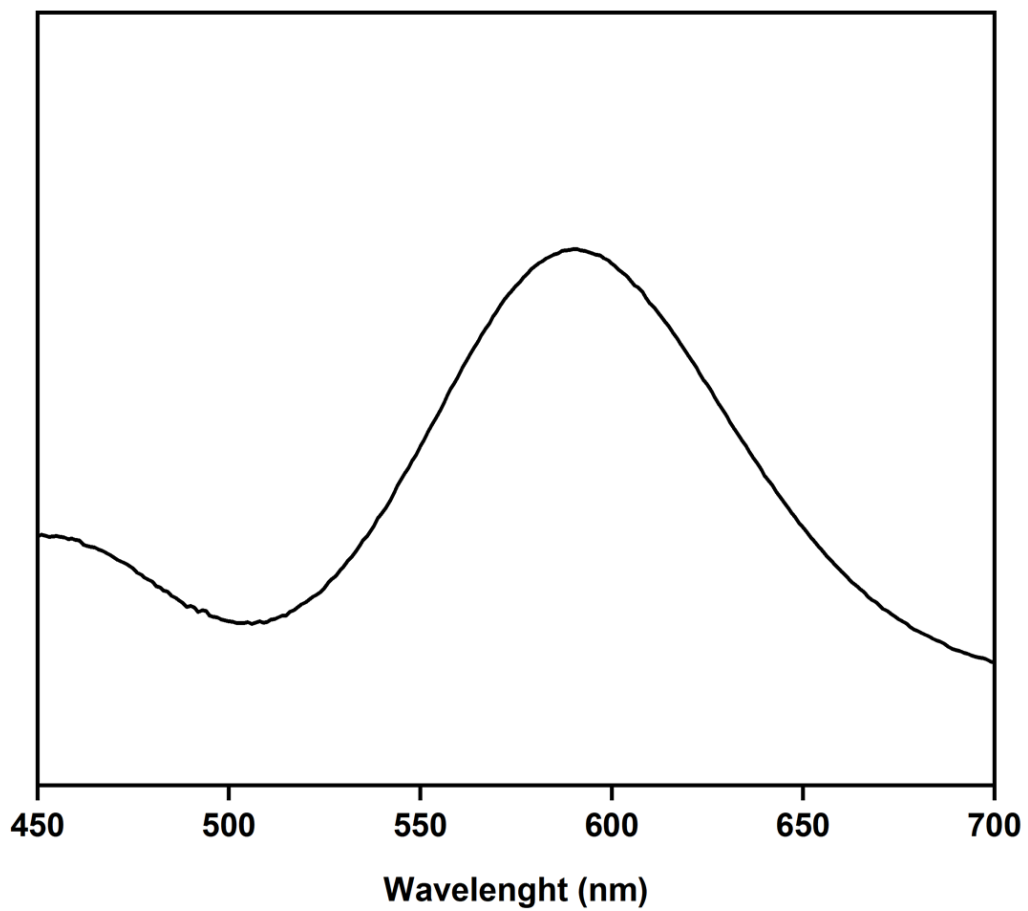


Figure S26. UV-Vis spectrum of a DMF solution of $\text{Rh}_{12}\text{L}^1\text{L}^5\text{L}^6$. The maximum of adsorption band I (λ_{max}) of $\text{Rh}_{12}\text{L}^1\text{L}^5\text{L}^6$ is centered at 591 nm.

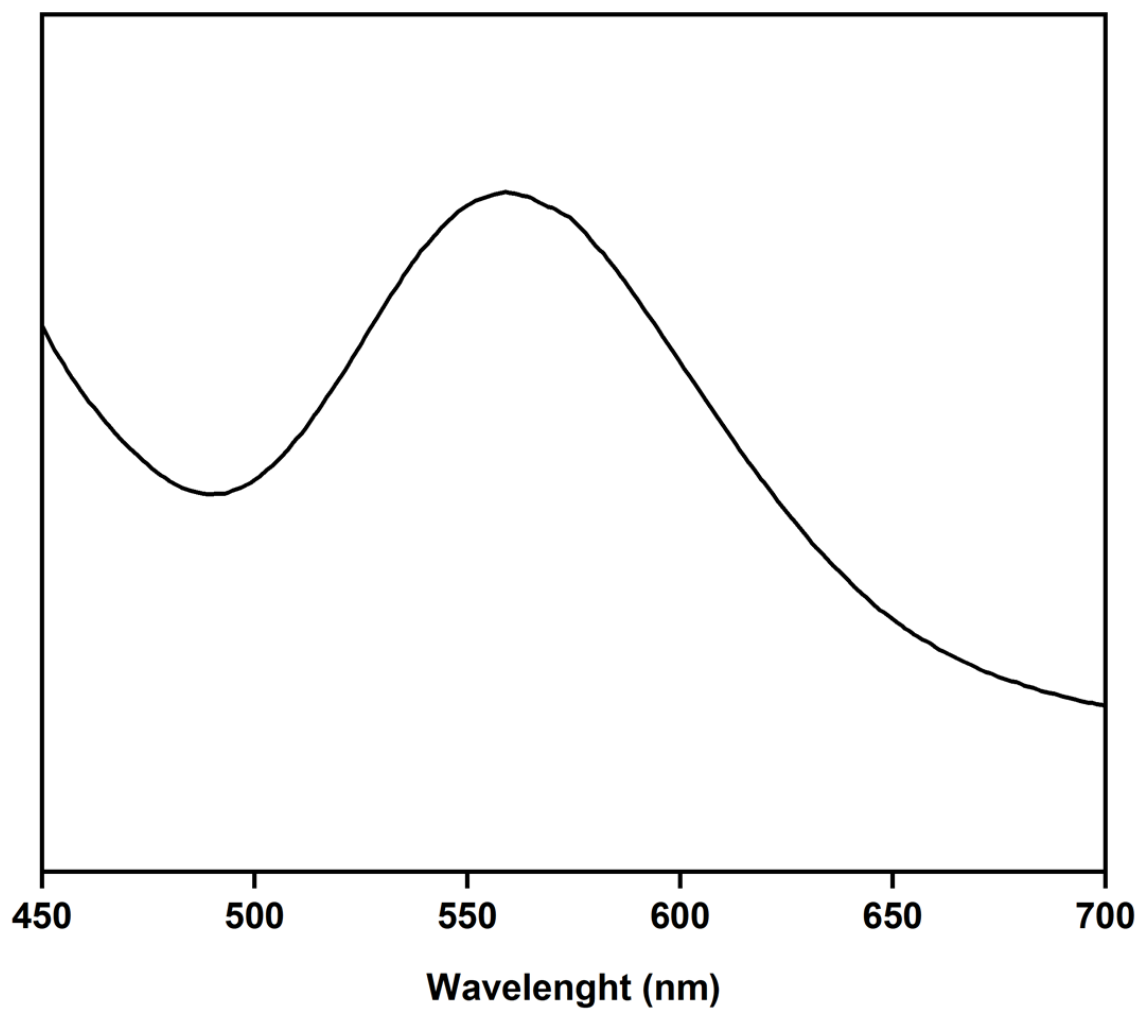


Figure S27. UV-Vis spectrum of a DMF solution of $\text{Rh}_{12}\text{L}^1\text{L}^{5'}_6$ coordinated to equivalents of isonicotinic acid. The maximum of adsorption band I (λ_{max}) of $\text{Rh}_{12}\text{L}^1\text{L}^{5'}_6$ is centered at 559 nm.

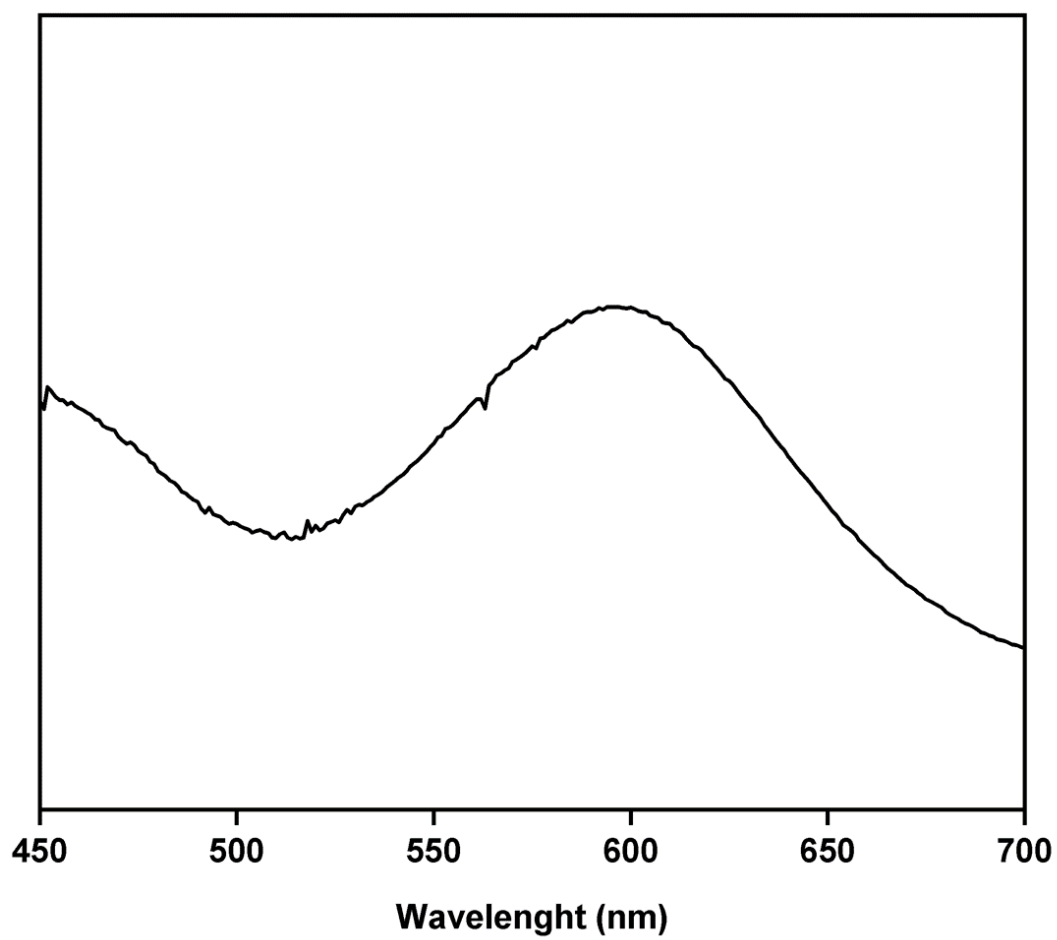


Figure S28. UV-Vis spectrum of a DMA solution of $\text{Rh}_{12}\text{L}^1_6\text{L}^6_6$. The maximum of adsorption band I (λ_{max}) of $\text{Rh}_{12}\text{L}^1_6\text{L}^6_6$ is centered at 597 nm.

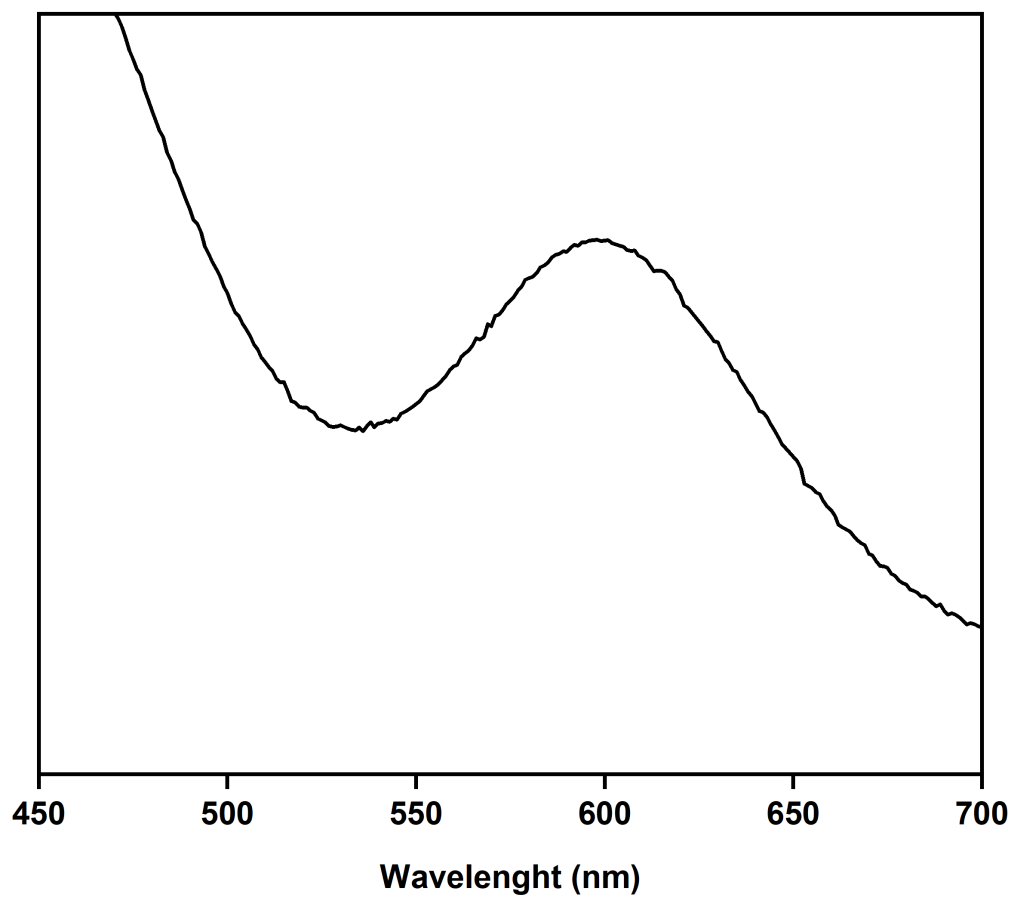


Figure S29. UV-Vis spectrum of a DMF solution of Rh₁₂L₂L₆. The maximum of adsorption band I (λ_{max}) of Rh₁₂L₂L₆ is centered at 599 nm.

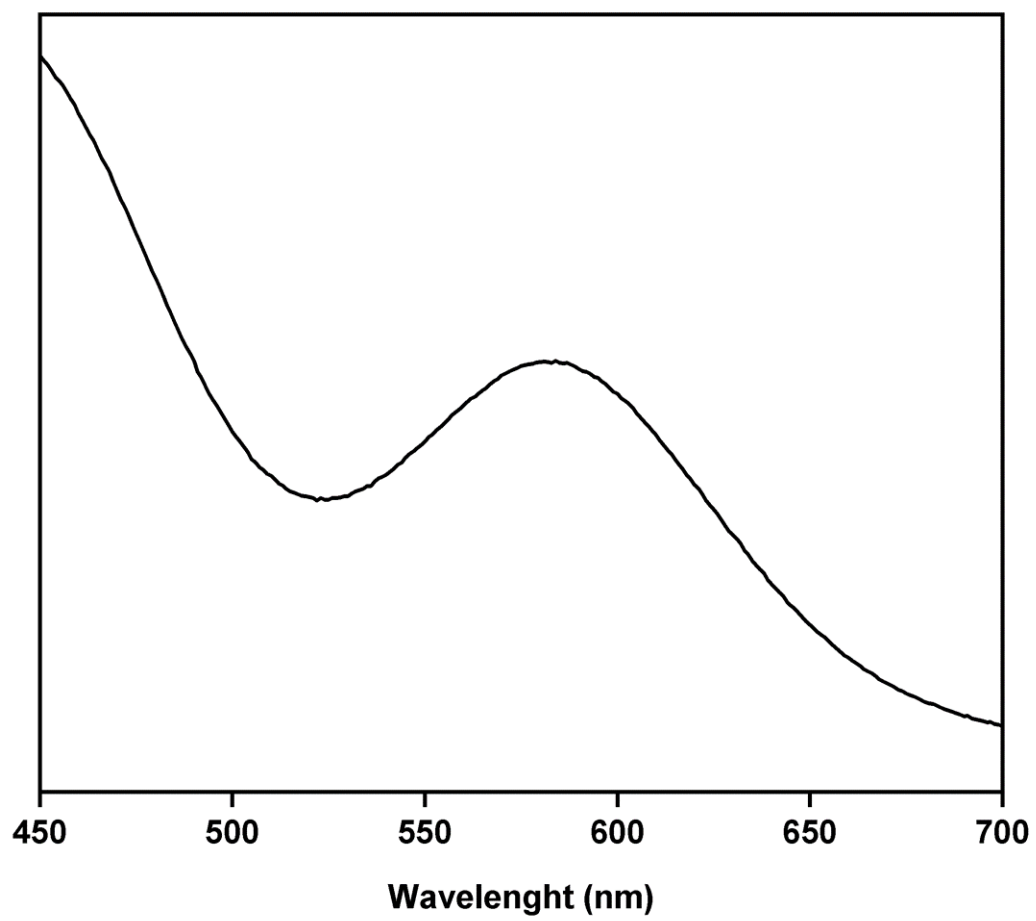


Figure S30. UV-Vis spectrum of a DMF solution of $\text{Rh}_{12}\text{L}^2_6\text{L}'_6$. The maximum of adsorption band I (λ_{max}) of $\text{Rh}_{12}\text{L}^2_6\text{L}'_6$ is centered at 583 nm.

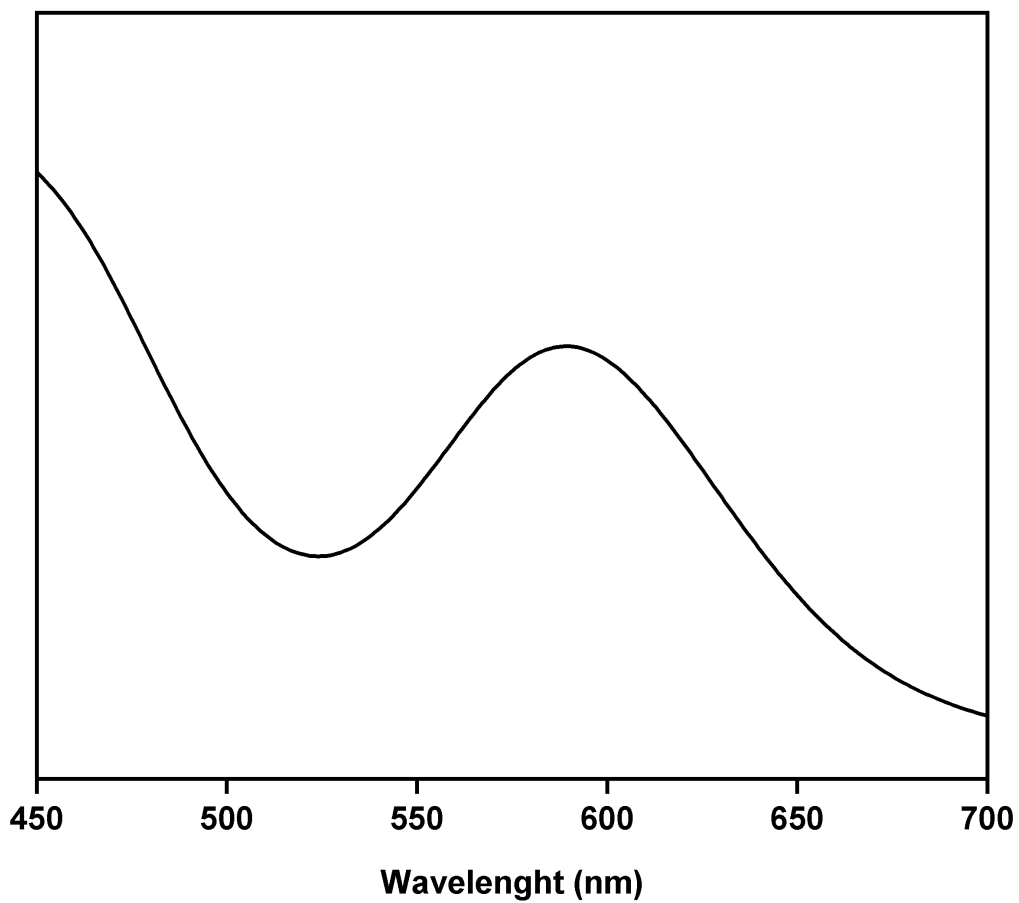


Figure S31. UV-vis spectrum of a DMF solution of $\text{Rh}_{12}\text{L}_2\text{L}'_6$. The maximum of adsorption band I (λ_{max}) of $\text{Rh}_{12}\text{L}_2\text{L}'_6$ is centered at 590 nm.

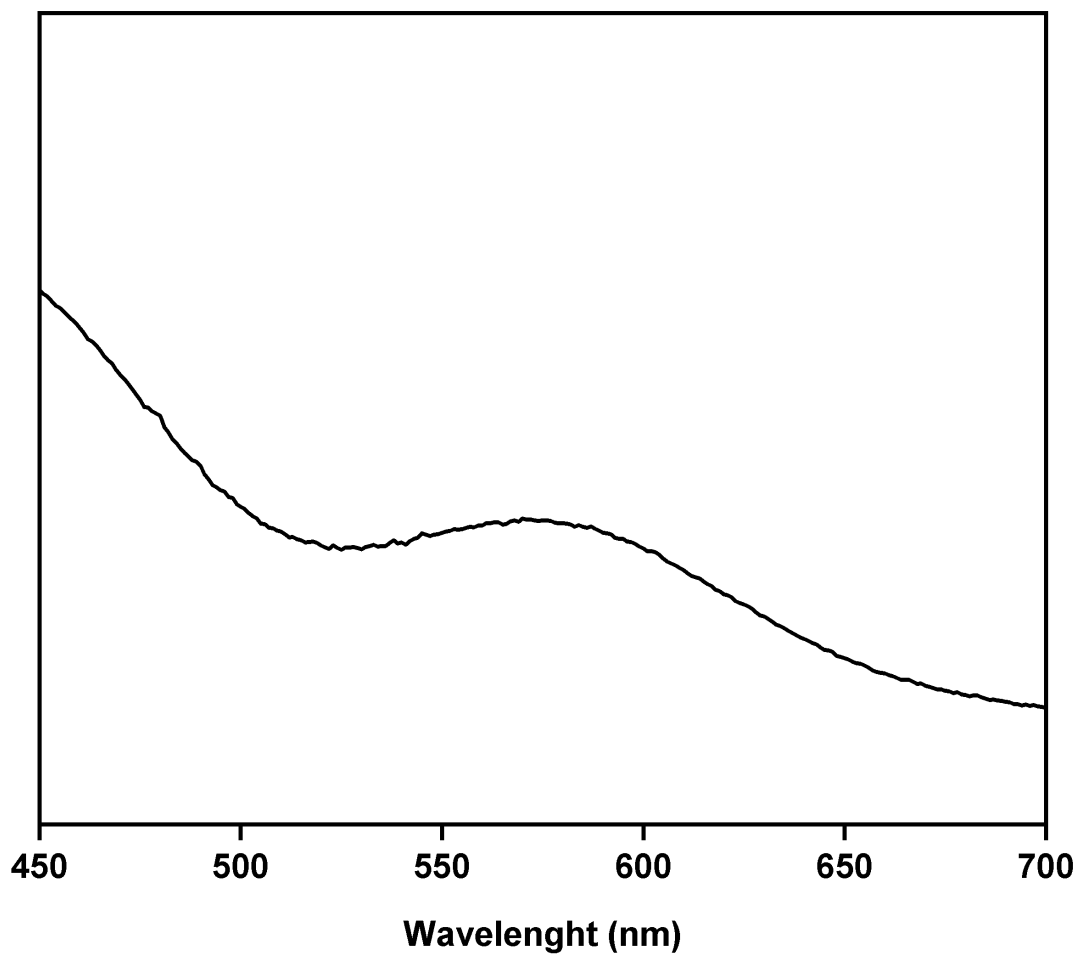


Figure S32: UV-vis spectrum of a DMF solution of Rh₁₂L²L'⁶. The maximum of adsorption band I (λ_{max}) of Rh₁₂L²L'⁶ is centered at 573 nm.

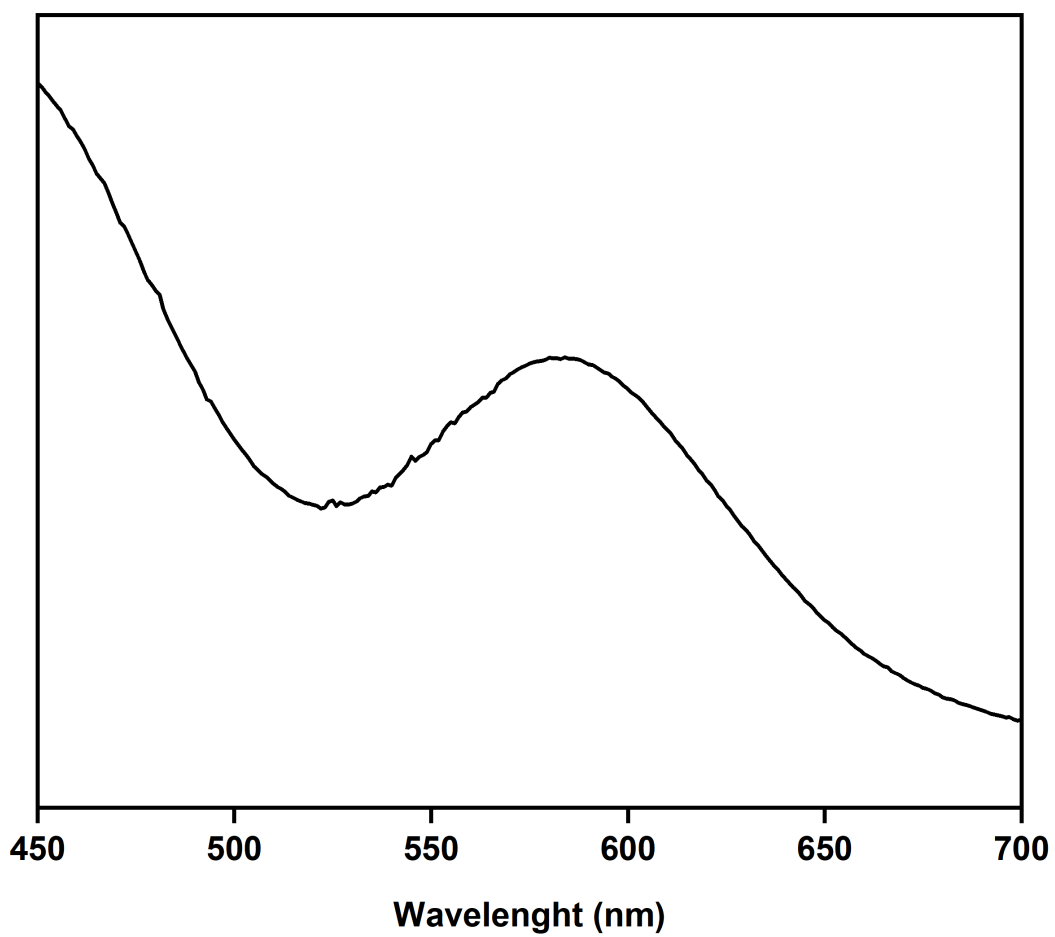


Figure S33. UV-Vis spectrum of a $\text{Rh}_{12}\text{L}^2_6\text{L}^4_6$ solution of DMF. The maximum of adsorption band I (λ_{max}) of $\text{Rh}_{12}\text{L}^2_6\text{L}^4_6$ is centered at 611 nm.

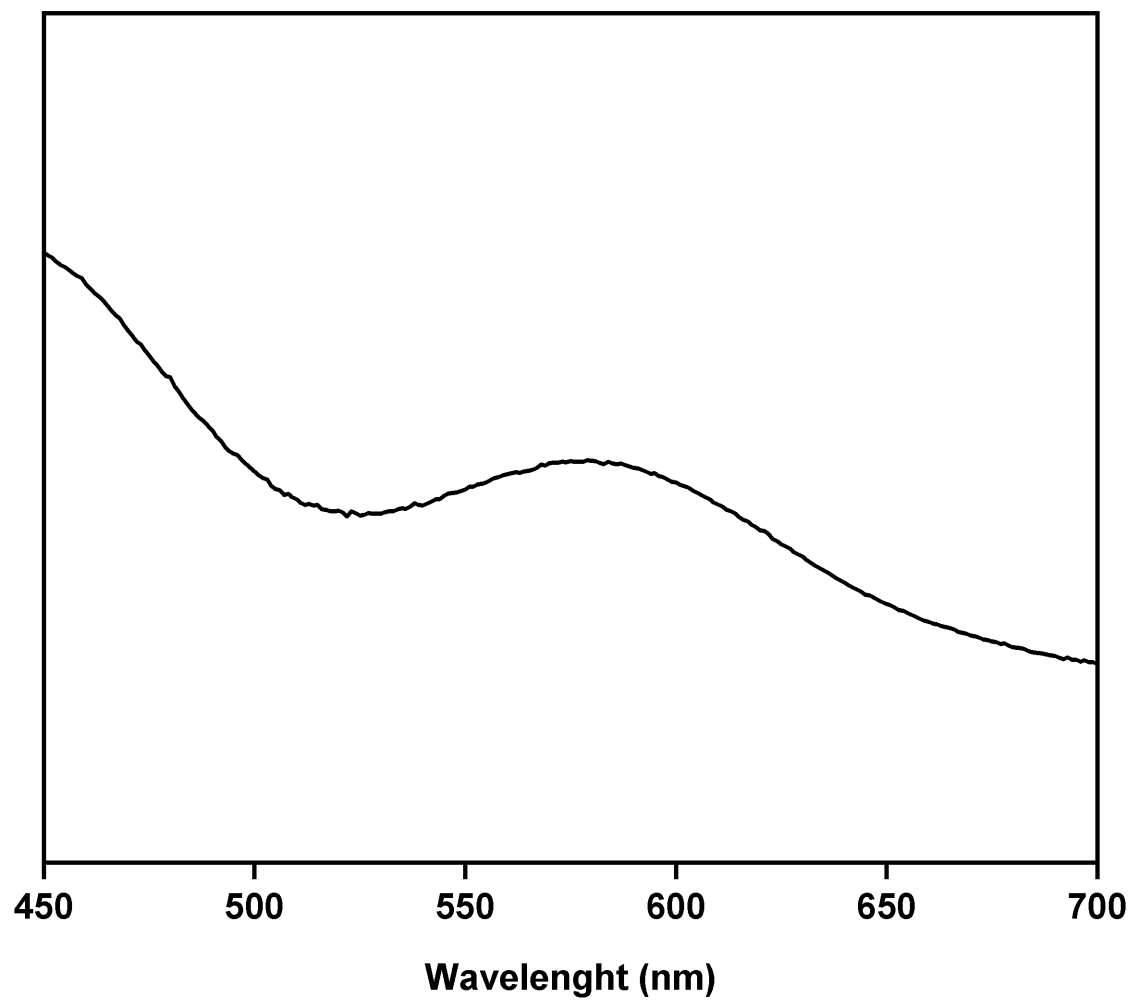


Figure S34. UV-Vis spectrum of a DMF solution of $\text{Rh}_{12}\text{L}^2\text{L}^{5'}_6$. The maximum of adsorption band I (λ_{max}) of $\text{Rh}_{12}\text{L}^2\text{L}^{5'}_6$ is centered at 579 nm.

S5.2.3 MALDI-TOF spectra

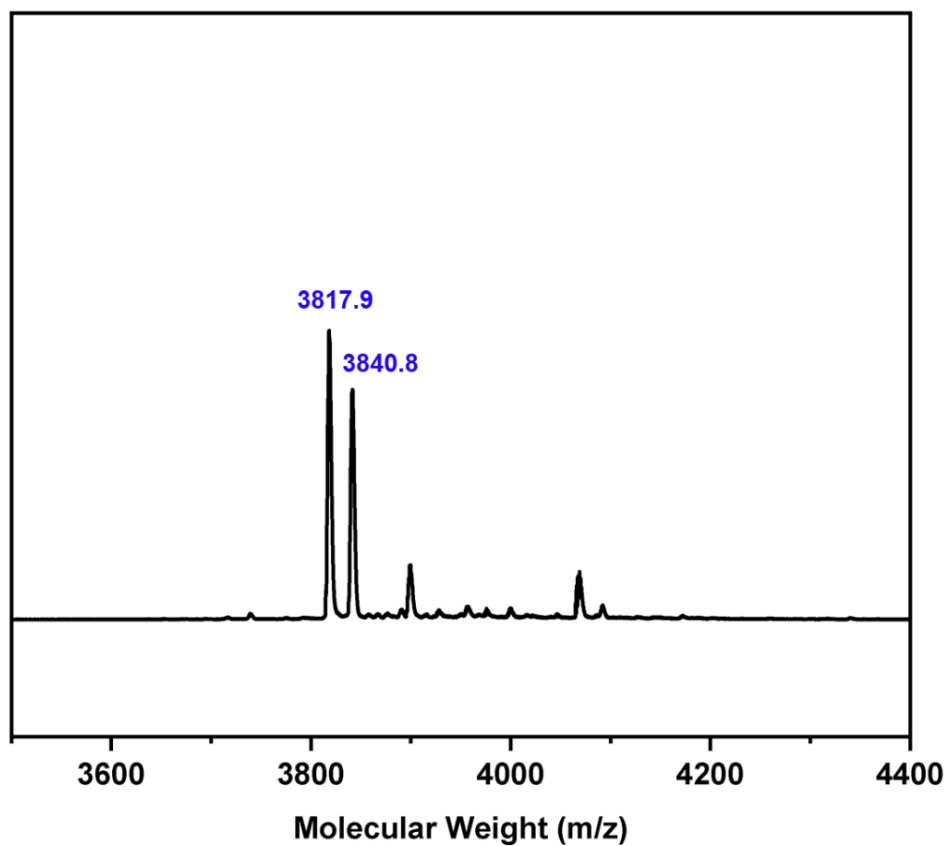


Figure S35. MALDI-TOF spectrum of $\text{Rh}_{12}\text{L}^1_6\text{L}'_6$. The weight corresponding to the formula $[(\text{Rh}_{12}(\text{L}^1)_6\text{L}'_6) + \text{H}]^+$ has been highlighted: expected = 3816.3 g/mol; found = 3817.9 g/mol.

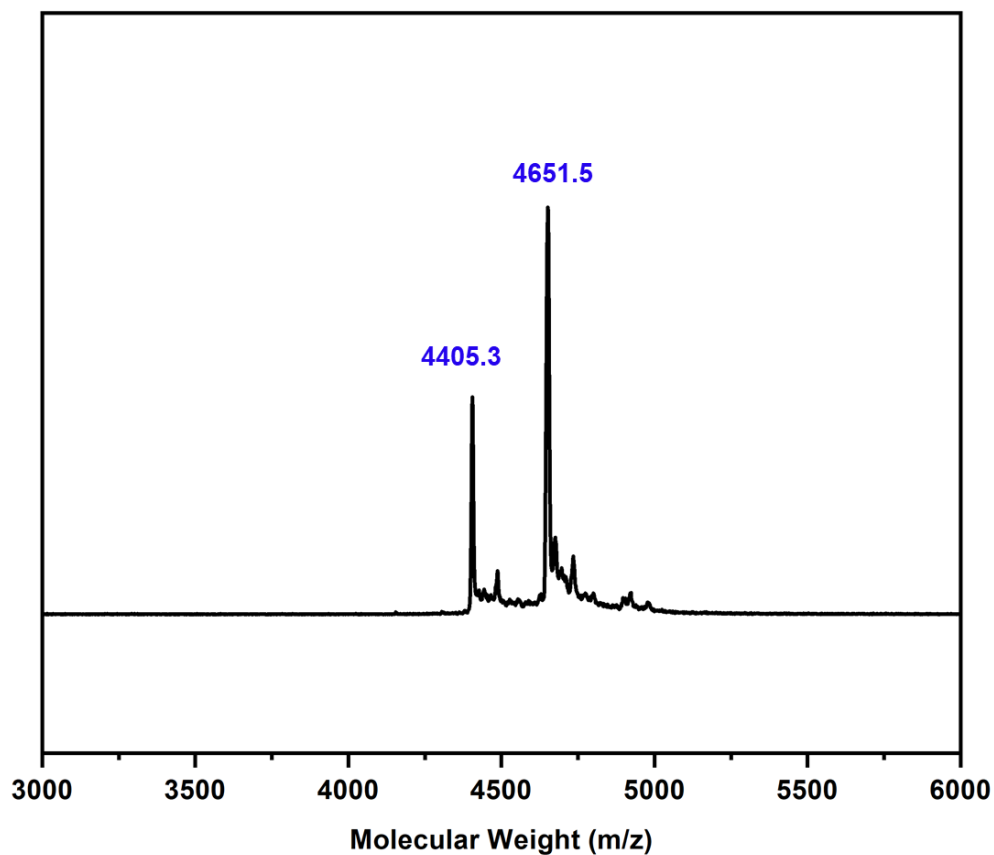


Figure S36. MALDI-TOF spectrum of $\text{Rh}_{12}\text{L}^1_6\text{L}'^6_6$. The weight corresponding to the formula $[\text{Rh}_{12}(\text{L}^1)_6(\text{L}'^2)_6(\text{DMA})(\text{H}_2\text{O})_2(\text{MeOH})_4 + \text{H}]^+$ has been highlighted: expected = 4403.8 g/mol; found = 4405.3 g/mol. The weight corresponding to the formula $[\text{Rh}_{12}(\text{L}^1)_6(\text{L}'^2)_6(\text{H}_2\text{O})_2(\text{DMA})_2(\text{CH}_3\text{CN})_7 + \text{H}]^+$ has been highlighted: expected = 4650.0 g/mol; found = 4651.48 g/mol.

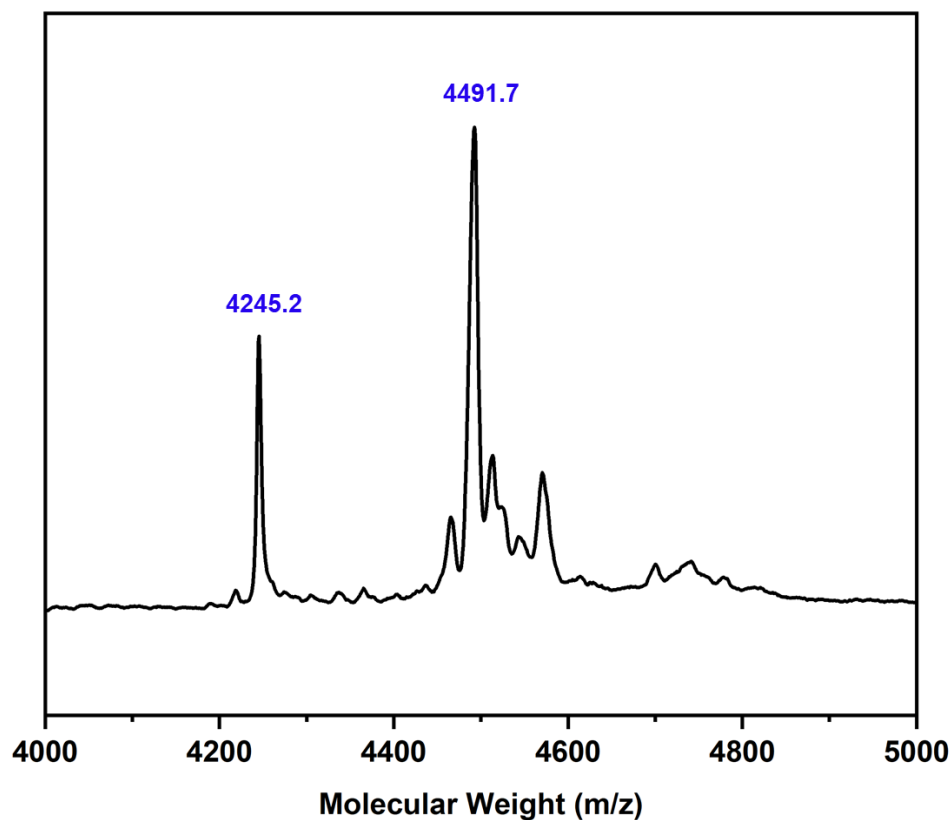


Figure S37. MALDI-TOF spectrum of $\text{Rh}_{12}\text{L}^1_6\text{L}^{3'}_6$. The weight corresponding to the formula $[(\text{Rh}_6(\text{L}^1)_6(\text{L}^{3'})_6 + \text{H})^+]$ has been highlighted: expected = 4248.6 g/mol; found = 4245.2 g/mol. The weight corresponding to the formula $[(\text{Rh}_6(\text{L}^1)_6(\text{L}^{3'})_6(\text{DMA})_2(\text{H}_2\text{O})_2(\text{MeOH}) + \text{H})^+]$ has been highlighted: expected = 4490.8 g/mol found = 4491.7 g/mol.

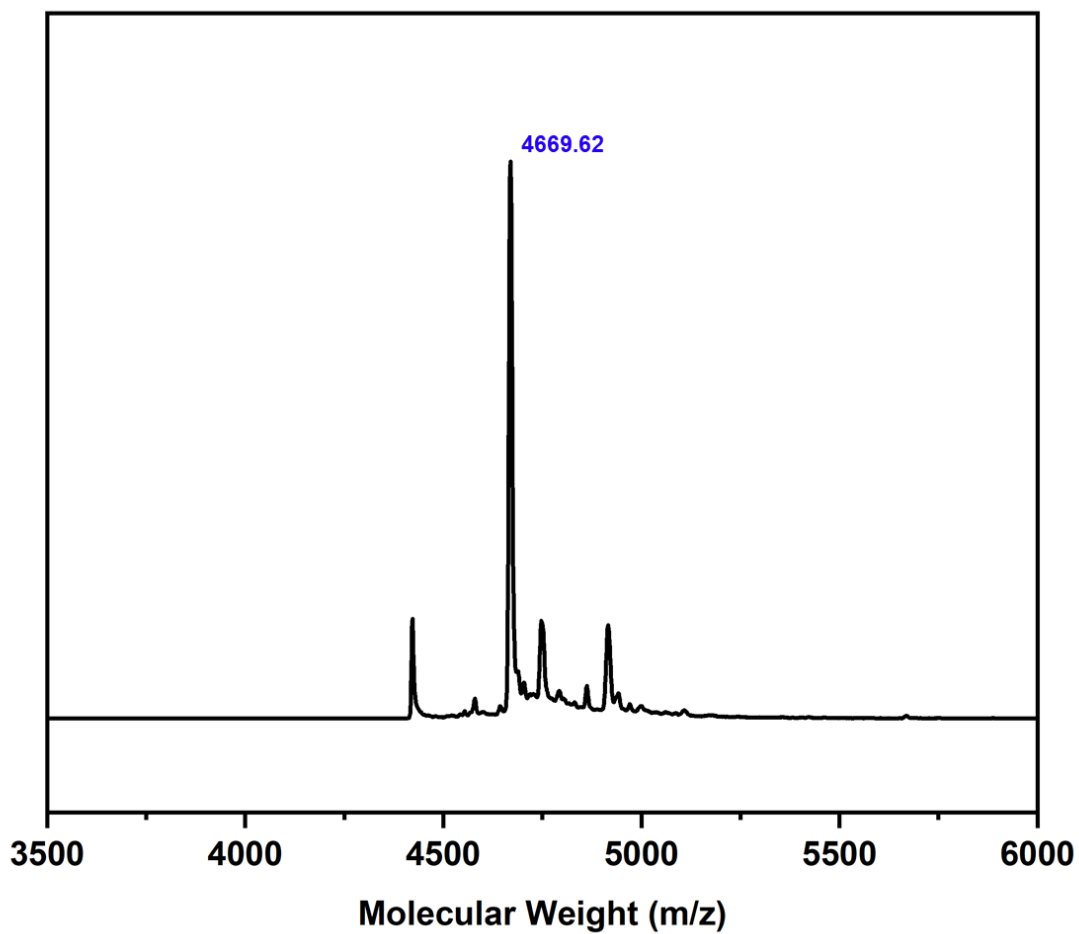


Figure S38: MALDI-TOF spectra of $\text{Rh}_{12}\text{L}^1_6\text{L}'_6$. The weight corresponding to the formula $[\text{Rh}_{12}(\text{L}^1)_6(\text{L}'^4)_6(\text{DMA})_2(\text{H}_2\text{O})_4 + \text{H}]^+$ has been highlighted: expected = 4662.98; found = 4669.62.

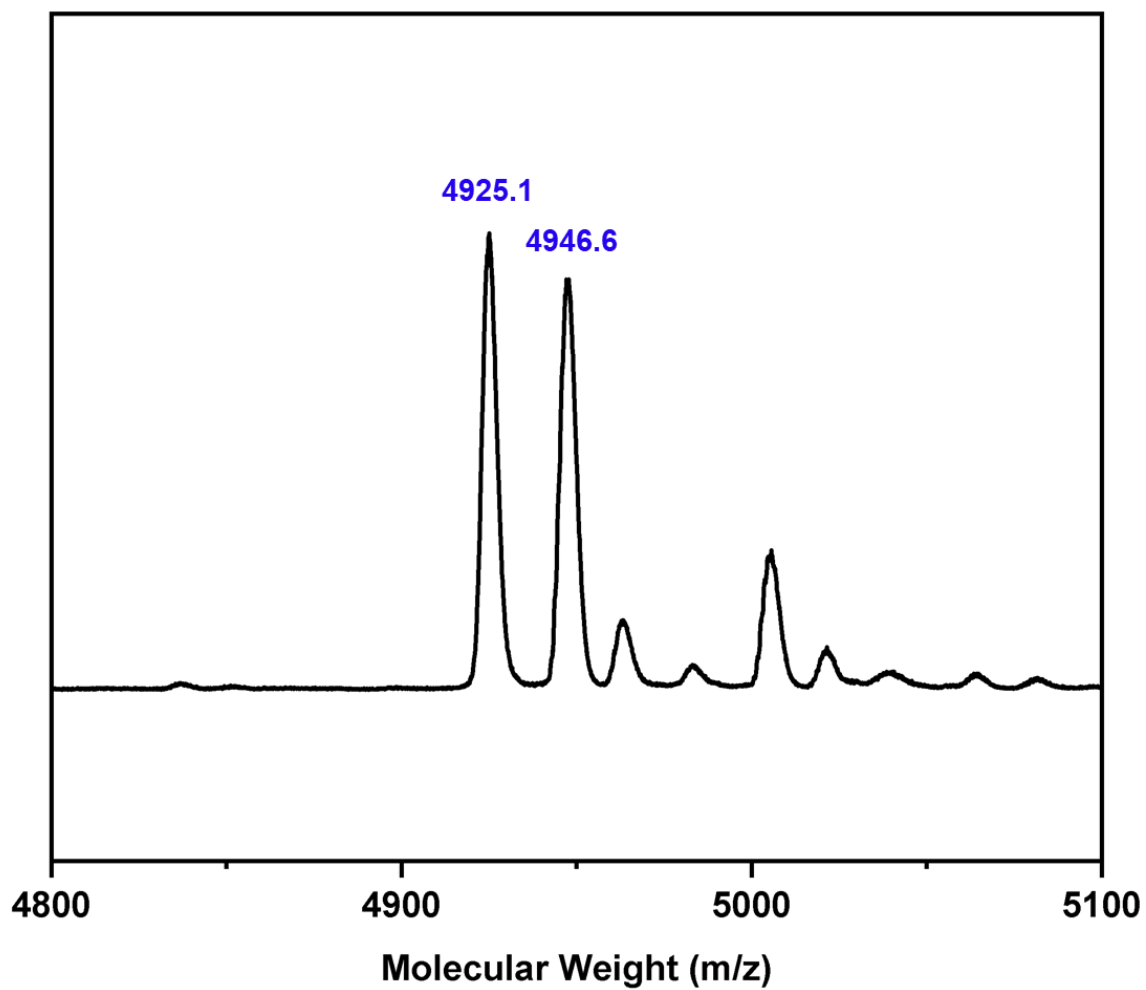


Figure S39. MALDI-TOF spectrum of $\text{Rh}_{12}\text{L}^1_6\text{L}^{5^*}_6$. The weight corresponding to the formula $[(\text{Rh}_6(\text{L}^1)_6(\text{L}^{5^*})_6 + \text{H})^+]$ has been highlighted: expected = 4921.4 g/mol; found = 4925.1 g/mol.

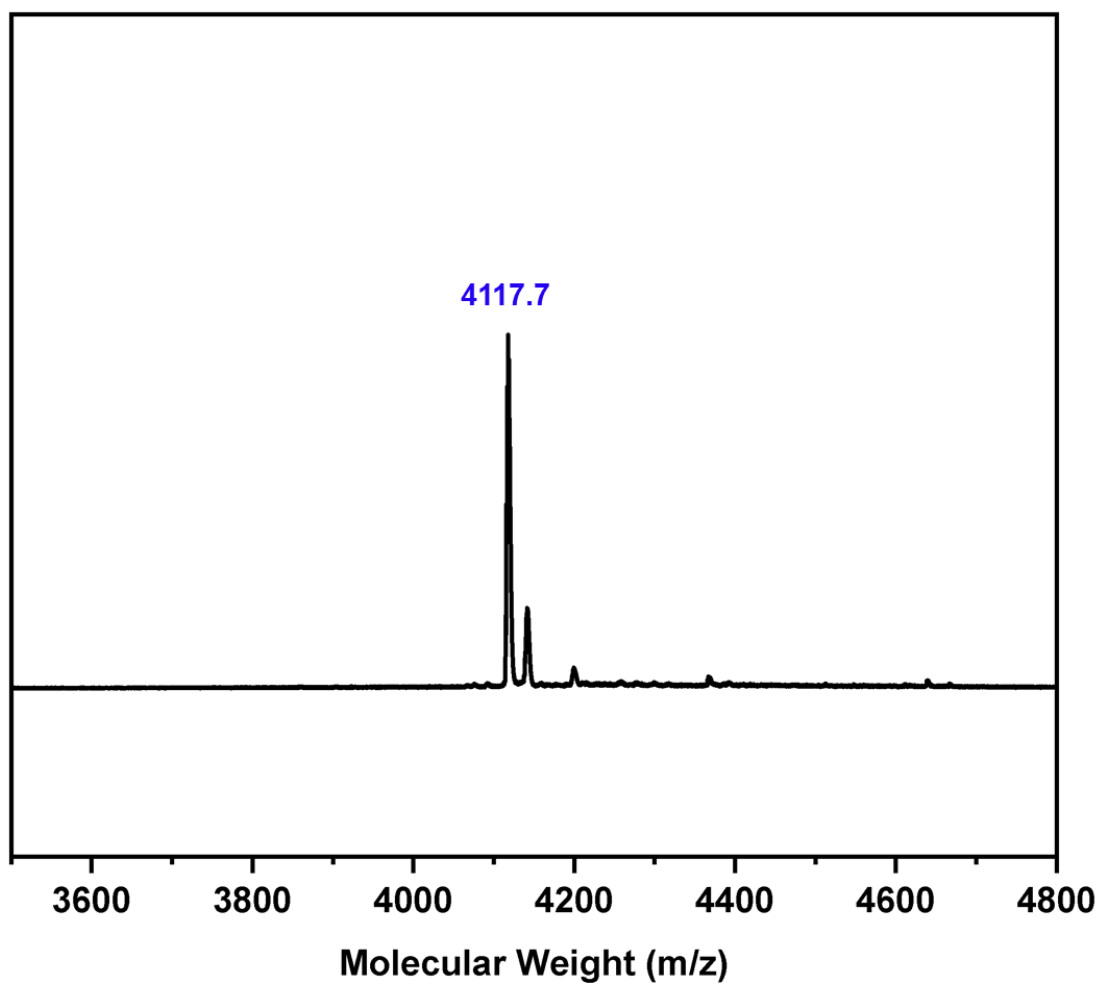


Figure S40. MALDI-TOF spectrum of $\text{Rh}_{12}\text{L}^1\text{L}^6$. The weight corresponding to the formula $[(\text{Rh}_6(\text{L}^1)_6(\text{L}^6)_6 + \text{H})^+]$ has been highlighted: expected = 4116.4 g/mol; found = 4117.7 g/mol.

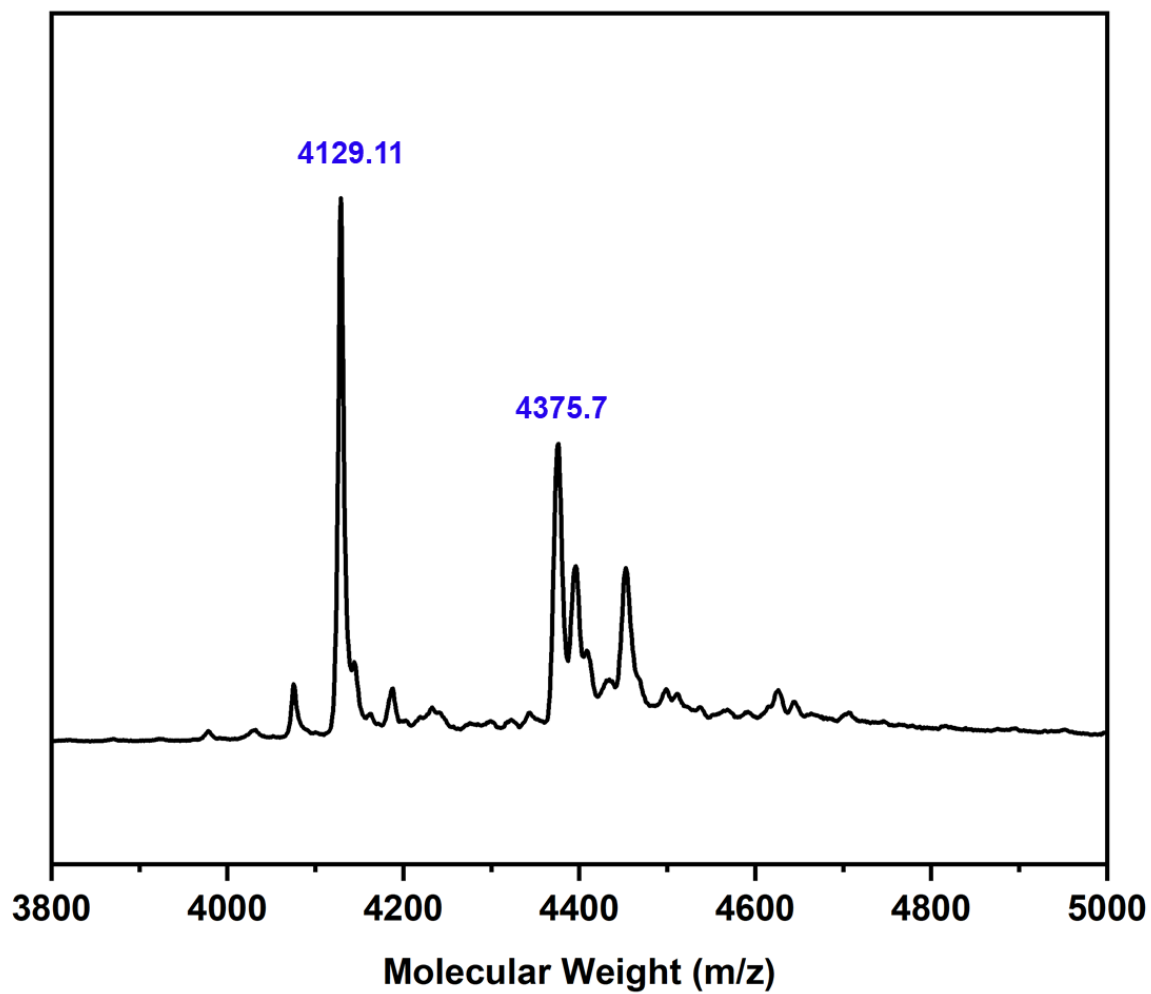


Figure S41. MALDI-TOF spectrum of $\text{Rh}_{12}\text{L}^2_6\text{L}^6_6$. The weight corresponding to the formula $[\text{Rh}_{12}(\text{L}^2)_6(\text{L}^6)_6 + \text{H}]^+$ has been highlighted: expected = 4128.3; found = 4129.1.

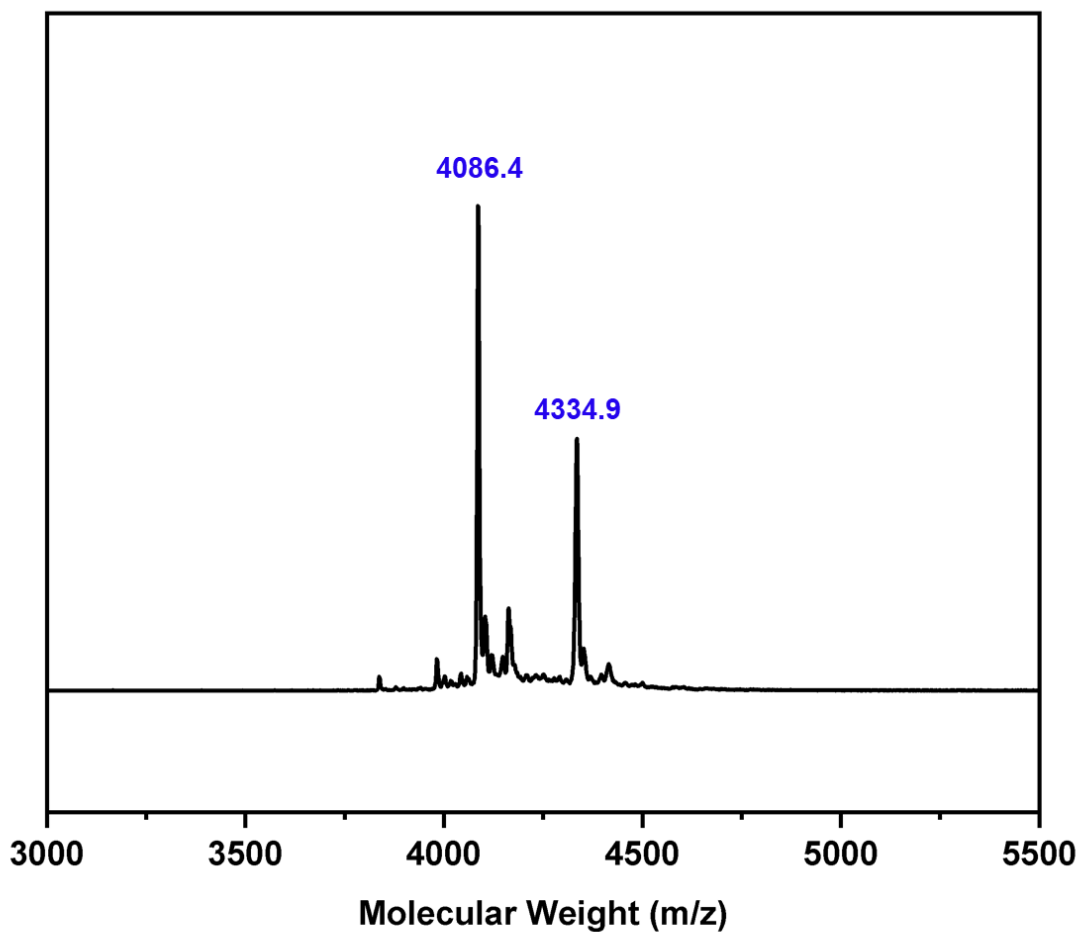


Figure S42. MALDI-TOF spectrum of $\text{Rh}_{12}\text{L}^2_6\text{L}'_6$. The weight corresponding to the formula $[\text{Rh}_{12}(\text{L}^2)_6(\text{L}^1)_6(\text{H}_2\text{O})_3(\text{DMA})_2(\text{MeOH}) + \text{H}]^+$ has been highlighted: expected = 4088.4; found = 4086.4. The weight corresponding to the formula $[\text{Rh}_{12}(\text{L}^2)_6(\text{L}^1)_6(\text{H}_2\text{O})_4(\text{DMA})_5 + \text{H}]^+$ has also been highlighted: expected = 4335.6; found = 4334.9.

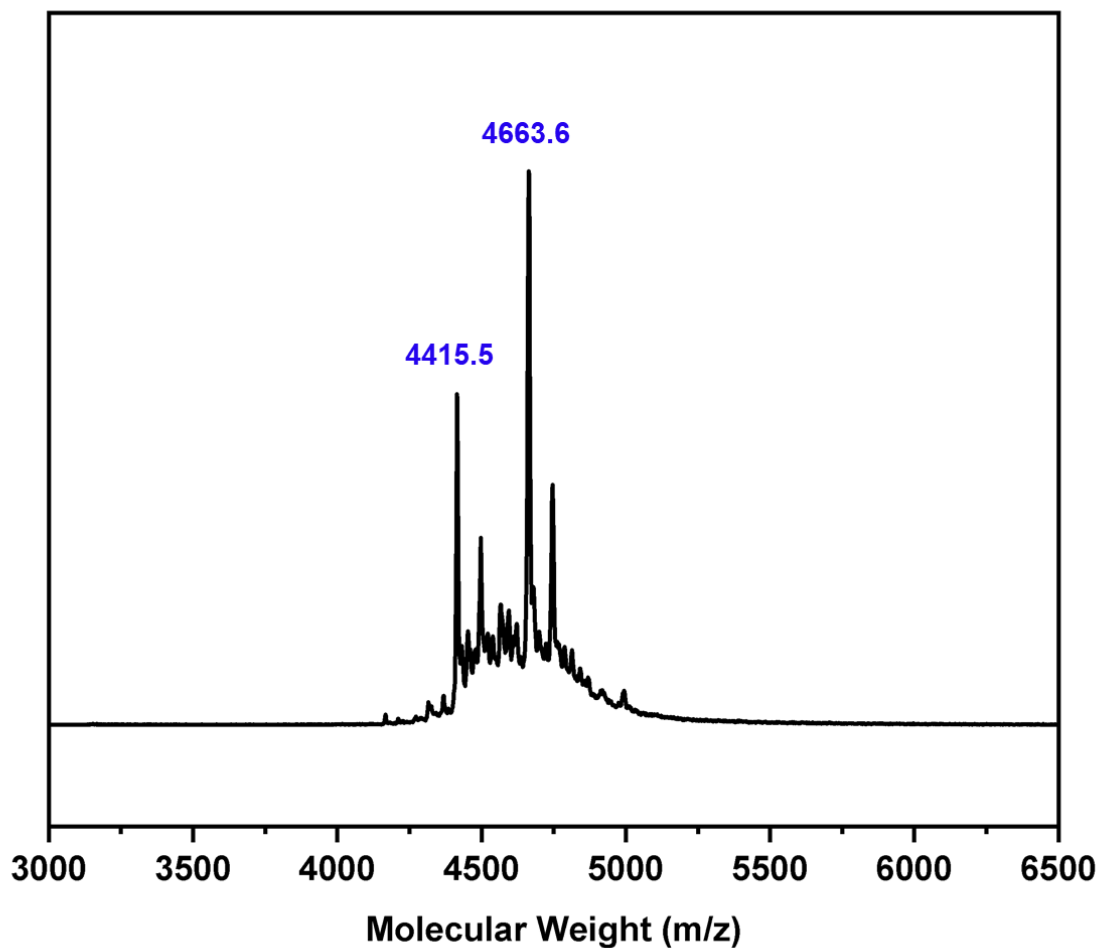


Figure S43. MALDI-TOF spectrum of $\text{Rh}_{12}\text{L}^2_6\text{L}'^2_6$. The weight corresponding to the formula $[\text{Rh}_{12}(\text{L}^2)_6(\text{L}'^2)_6(\text{MeOH})(\text{DMF})_3 + \text{H}]^+$ has been highlighted: expected = 4415.8; found = 4415.5. The weight corresponding to the formula $[\text{Rh}_{12}(\text{L}^2)_6(\text{L}'^2)_6(\text{H}_2\text{O})_4(\text{DMF})_5(\text{MeOH})_2 + \text{H}]^+$ has also been highlighted: expected = 4665.9; found = 4663.6.

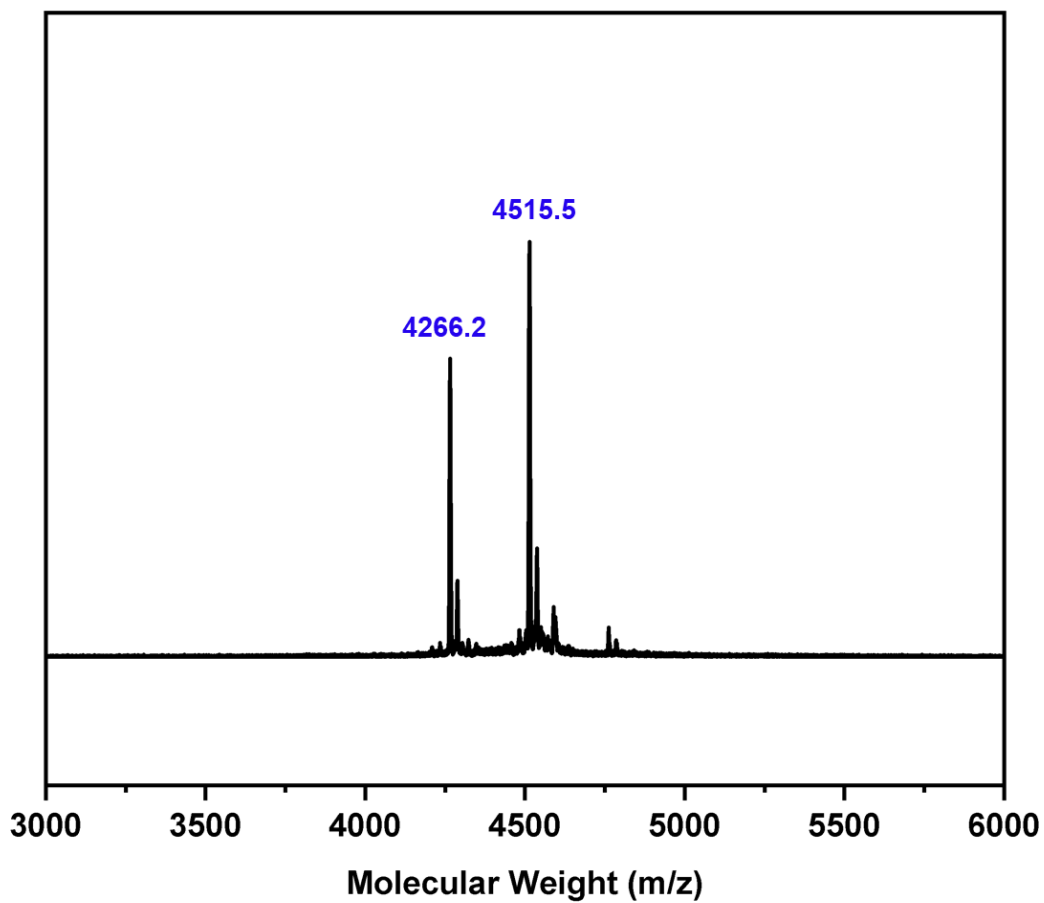


Figure S44: MALDI-TOF spectra of $\text{Rh}_{12}\text{L}^2_6\text{L}^{3'}_6$. The weight corresponding to the formula $[\text{Rh}_{12}(\text{L}^2)_6(\text{L}^{3'})_6 + \text{H}]^+$ has been highlighted: expected = 4260.6; found = 4266.2. The weight corresponding to the formula $[\text{Rh}_{12}(\text{L}^2)_6(\text{L}^{3'})_6(\text{H}_2\text{O})_2(\text{DMF})_3 + \text{H}]^+$ has been highlighted: expected = 4515.7; found = 4515.5.

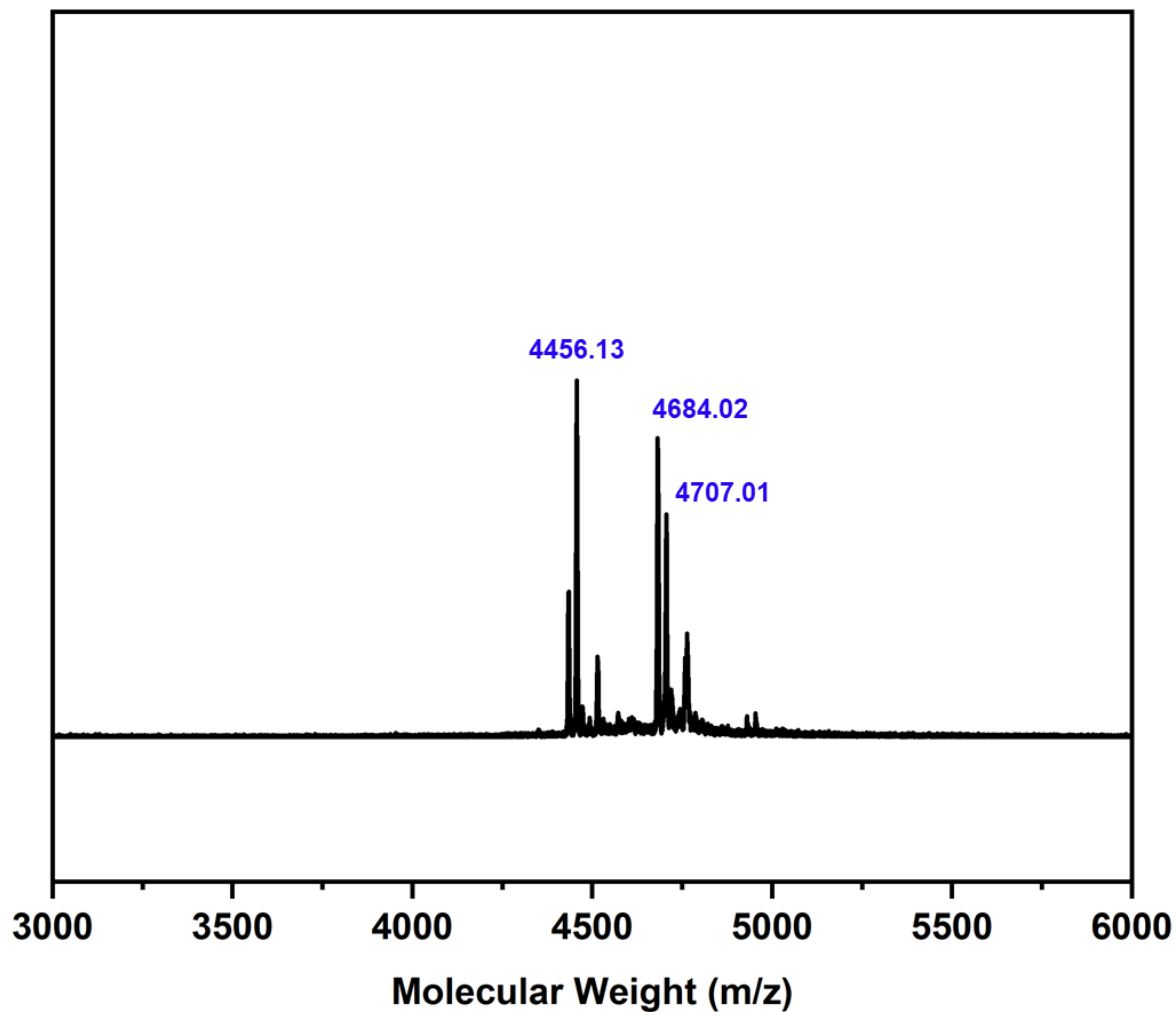


Figure S45. MALDI-TOF spectra of $\text{Rh}_{12}\text{L}^2_6\text{L}'_6$. The weight corresponding to the formula $[\text{Rh}_{12}(\text{L}^2)_6(\text{L}^4)_6(\text{MeOH}) + \text{H}]^+$ has been highlighted: expected = 4460.8; found = 4456.1. The weight corresponding to the formula $[\text{Rh}_{12}(\text{L}^2)_6(\text{L}^4)_6(\text{MeOH})_4(\text{H}_2\text{O})_3(\text{DMF}) + \text{H}]^+$ has been highlighted: expected = 4683.9; found = 4684.0.

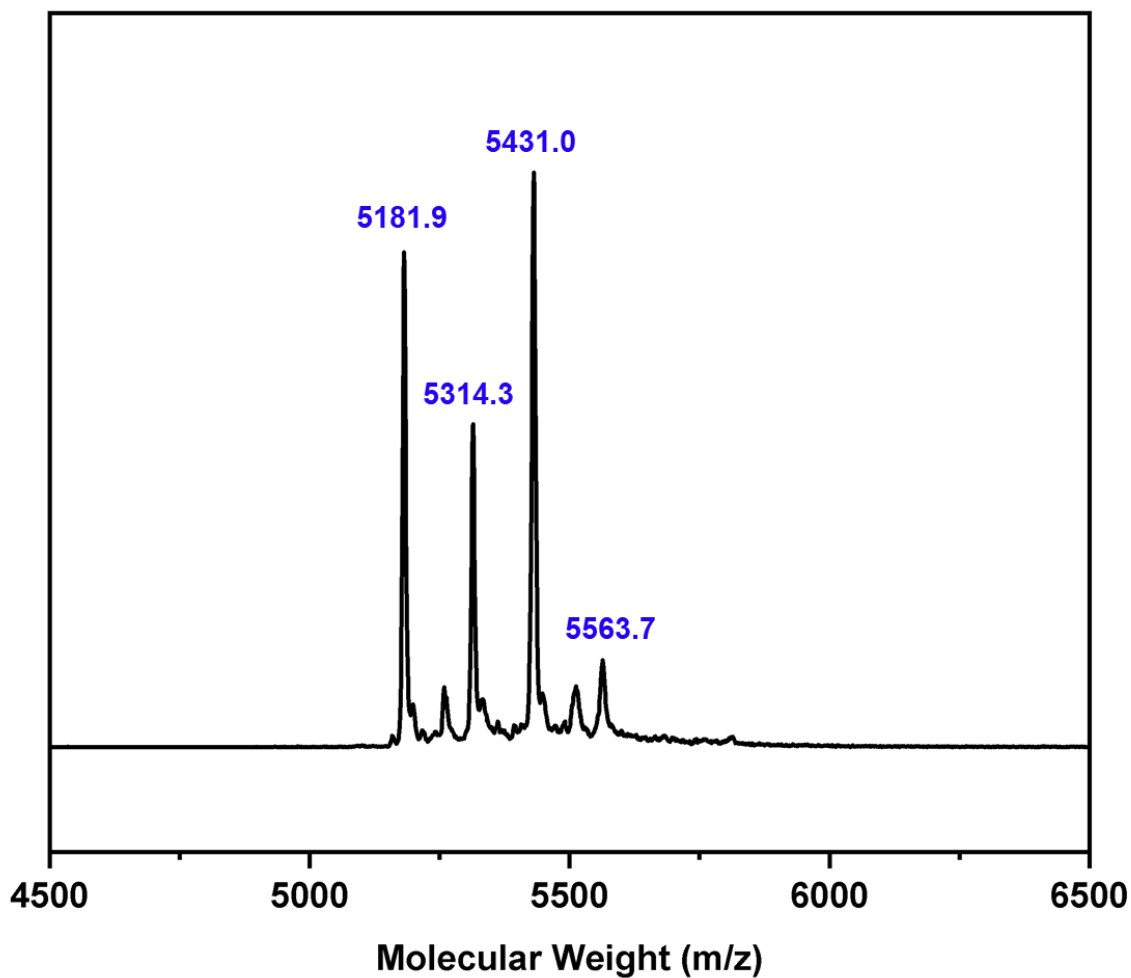


Figure S46. MALDI-TOF spectrum of $\text{Rh}_{12}\text{L}^2\text{L}^5_6$. The weight corresponding to the formula $[\text{Rh}_{12}(\text{L}^2)_6(\text{L}^5)_6(\text{H}_2\text{O})_4(\text{DMF})_2(\text{MeOH}) + \text{H}]^+$ has been highlighted: expected = 5183.5; found = 5181.9. The weight corresponding to the formula $[\text{Rh}_{12}(\text{L}^2)_6(\text{L}^5)_6(\text{H}_2\text{O})_2(\text{DMF})_5(\text{MeOH})_3 + \text{H}]^+$ has also been highlighted: expected = 5430.7; found = 5431.0

S5.2.4 Powder X-ray diffraction

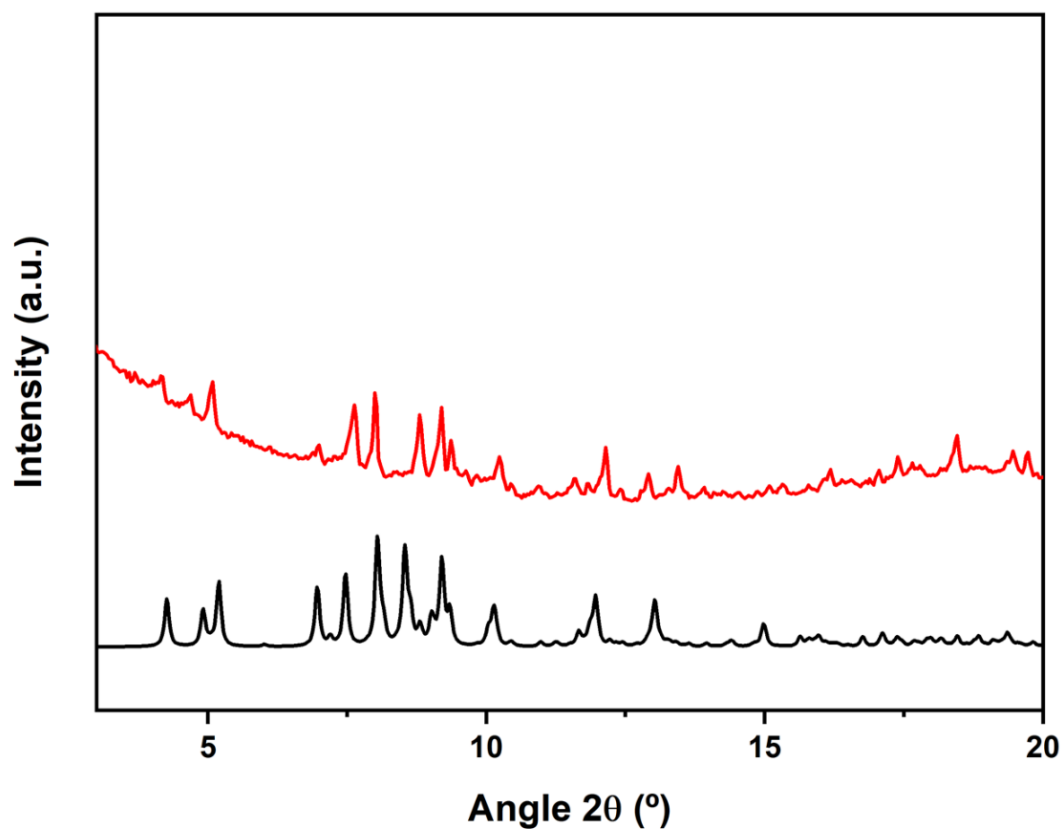


Figure S47. Simulated PXRD diffractogram of $\text{Rh}_{12}\text{L}^1\text{L}'_6$ from crystal structure (black) and experimental PXRD diffractogram of $\text{Rh}_{12}\text{L}^1\text{L}'_6$ crystals (red).

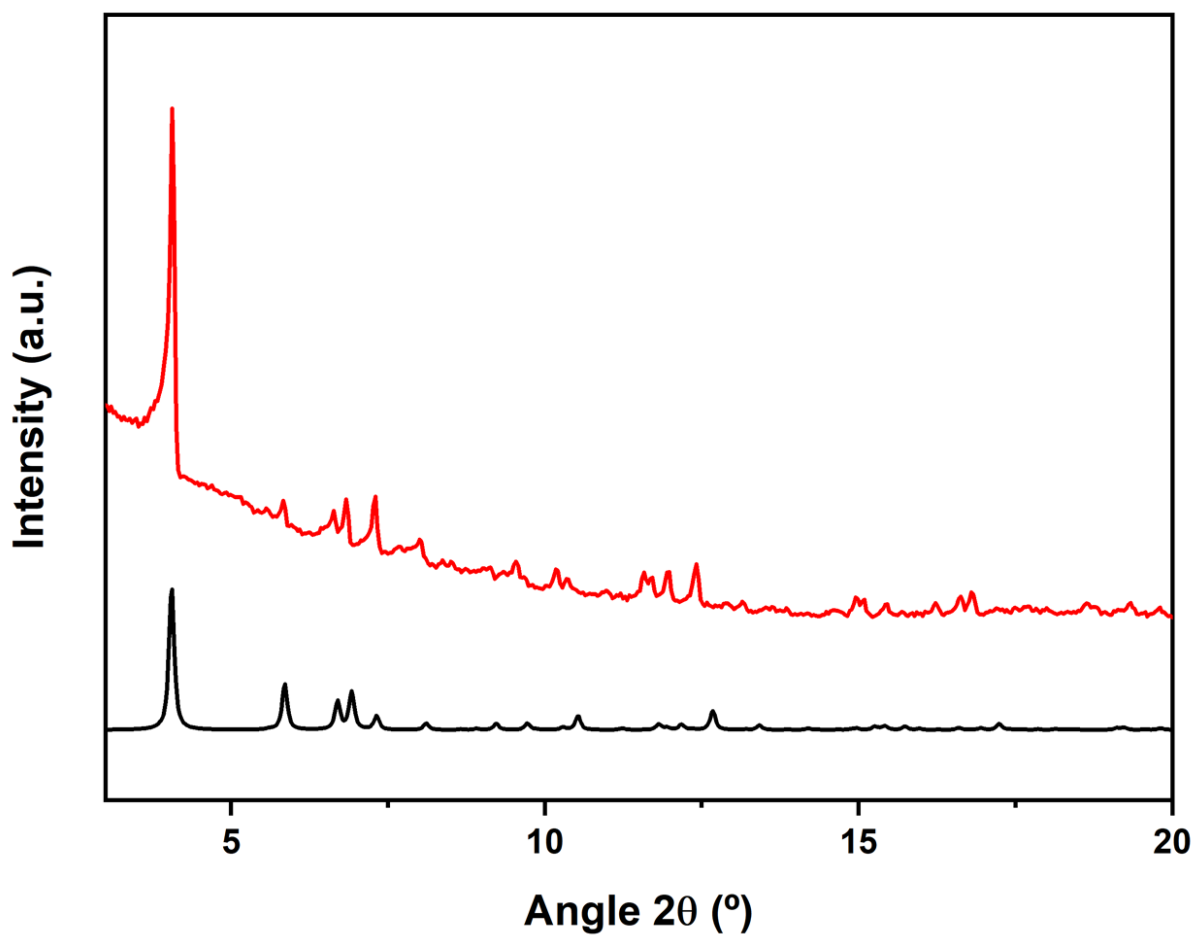


Figure S48. Simulated PXRd diffractogram of $\text{Rh}_{12}\text{L}^1_6\text{L}'^6_6$ from crystal structure (black) and experimental PXRd diffractogram of $\text{Rh}_{12}\text{L}^1_6\text{L}'^6_6$ crystals (red).

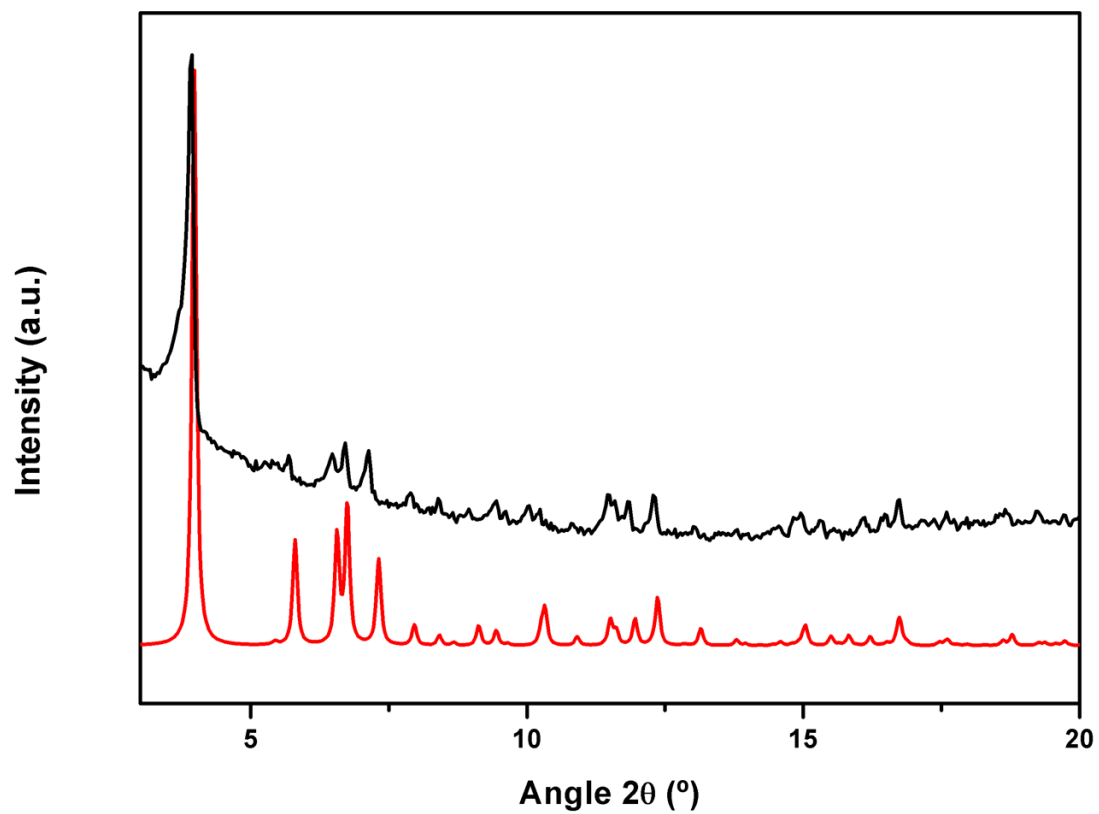


Figure S49. Simulated PXRd diffractogram of $\text{Rh}_{12}\text{L}^1_6\text{L}^{3'}_6$ from crystal structure (black) and experimental PXRd diffractogram of $\text{Rh}_{12}\text{L}^1_6\text{L}^{3'}_6$ crystals (red).

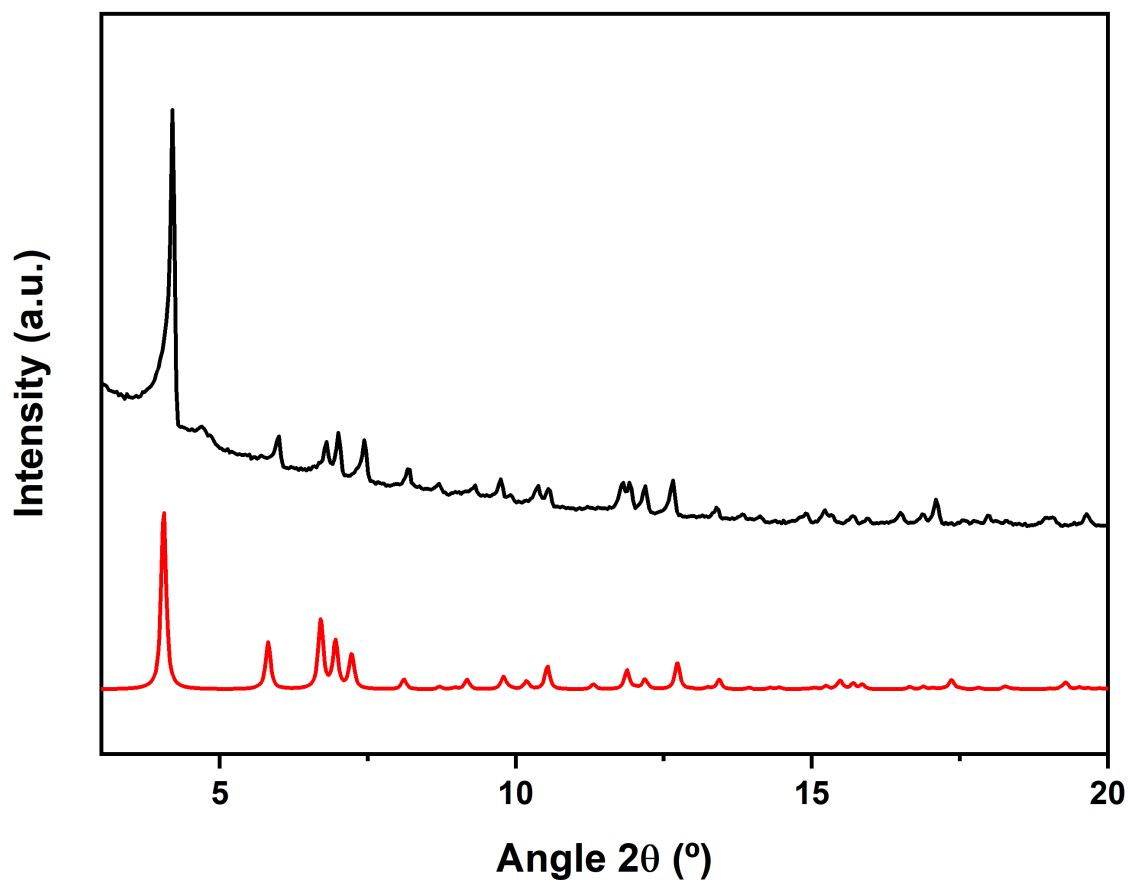


Figure S50. Simulated PXRd diffractogram of $\text{Rh}_{12}\text{L}^1\text{L}'_6$ from crystal structure (black) and experimental PXRd diffractogram of $\text{Rh}_{12}\text{L}^1\text{L}'_6$ crystals (red).

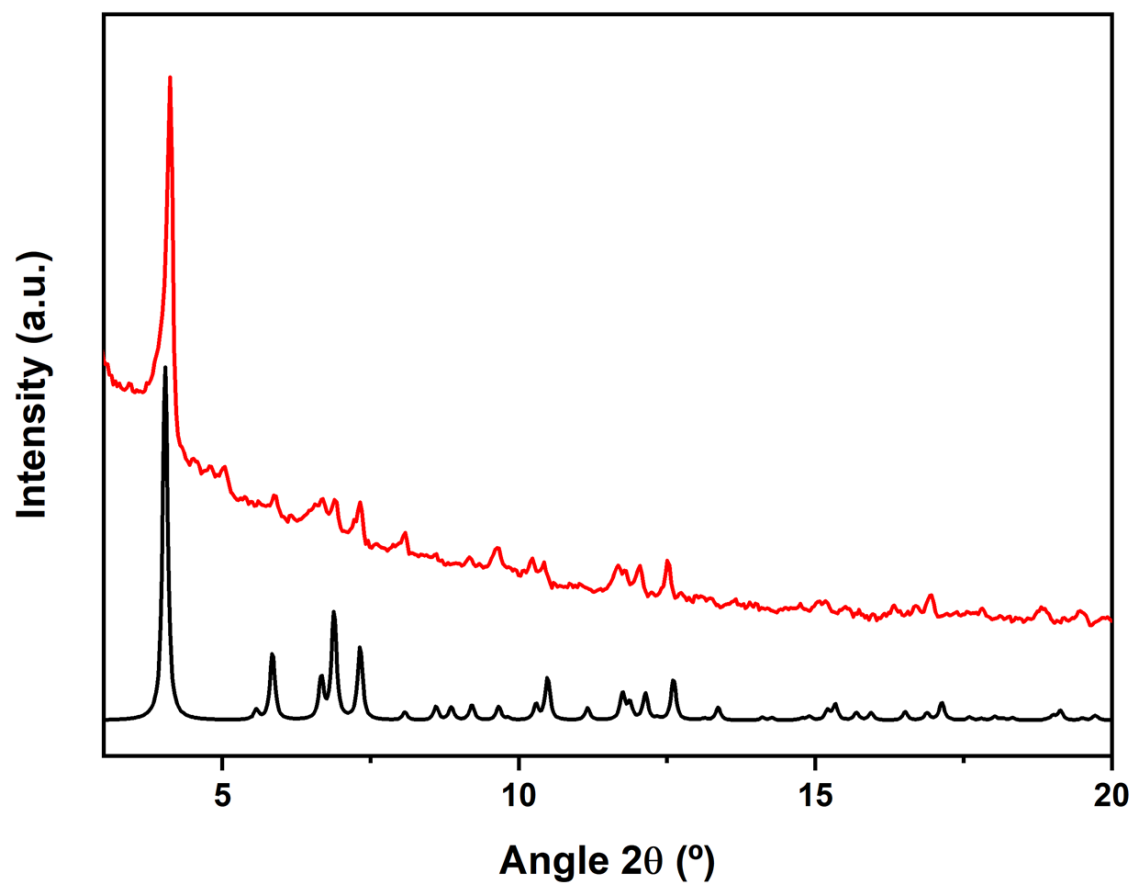


Figure S51. Simulated PXRd diffractogram of $\text{Rh}_{12}\text{L}^1_6\text{L}^{5'}_6$ from crystal structure (black) and experimental PXRd diffractogram of $\text{Rh}_{12}\text{L}^1_6\text{L}^{5'}_6$ crystals (red).

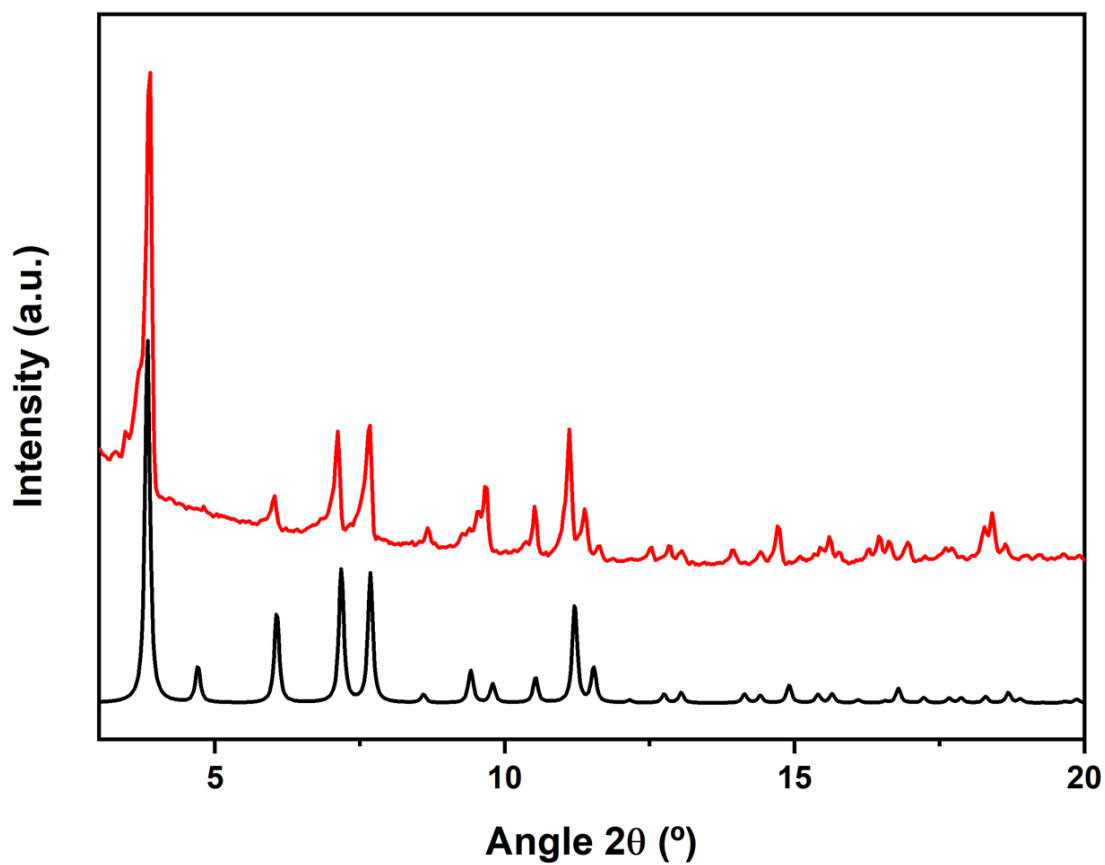


Figure S52. Simulated PXRd diffractogram of $\text{Rh}_{12}\text{L}^1\text{L}^6\%$ from crystal structure (black) and experimental PXRd diffractogram of $\text{Rh}_{12}\text{L}^1\text{L}^6\%$ crystals (red).

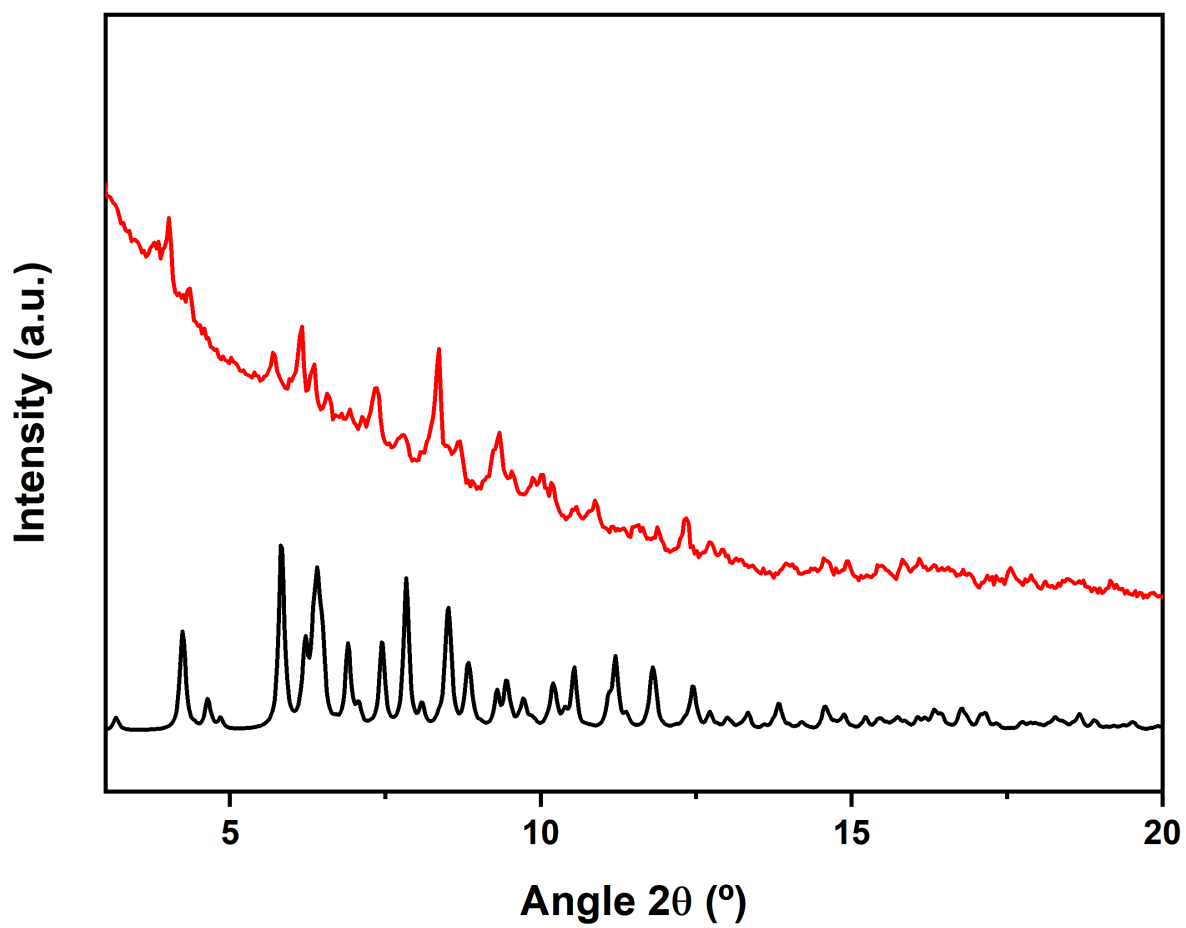


Figure S53. Simulated PXRD diffractogram of $\text{Rh}_{12}\text{L}^2_6\text{L}^6_6$ from crystal structure (black) and experimental PXRD diffractogram of $\text{Rh}_{12}\text{L}^2_6\text{L}^6_6$ crystals (red).

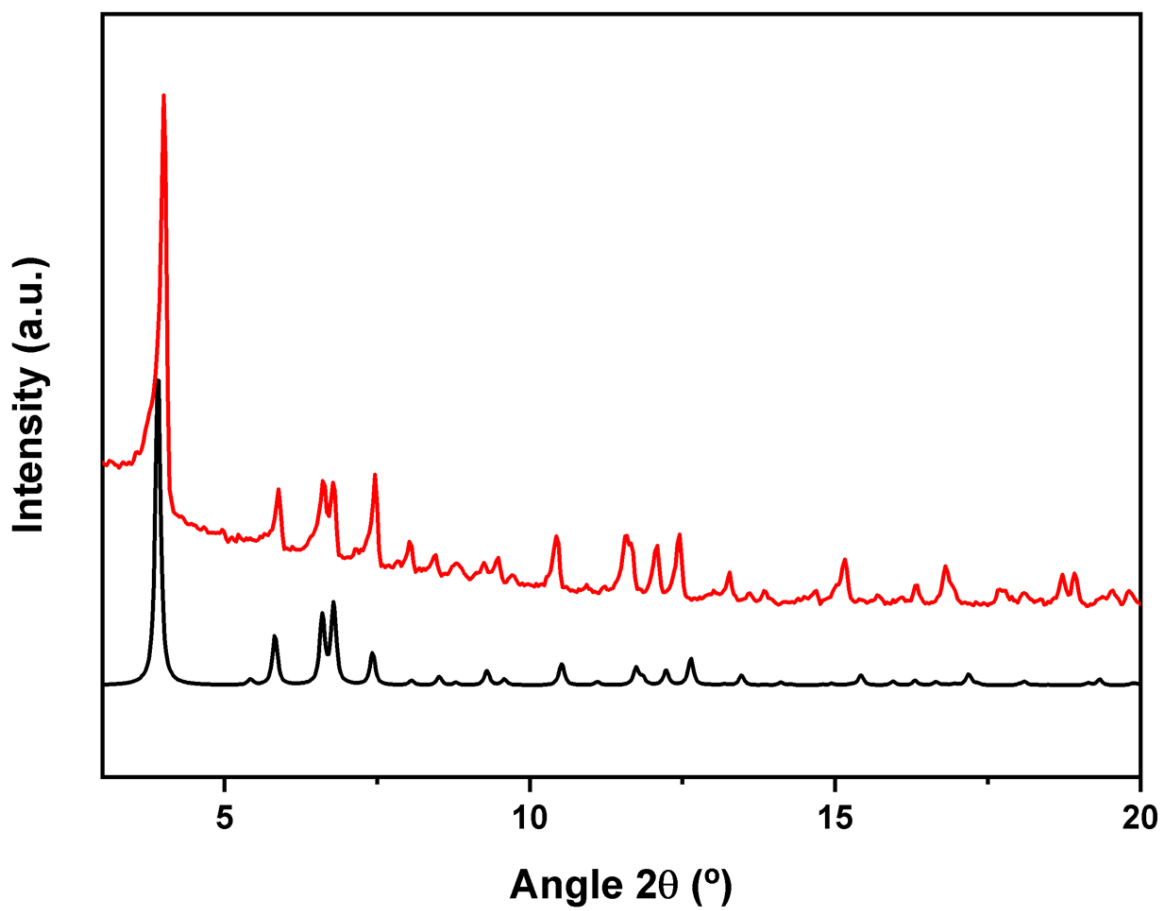


Figure S54. Simulated PXRd diffractogram of $\text{Rh}_{12}\text{L}^2\text{L}'_6$ from crystal structure (black) and experimental PXRd diffractogram of $\text{Rh}_{12}\text{L}^2\text{L}'_6$ crystals (red).

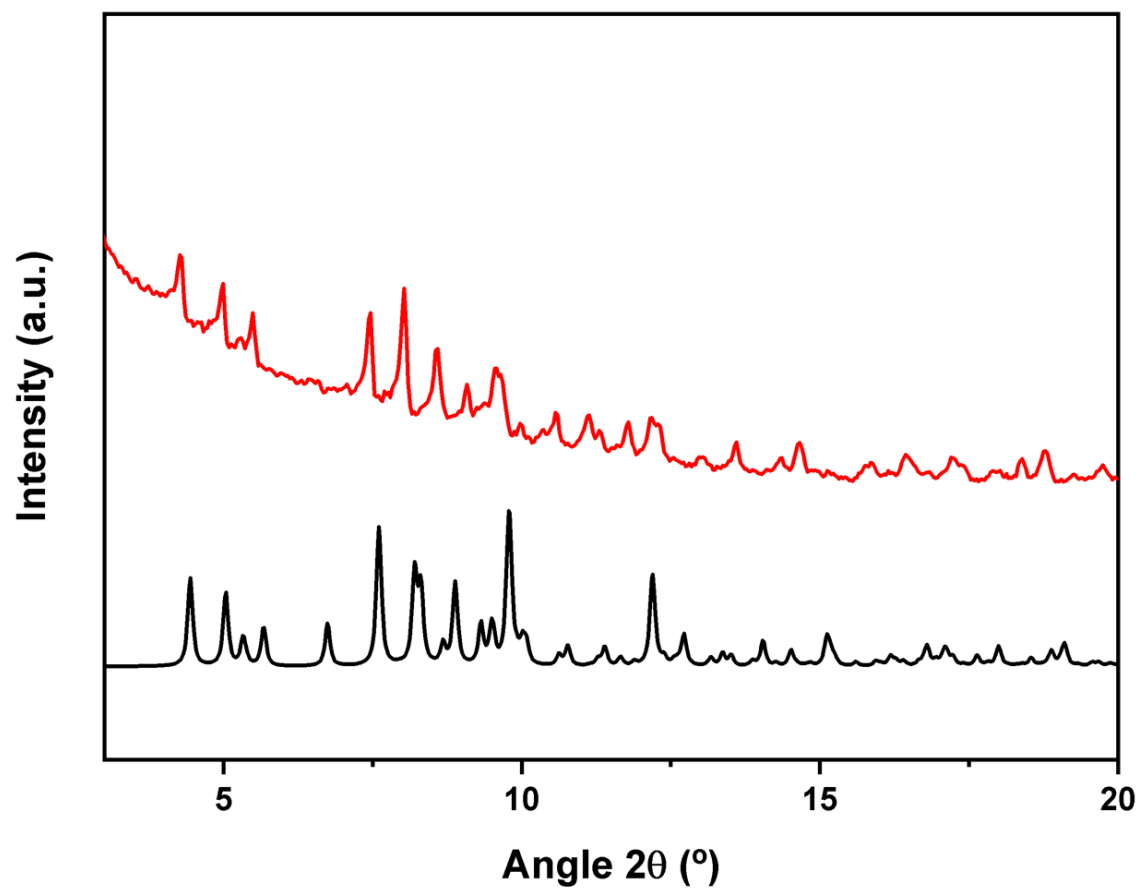


Figure S55. Simulated PXRD diffractogram of $\text{Rh}_{12}\text{L}^2_6\text{L}'_6$ from crystal structure (black) and experimental PXRD diffractogram of $\text{Rh}_{12}\text{L}^2_6\text{L}'_6$ crystals (red).

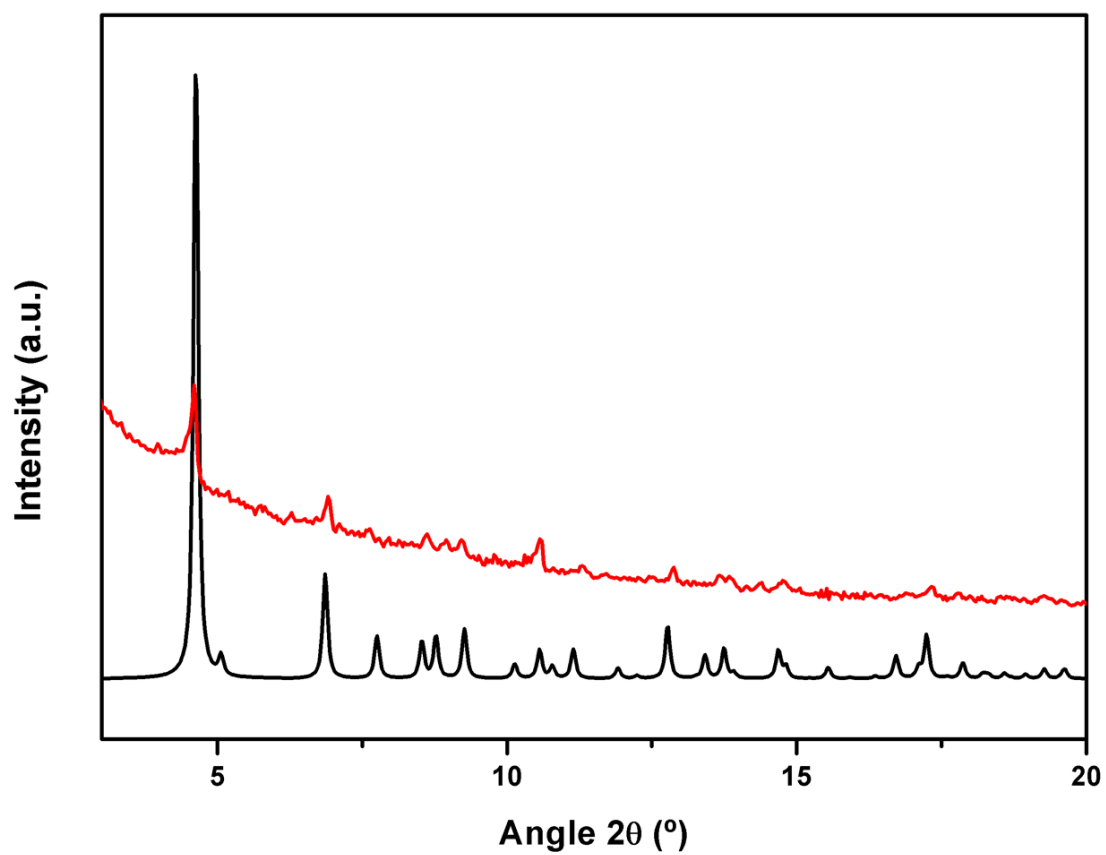


Figure S56. Simulated PXRD diffractogram of $\text{Rh}_{12}\text{L}^2_6\text{L}^{3'}_6$ from crystal structure (black) and experimental PXRD diffractogram of $\text{Rh}_{12}\text{L}^2_6\text{L}^{3'}_6$ crystals (red).

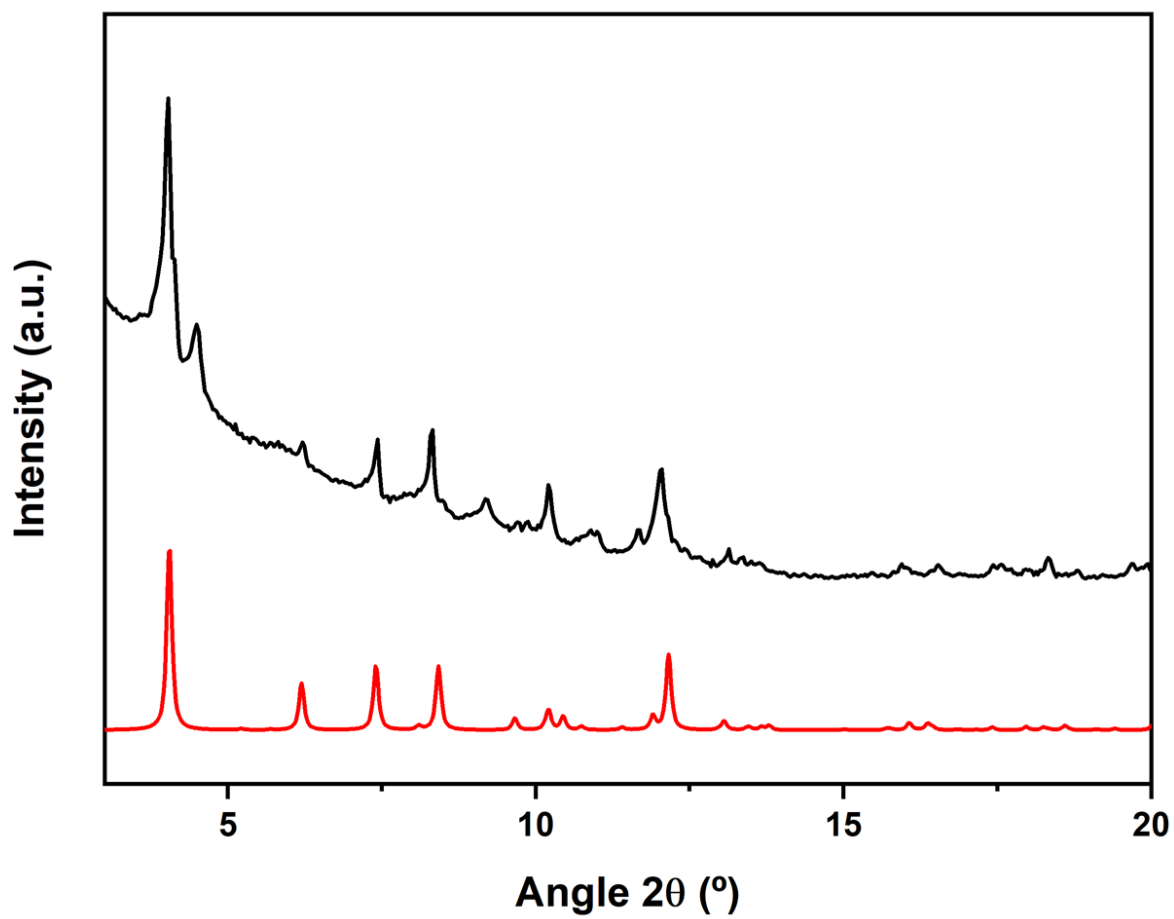


Figure S57. Simulated PXRd diffractogram of $\text{Rh}_{12}\text{L}^2_6\text{L}^4_6$ from crystal structure (black) and experimental PXRd diffractogram of $\text{Rh}_{12}\text{L}^2_6\text{L}^4_6$ crystals (red).

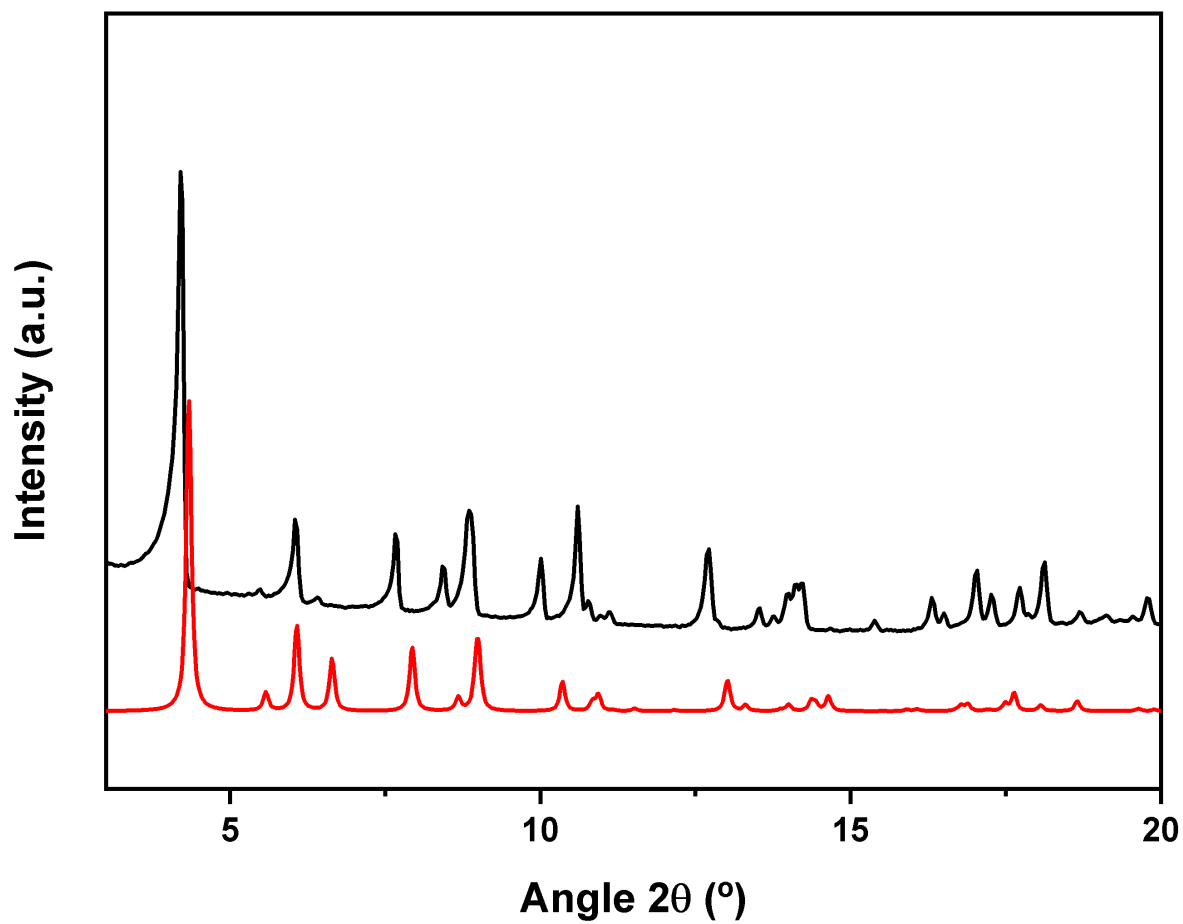


Figure S58. Simulated PXRd diffractogram of $\text{Rh}_{12}\text{L}^2\text{L}^{5\%}$ from crystal structure (black) and experimental PXRd diffractogram of $\text{Rh}_{12}\text{L}^2\text{L}^{5\%}$ crystals (red).

S5.2.1 N₂ adsorption-desorption isotherms

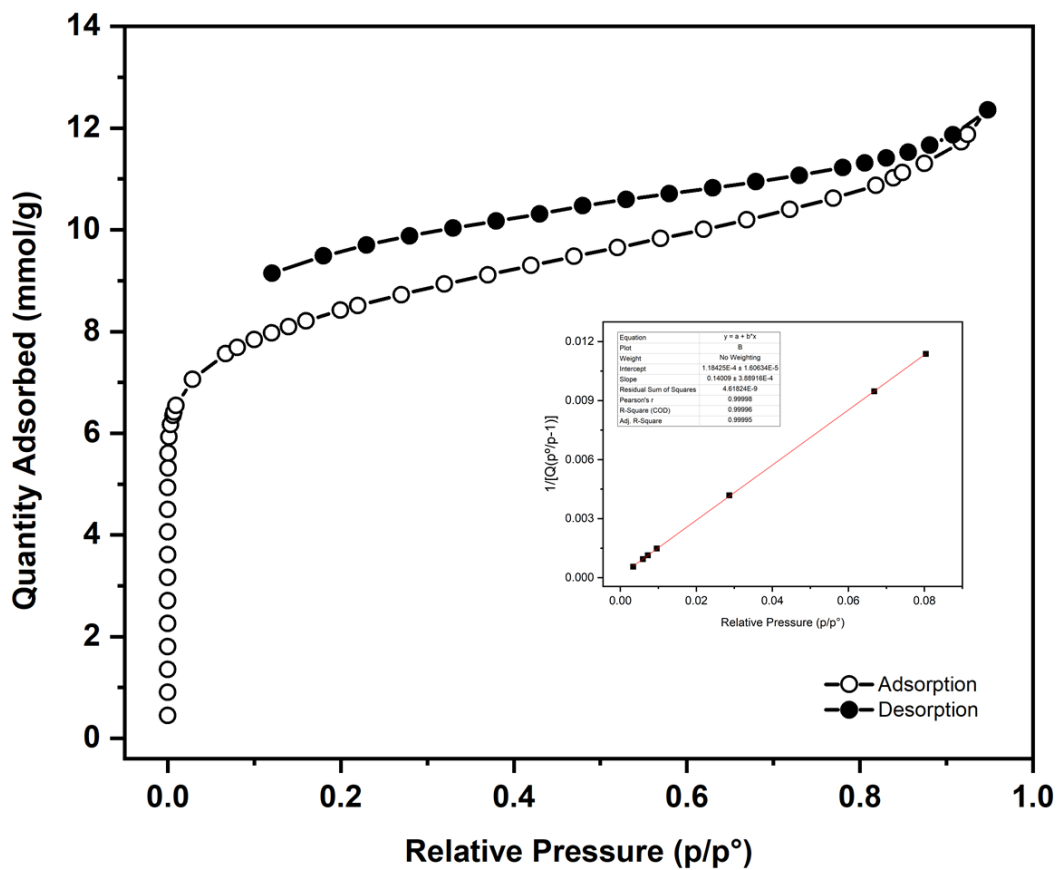


Figure S59. N₂ adsorption-desorption isotherm for Rh₁₂L₆L'₆ at 77 K ($S_{\text{BET}} = 696 \text{ m}^2/\text{g}$).

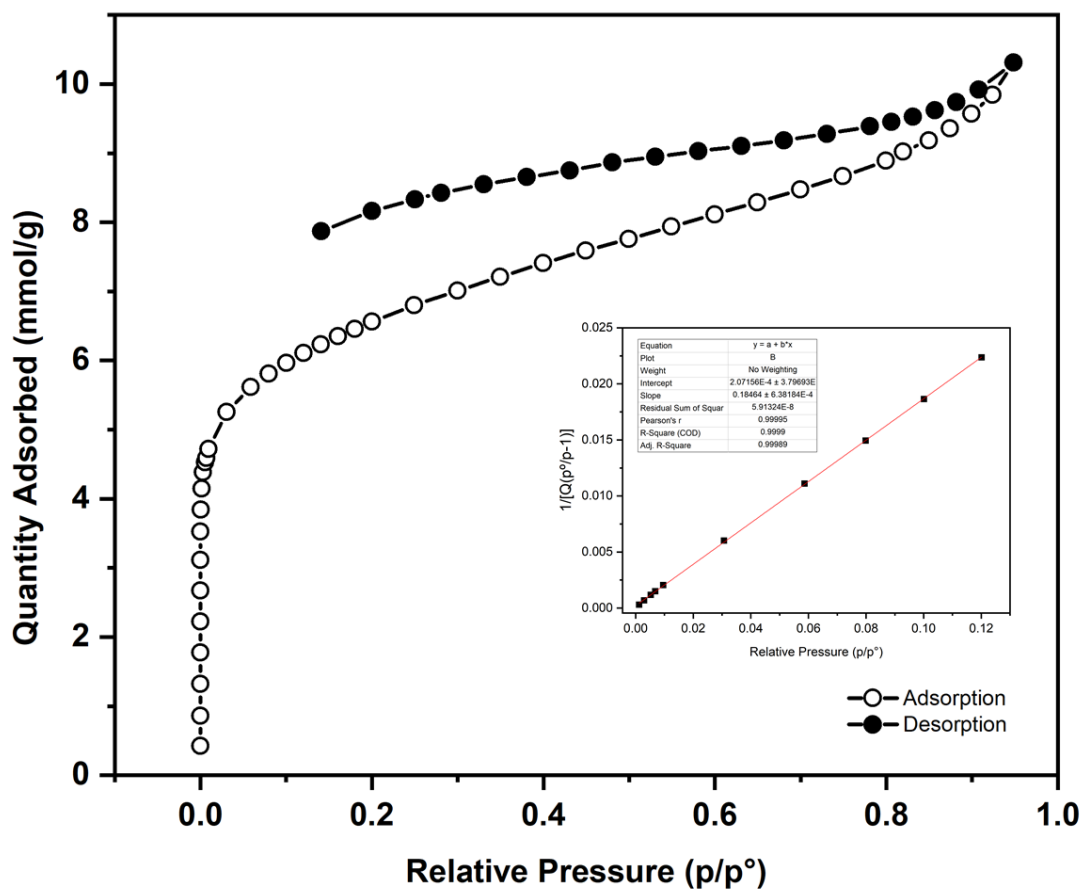


Figure S60. N_2 adsorption-desorption isotherm for $\text{Rh}_{12}\text{L}'_6$ at 77 K ($S_{\text{BET}} = 528 \text{ m}^2/\text{g}$).

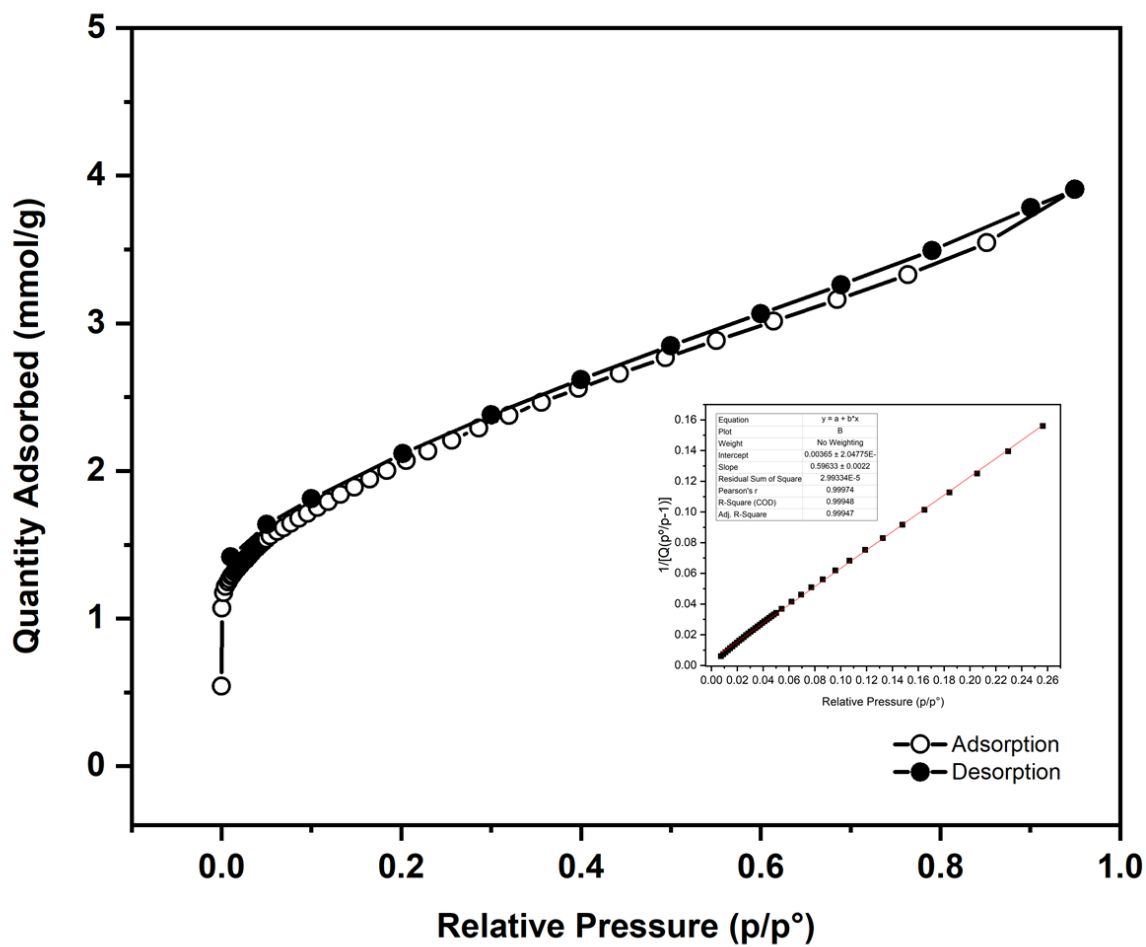


Figure S61. N₂ adsorption-desorption isotherm for Rh₁₂L₁₆L_{3'}₆ at 77 K ($S_{\text{BET}} = 163 \text{ m}^2/\text{g}$).

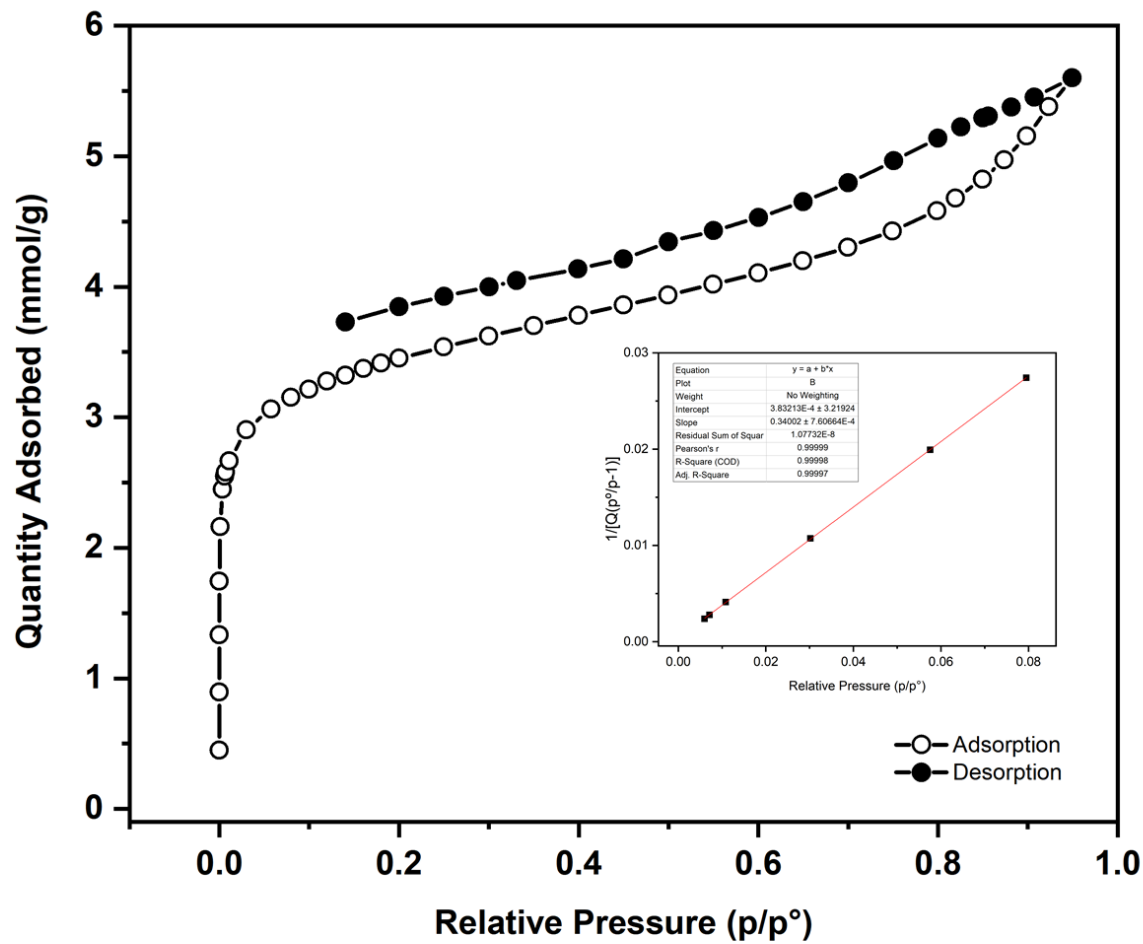


Figure S62. N_2 adsorption-desorption isotherm for $Rh_{12}L^1_6L^4'_6$ at 77 K ($S_{BET} = 287 \text{ m}^2/\text{g}$).

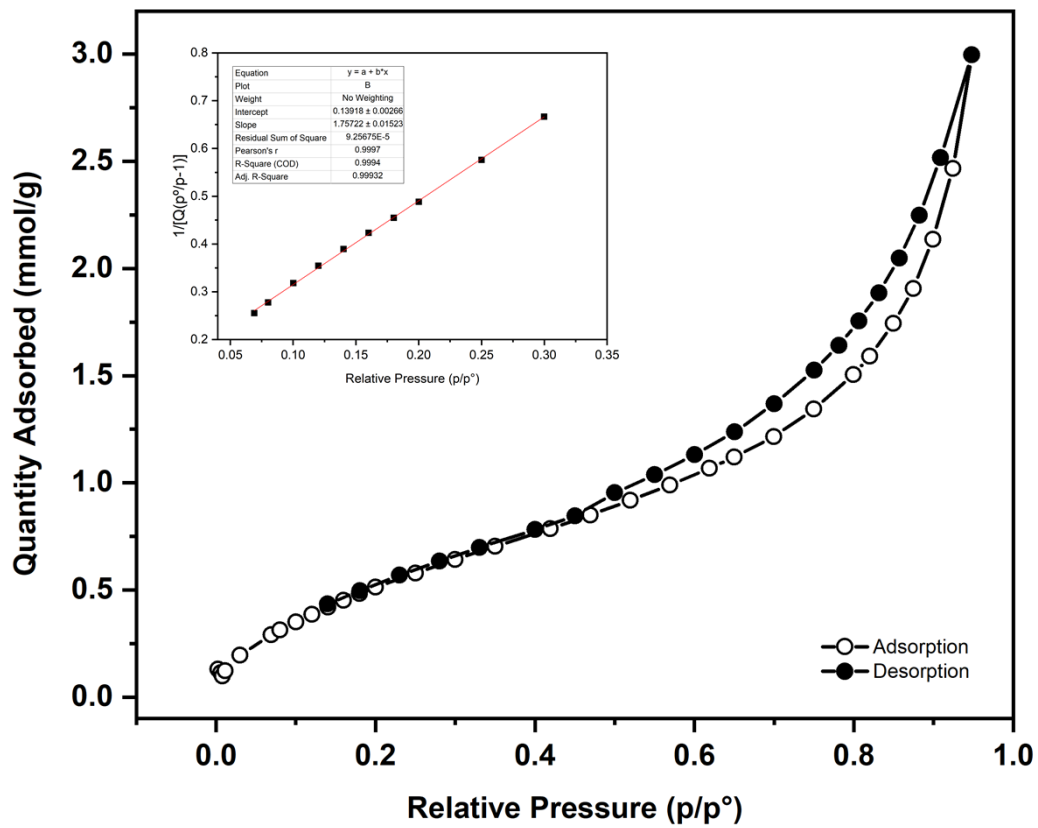


Figure S63. N_2 adsorption-desorption isotherm for $Rh_{12}L_6L_5^*6$ at 77 K ($S_{BET} = 51 \text{ m}^2/\text{g}$).

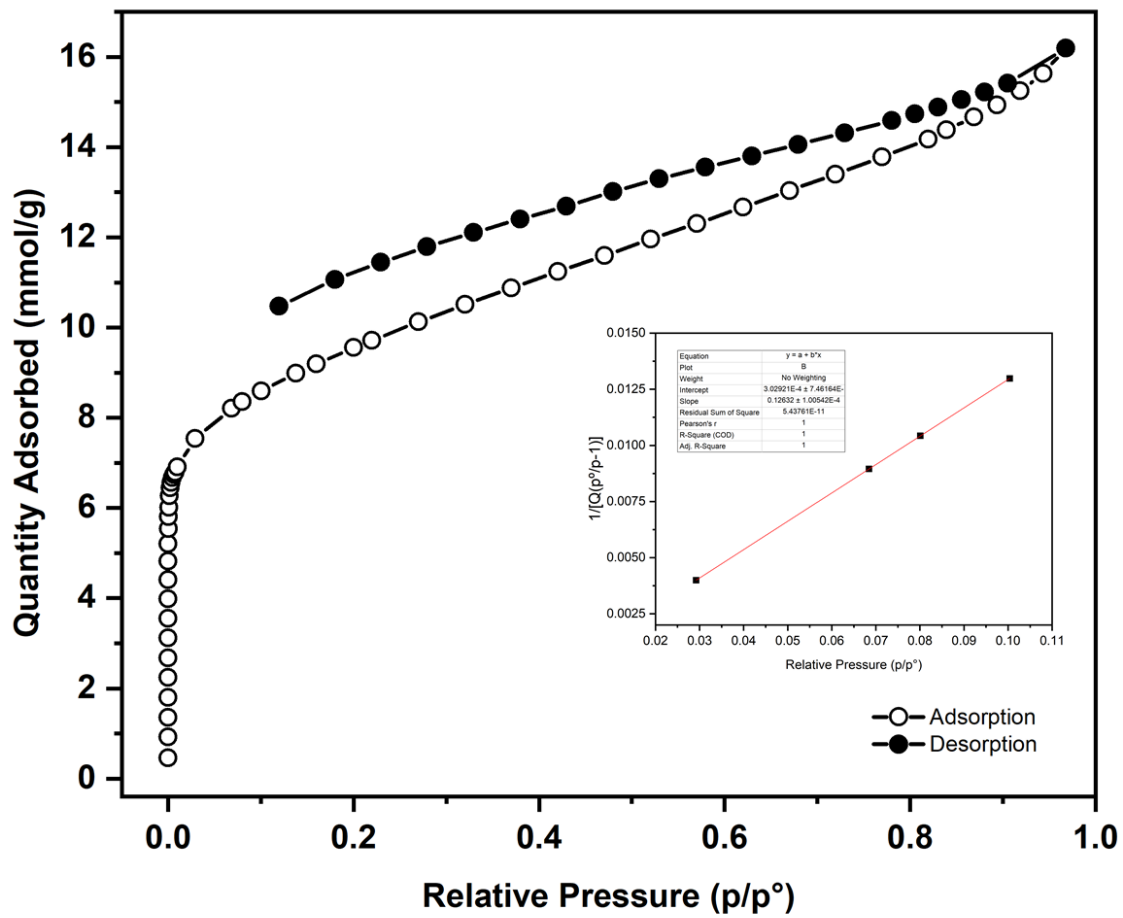


Figure S64. N₂ adsorption-desorption isotherm for Rh₁₂L₁₆L'₆ at 77 K (S_{BET} = 770 m²/g).

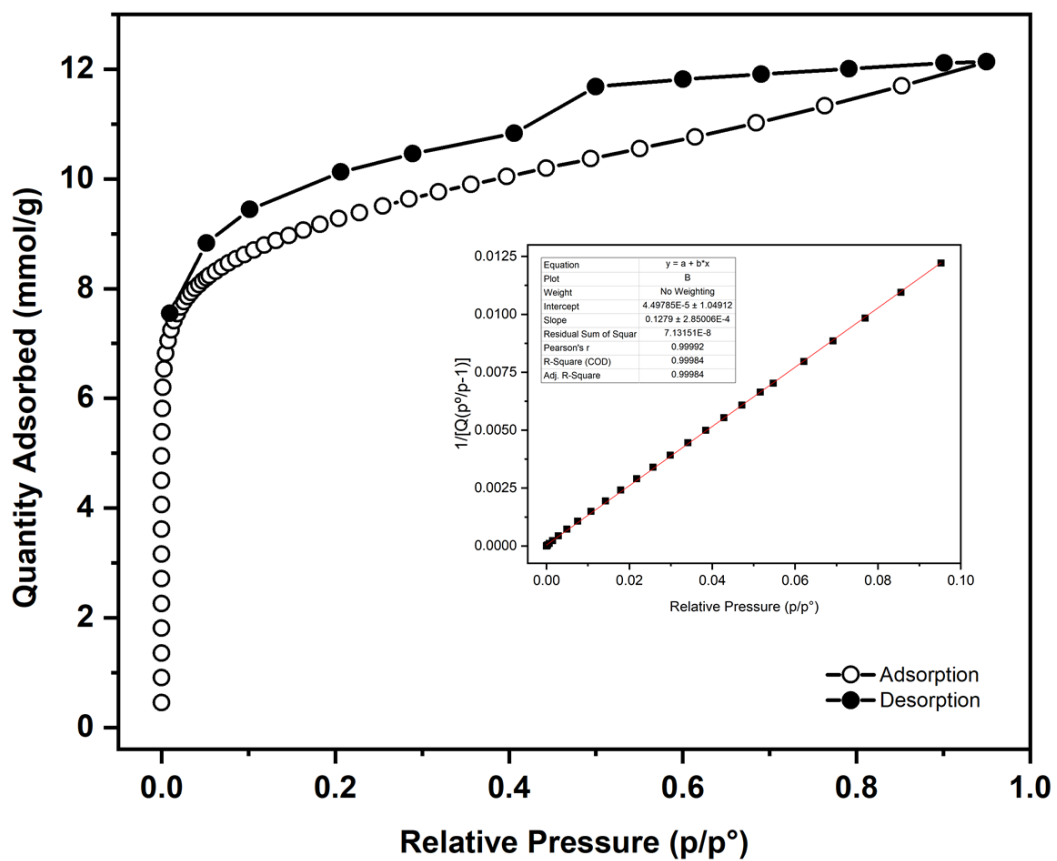


Figure S65. N₂ adsorption-desorption isotherm for Rh₁₂L₂₆L₆ at 77 K ($S_{\text{BET}} = 762 \text{ m}^2/\text{g}$).

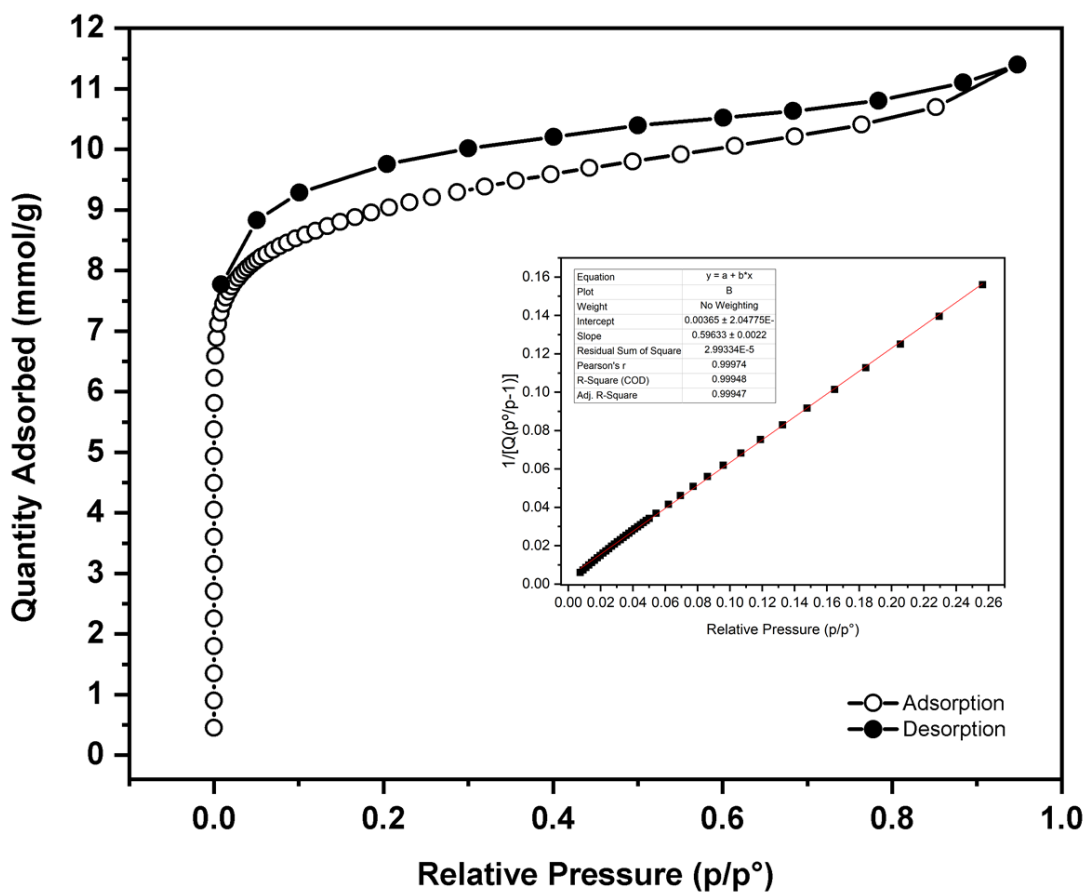


Figure S66. N₂ adsorption-desorption isotherm for Rh₁₂L₂₆L'₆ at 77 K ($S_{\text{BET}} = 761 \text{ m}^2/\text{g}$).

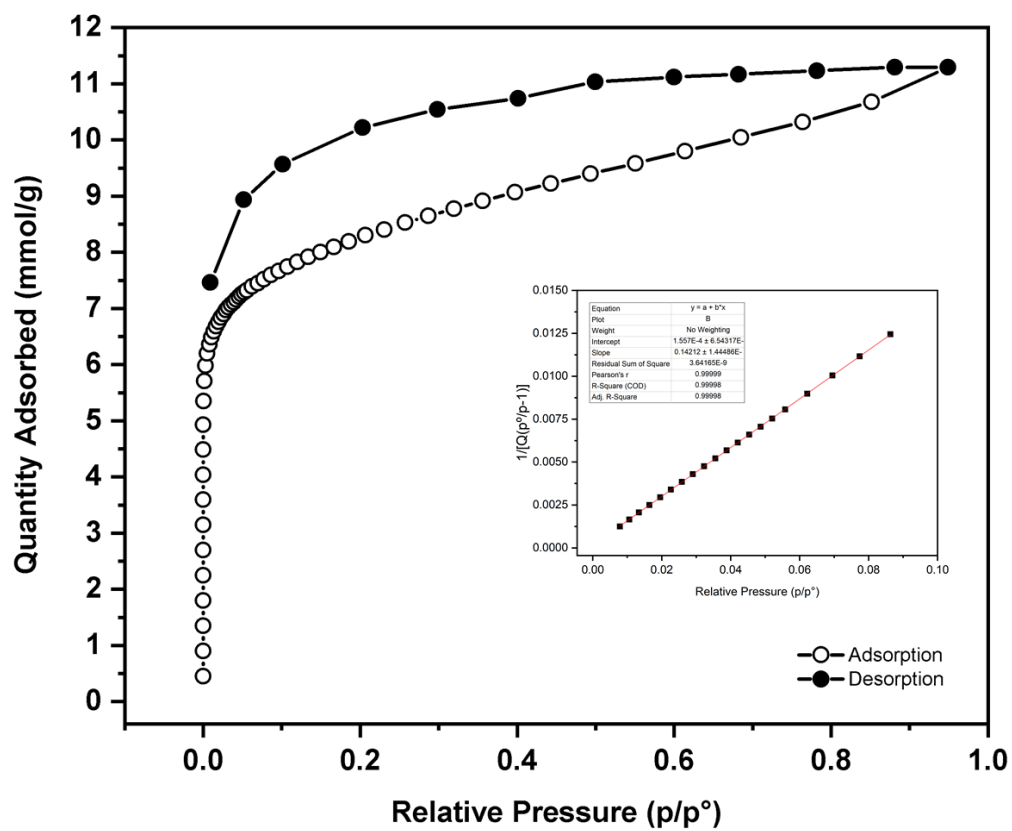


Figure S67. N_2 adsorption-desorption isotherm for $\text{Rh}_{12}\text{L}'_6\text{L}^2_6$ at 77 K ($S_{\text{BET}} = 686 \text{ m}^2/\text{g}$).

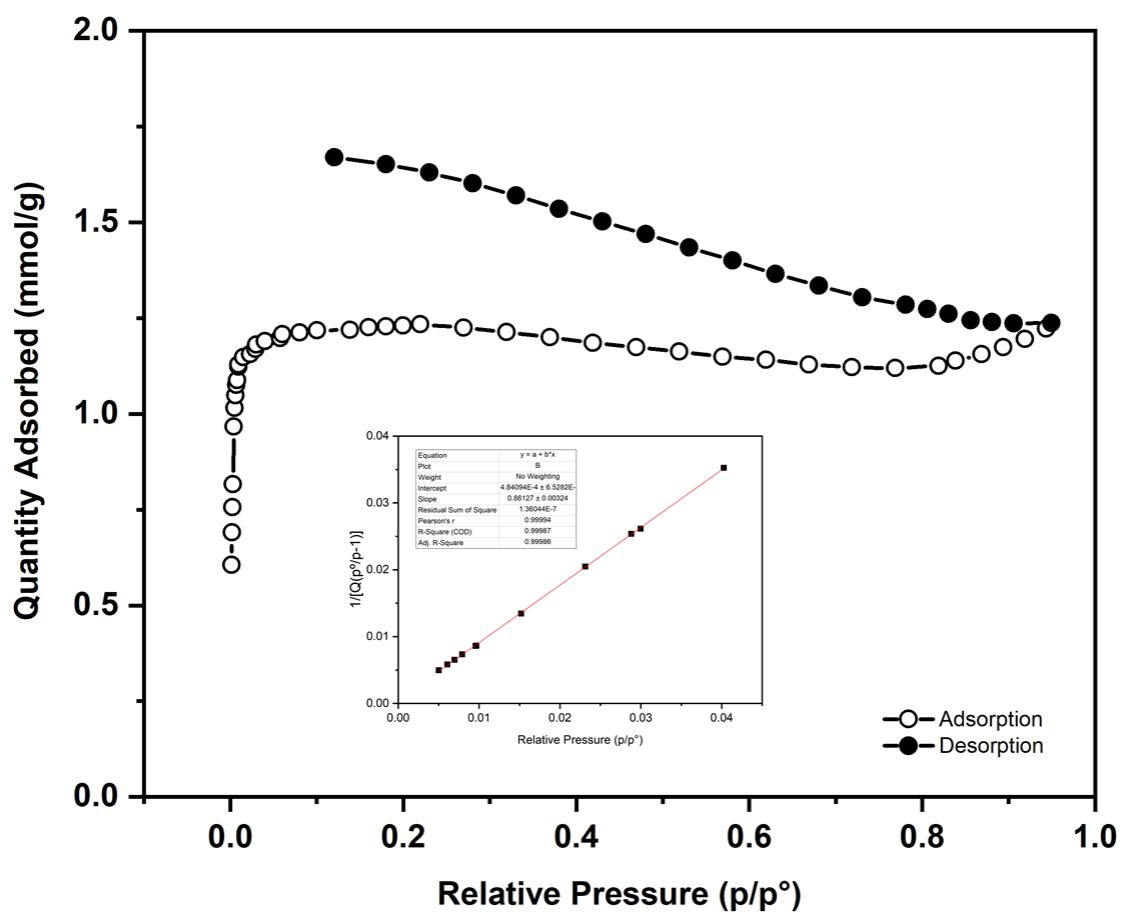


Figure S68. N_2 adsorption-desorption isotherm for $Rh_{12}L^2_6L^3'_6$ at 77 K ($S_{BET} = 113 \text{ m}^2/\text{g}$).

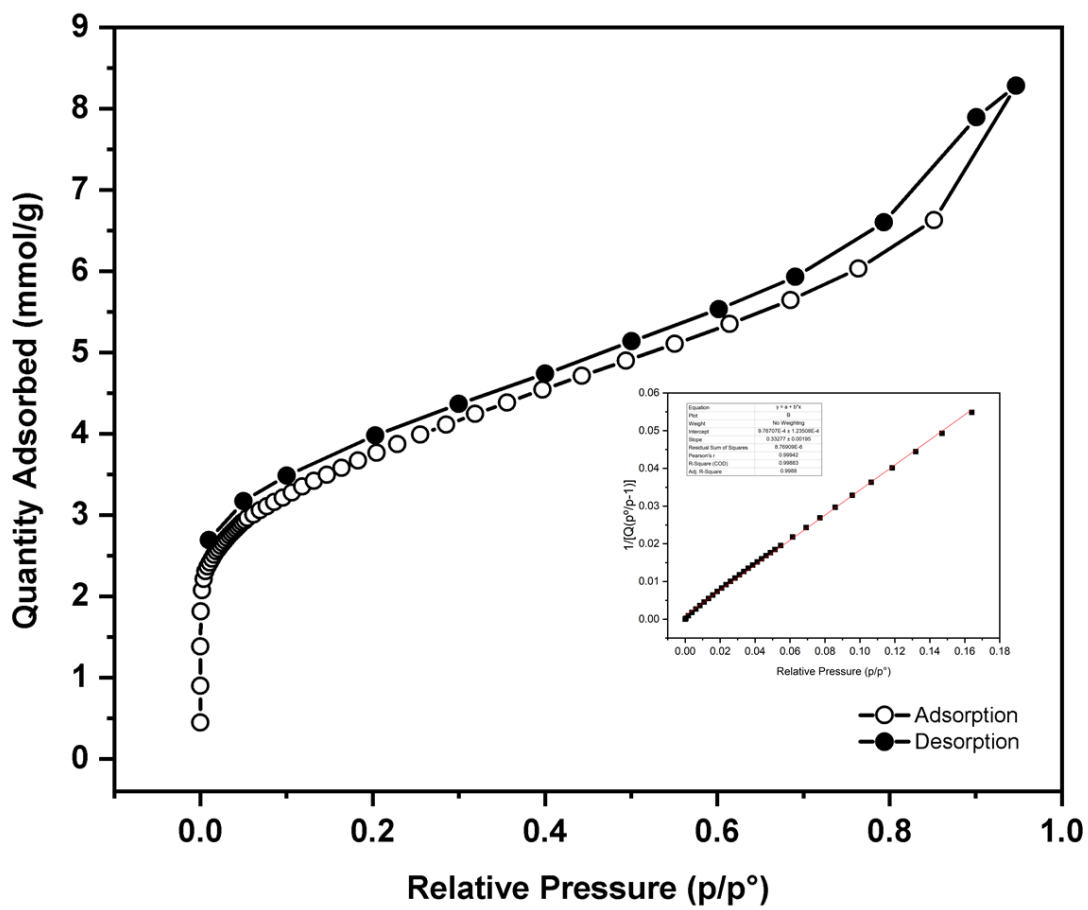


Figure S69. N₂ adsorption-desorption isotherm for Rh₁₂L₂₆L'₆ at 77 K (S_{BET} = 292 m²/g).

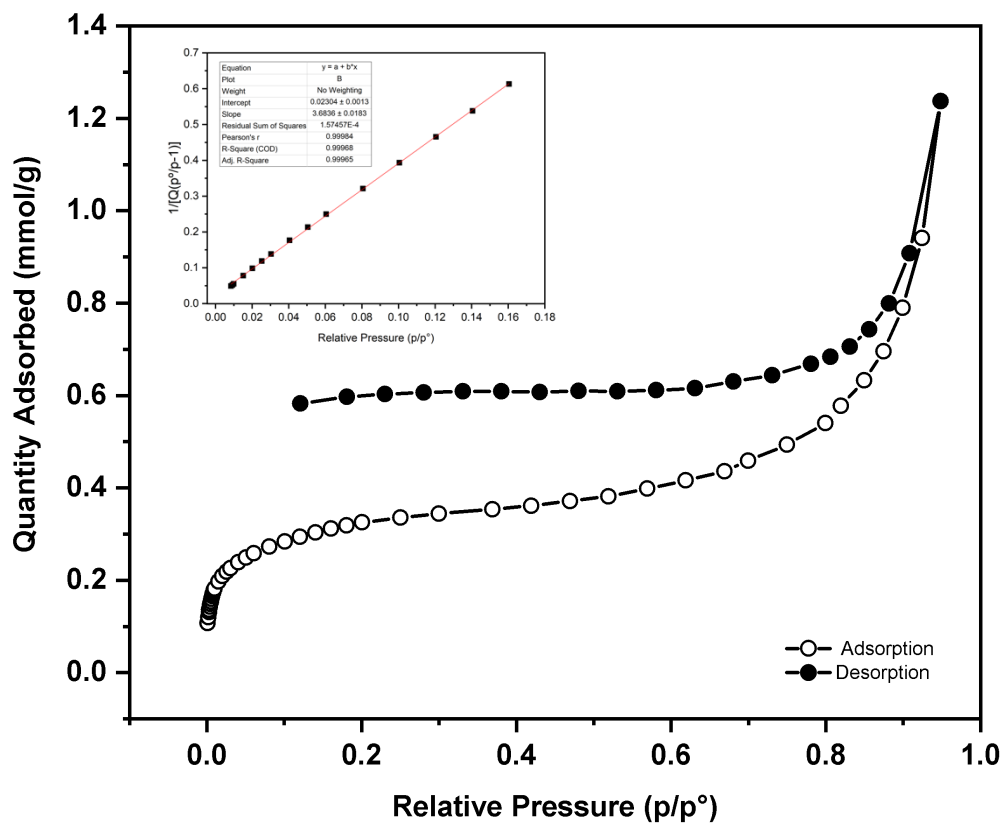


Figure S70. N_2 adsorption-desorption isotherm for $\text{Rh}_{12}\text{L}^2_6\text{L}^5_6$ at 77 K ($S_{\text{BET}} = 26 \text{ m}^2/\text{g}$).

S5.2.1 CO₂ adsorption-desorption isotherms

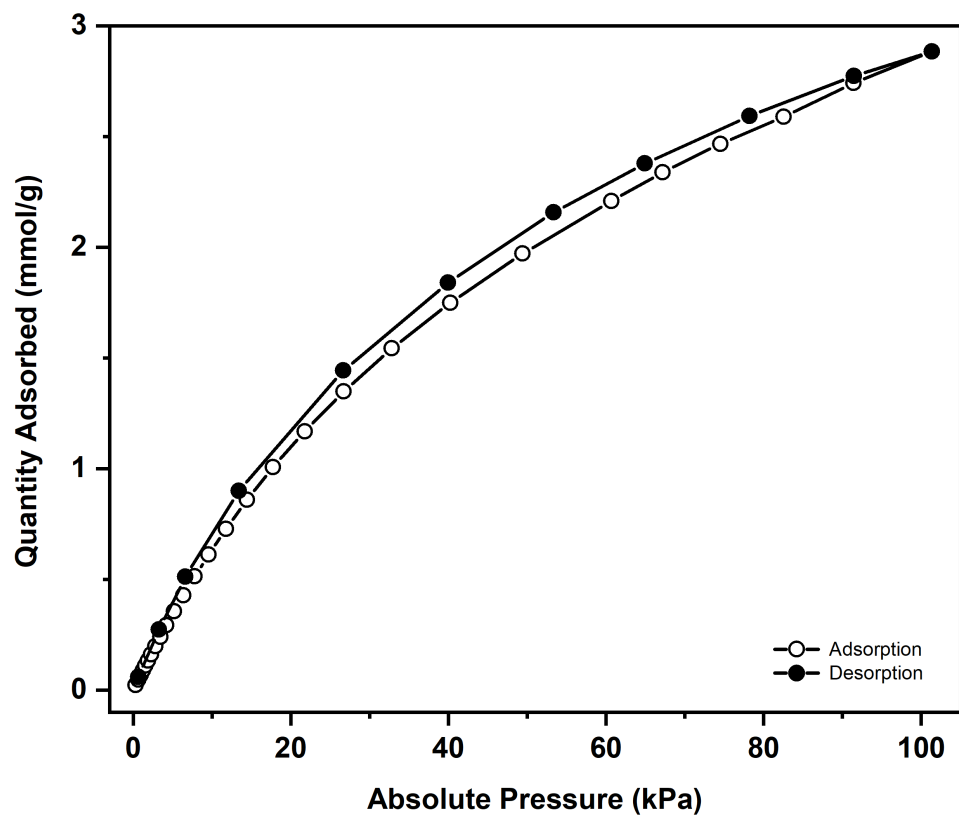


Figure S71. CO₂ adsorption-desorption isotherm for Rh₁₂L¹₆L^{1'}₆ at 298 K.

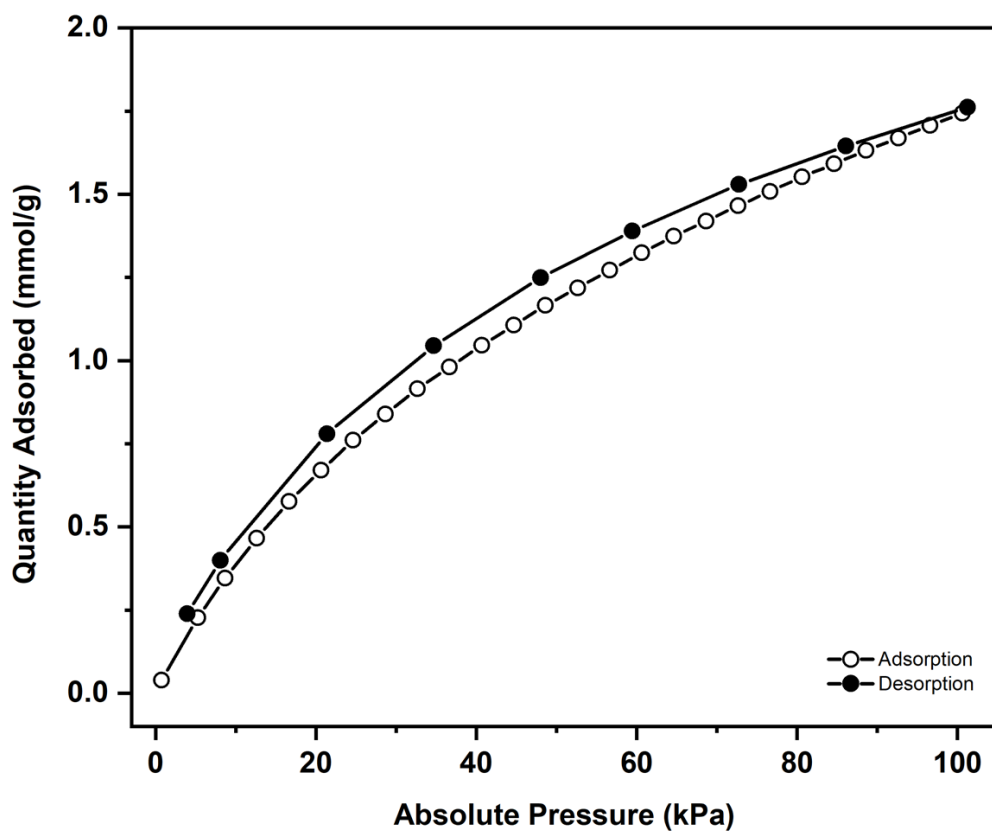


Figure S72. CO₂ adsorption-desorption isotherm for Rh₁₂L¹₆L²'₆ at 298 K.

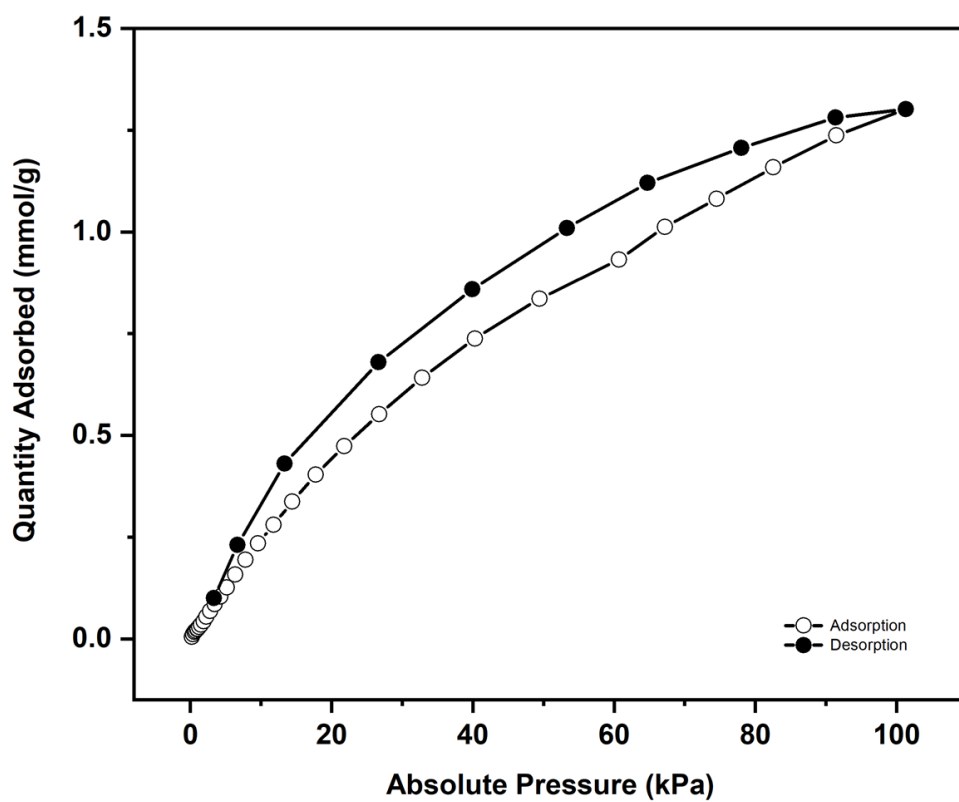


Figure S73. CO₂ adsorption-desorption isotherm for Rh₁₂L¹L^{3'}₆ at 298 K.

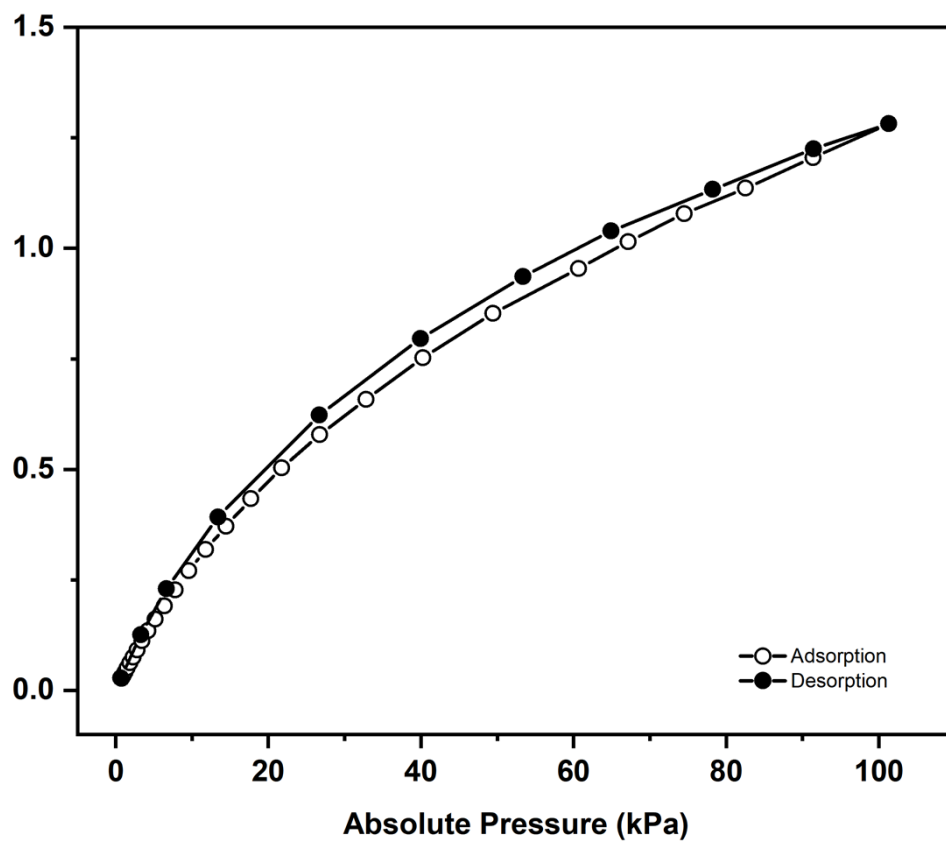


Figure S74. CO₂ adsorption-desorption isotherm for Rh₁₂L¹₆L^{4'} at 298 K.

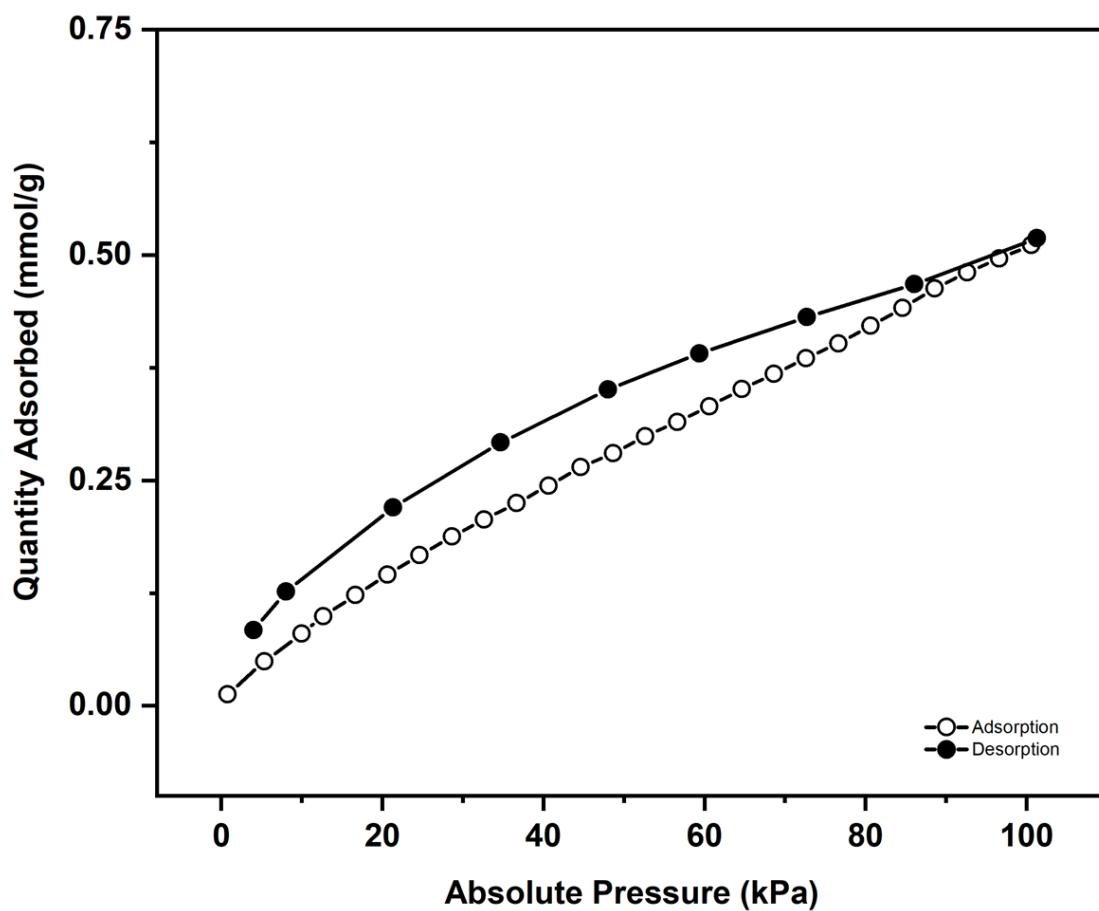


Figure S75. CO₂ adsorption-desorption isotherm for Rh₁₂L¹L⁵ at 298 K.

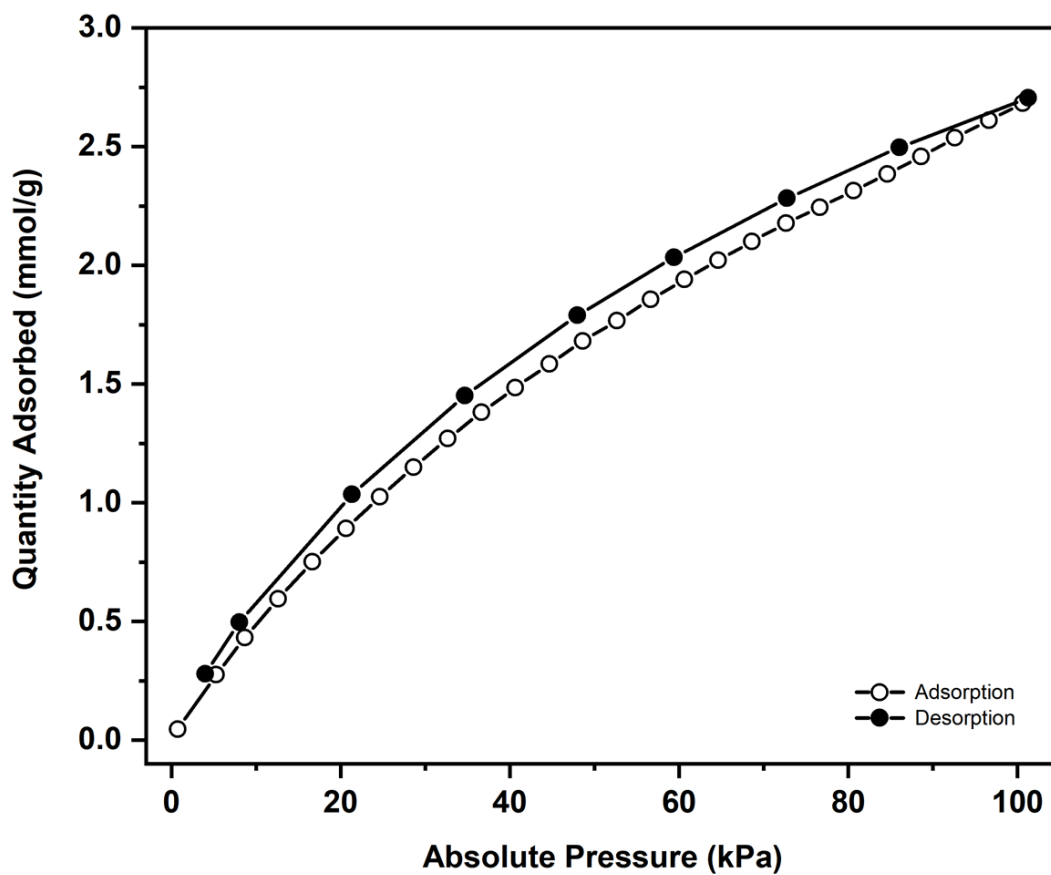


Figure S76. CO₂ adsorption-desorption isotherm for Rh₁₂L¹₆L⁶ at 298 K.

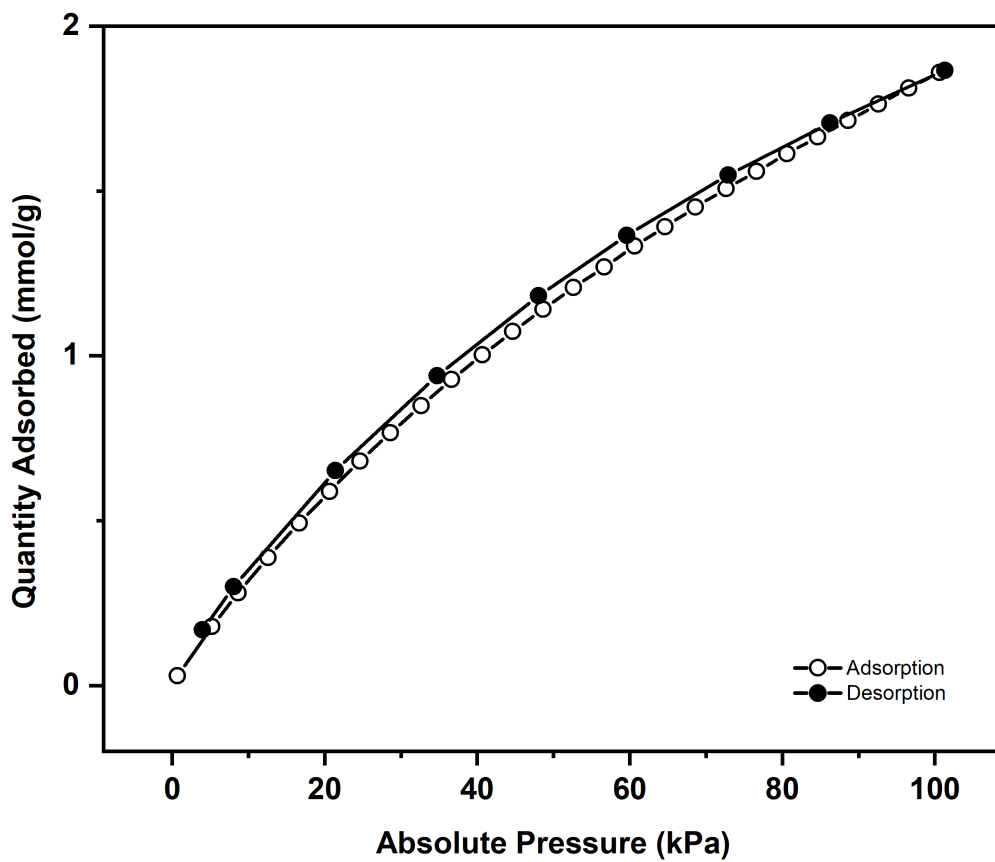


Figure S77. CO₂ adsorption-desorption isotherm for Rh₁₂L²₆L⁶ at 298 K.

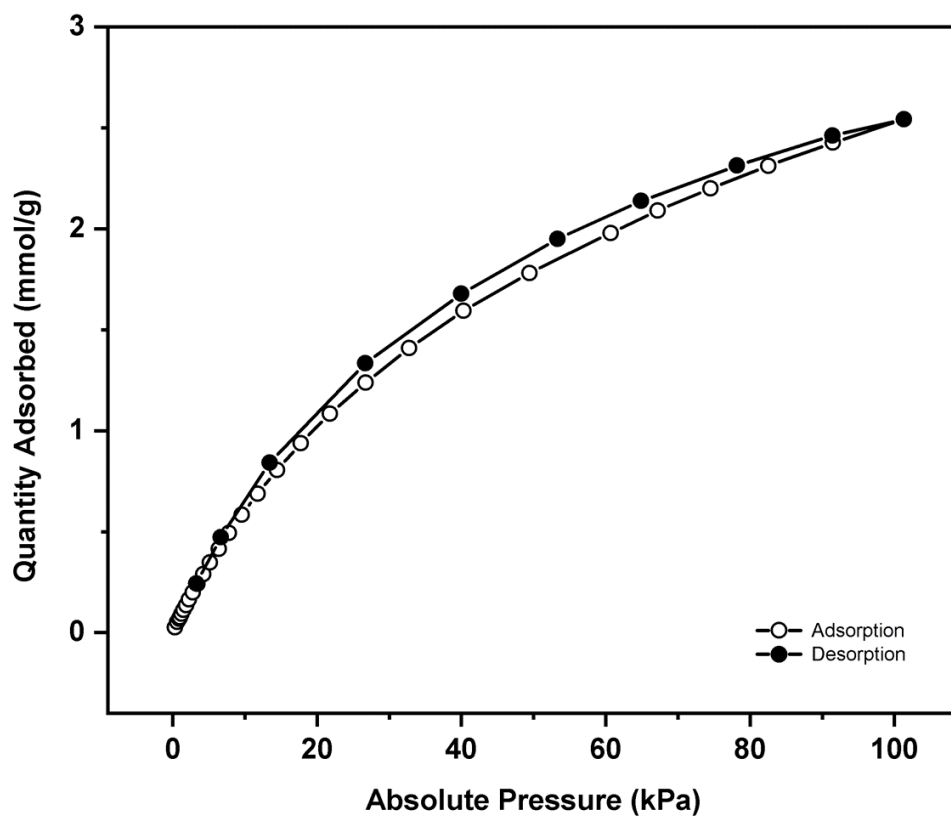


Figure S78. CO₂ adsorption-desorption isotherm for Rh₁₂L₂₆L'₆ at 298 K.

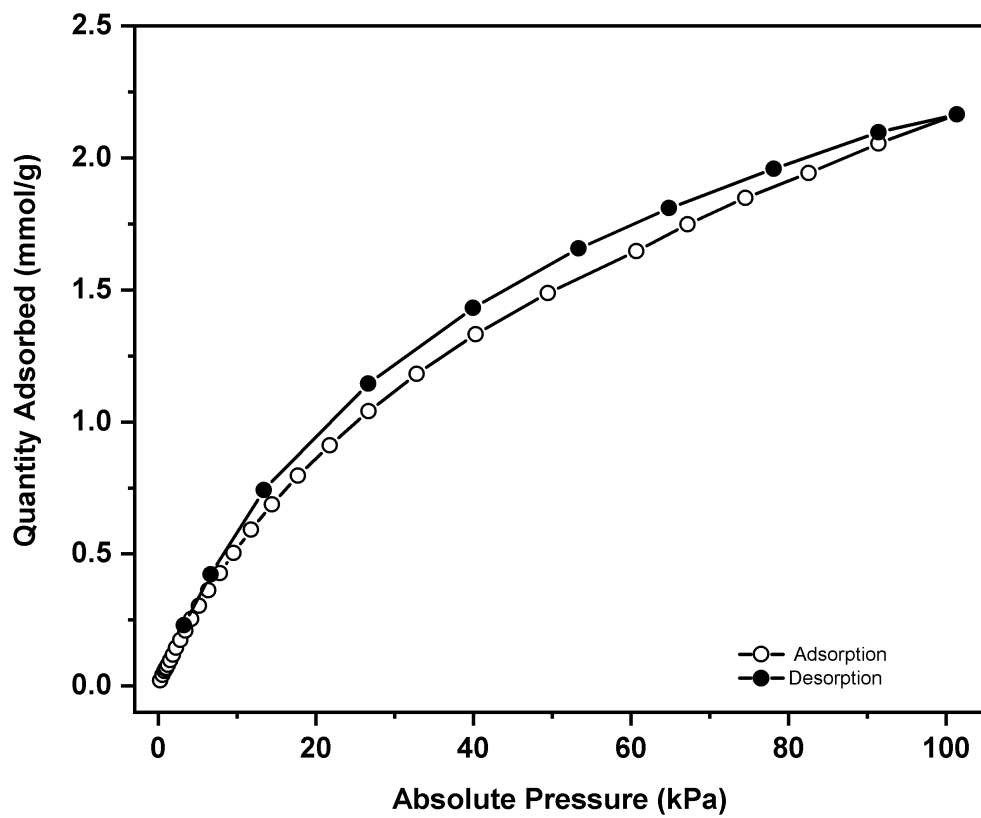


Figure S79. CO₂ adsorption-desorption isotherm for Rh₁₂L₂₆L'₆ at 298 K.

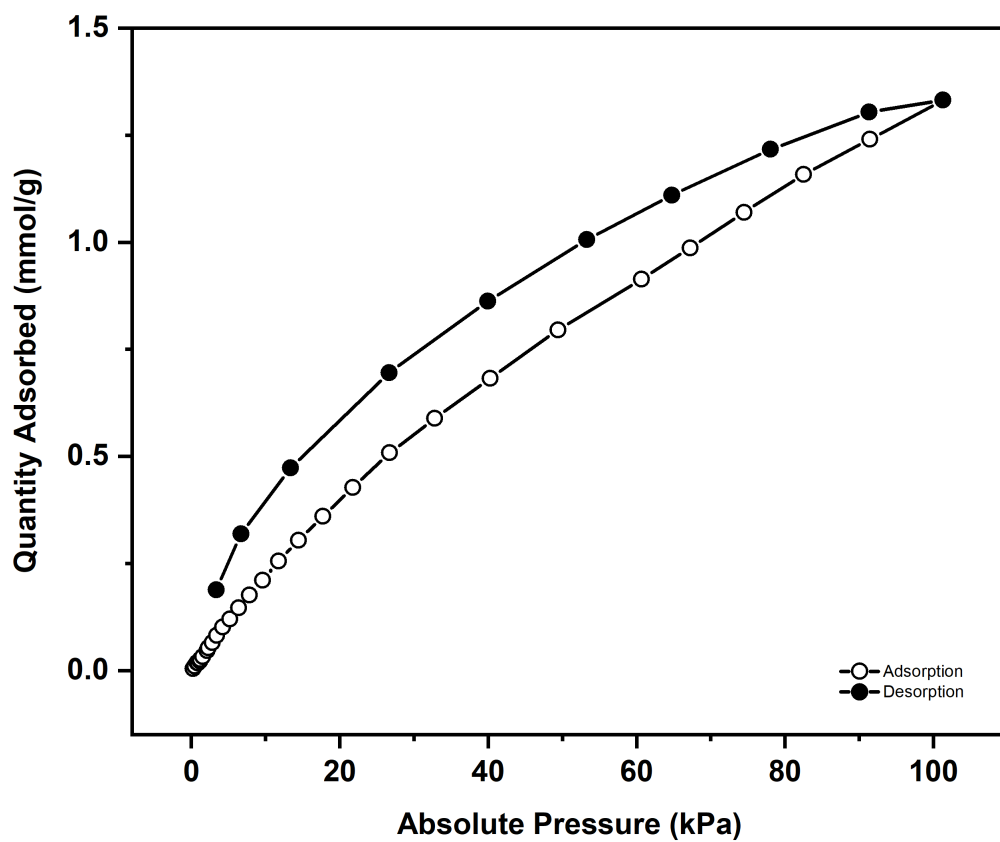


Figure S80. CO₂ adsorption-desorption isotherm for Rh₁₂L₂₆L_{3'}₆ at 298 K.

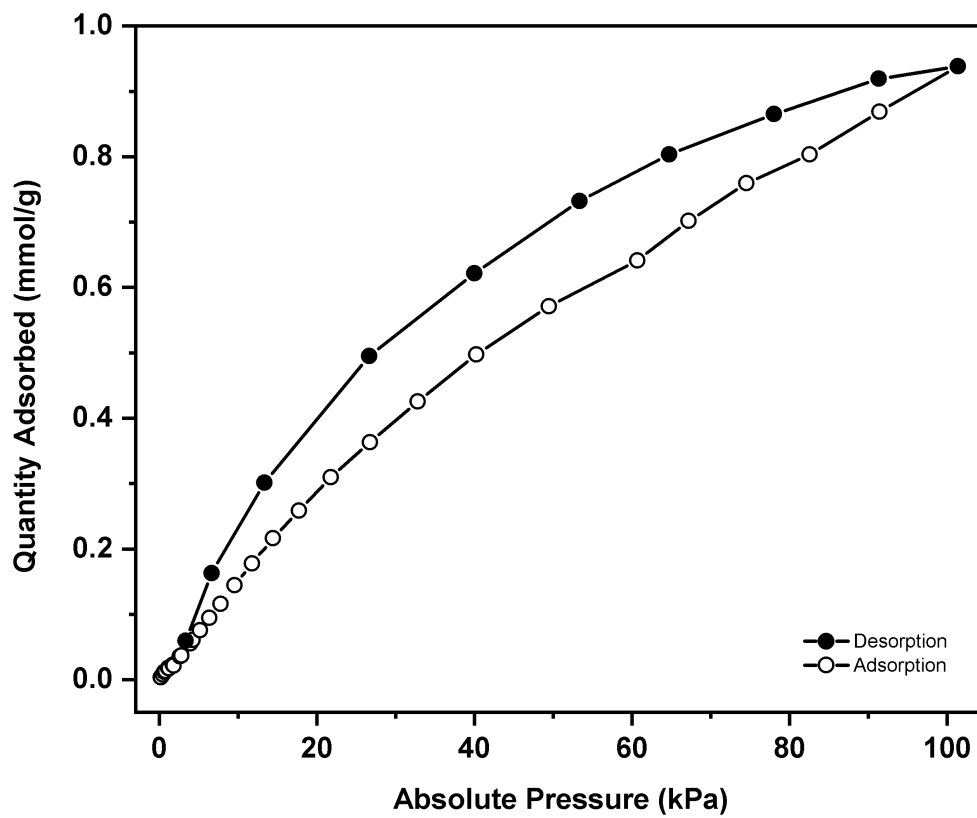


Figure S81. CO₂ adsorption-desorption isotherm for Rh₁₂L²₆L^{4'} at 298 K.

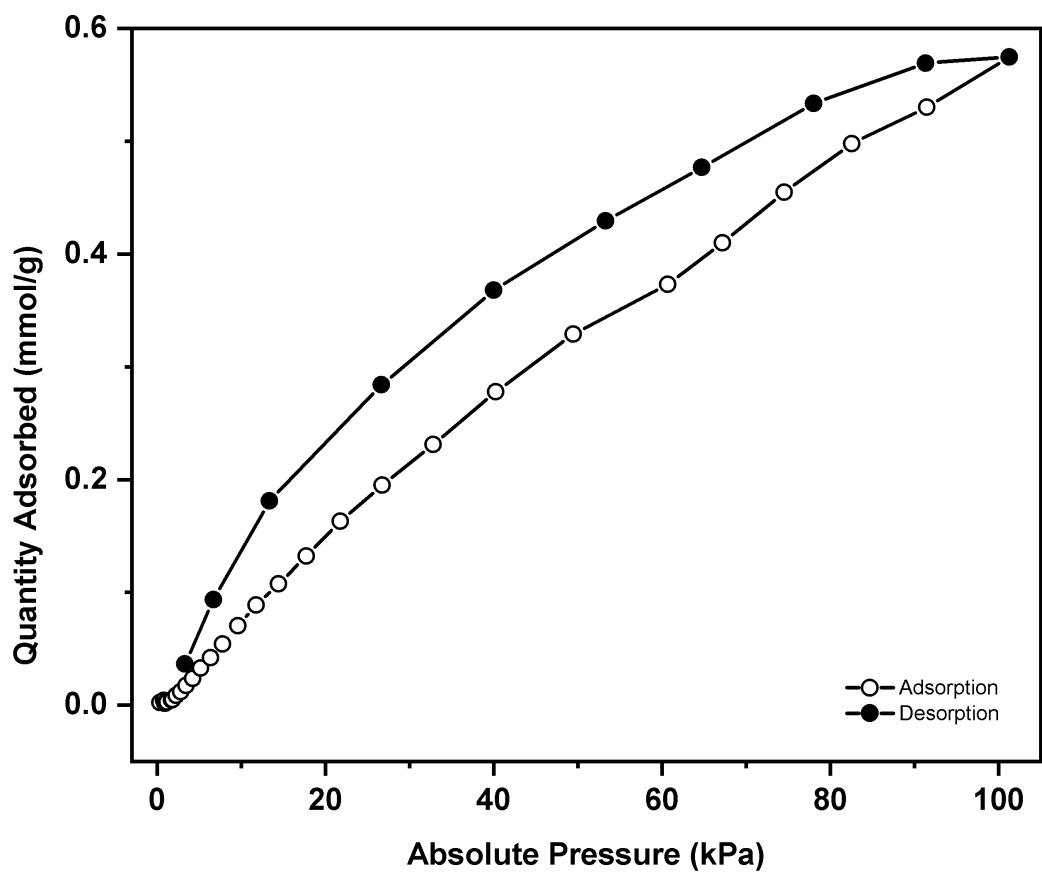


Figure S82. CO₂ adsorption-desorption isotherm for Rh₁₂L²₆L^{5'}₆ at 298 K.

S5. References

- (1) Juanhuix, J.; Gil-Ortiz, F.; Cuní, G.; Colldelram, C.; Nicolás, J.; Lidón, J.; Boter, E.; Ruget, C.; Ferrer, S.; Benach, J.; *J. Synchrotron Radiat.* 2014, 21, 679-689.
- (2) Kabsch, W. *Acta Cryst. D* 2010, 66, 125-132.
- (3) Bruker. APEX2, SAINT and SADABS; Bruker AXS Inc.: Madison, Wisconsin, USA 2012.
- (4) Sheldrick, G. M. *Acta Cryst. C* 2015, 71, 3-8.
- (5) Farrugia, L. J. *J. Appl. Cryst.* 2012, 45, 849-854.
- (6) Dolomanov, O. V.; Bourhis, L. J.; Gildea, R. J.; Howard, J. A. K.; Puschmann, H. *J. Appl. Cryst.* 2009, 42, 339-341.
- (7) Spek, A. J. *J. Appl. Cryst.* 2003, 36, 7-13.